# Non-linear Phenomena in Dipolar Bose-Einstein Condensates

Von der Fakultät für Mathematik und Physik
der Gottfried Wilhelm Leibniz Universität Hannover
zur Erlangung des Grades

Doktor der Naturwissenschaften
- Dr. rer. nat. -

genehmigte Dissertation von

**M. Sc. Rejish Nath Gopinathan Rejani**

geboren am 12 Februar 1982 in Kollam, Kerala, Indien.

Institut für Theoretische Physik
Gottfried Wilhelm Leibniz Universität Hannover

2009

Referent : Prof. Dr. Luis Santos
Koreferent : Prof. Dr. Eric Jeckelmann
Tag der Promotion : 24. June 2009

*To Achan, Amma, Chettan and Chechi.*

It is not the strongest of the species that survives, nor the most intelligent that survives. It is the one that is the most adaptable to change.

– Charles Darwin.

# Zusammenfassung

Atom-Atom Wechselwirkungen induzieren eine inhärente nichtlineare Physik in Bose-Einstein Kondensaten, die eine beachtliche Ähnlichkeit zur nichtlinearen Optik aufweist. Üblicherweise haben nur kurzreichweitige Wechselwirkungen eine Rolle in Experimenten gespielt. Allerdings pflastern eine neue Generation von Experimenten zu magnetischen atomaren Dipolen und polaren Molekülen den Weg für das sich schnell entwickelnde Gebiet der dipolaren Gase, in denen die Dipol-Dipol Wechselwirkung signifikant oder sogar dominant vorliegt. In dieser Arbeit untersuchen wir neue von der Dipol-Dipol Wechselwirkung verursachte nichtlineare Physik in Bose-Einstein Kondensaten.

Wir zeigen, dass die von der Dipol-Dipol Wechselwirkung veursachte Nichtlokalität mehrdimensionale Solitonen stabilisieren kann. Insbesondere können hinreichend große Dipol-Dipol Wechselwirkungen zwei-dimensionale helle Solitonen und (falls ein optisches Gitter vorhanden ist) drei-dimensionale stationäre dunkle Solitonen stabilisieren. Die Möglichkeit zwei-dimensionale helle Solitonen zu stabilisieren ermöglicht neue Streu-Szenarien für ultra-kalte Atomen, die wir in dieser Arbeit im Detail untersuchen.

Der teilweise anziehende Charakter der Dipol-Dipol Wechselwirkung wirft offensichtliche Bedenken bezüglich des Problems der Stabilität auf. Zwei- und drei-dimensionale kurzreichweitig wechselwirkende homogene Kondensate erfahren lokale Kollapse, wenn die Phononen im System instabil werden (Phononen-Instabilität). Im Gegensatz dazu zeigen wir, dass sich nach der Phononen-Instabilität die Dynamik in einem zwei-dimensionalen dipolaren Kondensat qualitativ anders verhält, da in diesen Systemen die Phonon-Instabilität kurzlebige Patterns und die Formation von zwei-dimensionalen hellen Solitonen nach sich zieht.

Außerdem zeigen wir, dass sich Faraday-Patterns, induziert durch externes modulieren der System-Nichtlinearität, in dipolaren Gasen mit einem Roton-Maxon Anregungsspektrum außergewöhnlich verändern. Während für nicht-dipolare Gase die Patternsgröße monoton mit der Modulations-Frequenz abfällt, weisen Patterns in dipolaren Gasen, auch für flache Roton-Minima, eine hoch nicht-triviale Frequenzabhängingkeit auf, die durch abrupte Übergange in der Patternsgröße charakterisiert werden, welche besonders ausgeprägt sind, wenn die dipolare Wechselwirkung moduliert wird. Deshalb stellen Faraday-Patterns ein optimales Werkzeug da, um die Entstehung des Roton-Minimums, einer bedeutenden Schlüsseleigenschaft dipolarer Gase aufzudecken.

In dieser Arbeit diskutieren wir auch experimentelle Möglichkeiten die oben beschriebenen Phänomene in laufenden Experimenten zu beobachten.

Stichwörter: Bose-Einstein Kondensation, Dipol-Dipol Wechselwirkung, Optische Gitter.

# Abstract

Atom-atom interactions induce an inherent nonlinear physics in Bose-Einstein condensates, which present remarkable resemblances with nonlinear optics. Typically only short-range interactions have played a role in experiments. However, a new generation of experiments on magnetic atomic dipoles and polar molecules is paving the path for the rapidly-developing field of dipolar gases, where the dipole-dipole interaction is significant or even dominant. In this thesis, we study the novel nonlinear physics introduced by the dipole-dipole interactions in Bose-Einstein condensates.

We show that nonlocality due to the dipole-dipole interactions may stabilize multi-dimensional solitons. In particular, sufficiently large dipole-dipole interactions may stabilize two-dimensional bright solitons and (in the presence of an additional optial lattice) three-dimensional stationary dark solitons. The possibility of stabilizing two-dimensional dipolar bright solitons offers novel inelastic soliton-soliton scattering scenarios in ultra-cold atoms, which we study in detail in this thesis.

The partially attractive character of the dipole-dipole interaction makes the issue of stability an issue of obvious concern. 2D and 3D short range interacting homogeneous condensates undergo local collapses if the phonons in the system are unstable (phonon instability). On the contrary, we show that post phonon instability dynamics is qualitatively different in two-dimensional dipolar condensates, since in these systems phonon instability is followed by a transient pattern formation, and the formation of two-dimensional bright solitons.

We show as well that Faraday patterns, induced by external driving of the system nonlinearity, are remarkably different in dipolar gases with a roton-maxon excitation spectrum. Whereas for non-dipolar gases the pattern size decreases monotonously with the driving frequency, patterns in dipolar gases present, even for shallow roton minima, a highly non trivial frequency dependence characterized by abrupt pattern size transitions, which are especially pronounced when the dipolar interaction is modulated. Faraday patterns constitute hence an optimal tool for revealing the onset of the roton minimum, a major key feature of dipolar gases.

In this thesis, we also discuss the experimental possibilities of observing the above mentioned phenomena in on-going experiments.

**Keywords**: Bose-Einstein Condensation, Dipole-dipole Interaction, Optical Lattices.

# Contents

**Zusammenfassung** vii

**List of Figures** xiii

**1. Introduction** 1
- 1.1. Bose-Einstein Condensation 1
  - 1.1.1. The Gross-Pitaevskii equation 3
  - 1.1.2. The External Potential 5
  - 1.1.3. Ground State of the GP Equation 6
  - 1.1.4. Reduced-dimensional GP Equations 9
  - 1.1.5. Solitons in BEC 10
  - 1.1.6. Elementary Excitations in BEC 13
- 1.2. Dipolar Bose-Einstein Condensation 14
  - 1.2.1. Dipole-dipole Interaction 15
  - 1.2.2. Tuning the Dipole-dipole Interaction 16
  - 1.2.3. Non-local Gross-Pitaevskii Equation 17
  - 1.2.4. Properties of Dipolar BEC 18
  - 1.2.5. Roton-maxon Spectrum in Dipolar BEC 19
- 1.3. Overview 22

**I. Solitons in Dipolar BEC** **25**

**2. Two-dimensional Bright Solitons in Dipolar BEC** 27
- 2.1. Two-dimensional Nonlocal GP Equation 27
- 2.2. Gaussian Ansatz 28
  - 2.2.1. Energy of the System 29
  - 2.2.2. Stability Conditions for a 2D Soliton 30
- 2.3. Time Dependent Variational Analysis 32
  - 2.3.1. Model of the System 32
  - 2.3.2. Evolution Equations for the Parameters 33
  - 2.3.3. Small Amplitude Shape Oscillations 34
- 2.4. Anisotropic Solitons 36

**3. Soliton-soliton Scattering in Dipolar BECs** 39
- 3.1. Scattering of 2D Bright Solitons in a Single Plane 39
- 3.2. Two-dimensional Bright Solitons in Double-well Potential 40
  - 3.2.1. Model of the Problem 40

3.2.2. Variational Method . . . . . . . . . . . . . . . . . . . . . . . . . . 41
3.2.3. Stationary Solution of the Two-coupled Solitons . . . . . . . . . 42
3.2.4. Lowest-lying excitations . . . . . . . . . . . . . . . . . . . . . . . 43
3.2.5. Scattering of Two-dimensional Solitons . . . . . . . . . . . . . . 45
3.3. One-dimensional Bright Solitons in Dipolar BEC . . . . . . . . . . . . . 46
3.4. Summary . . . . . . . . . . . . . . . . . . . . . . . . . . . . . . . . . 48

**4. Dark Solitons in Three Dimensional Dipolar Bose-Einstein Condensates 51**
4.1. Dark Solitons in 3D BEC . . . . . . . . . . . . . . . . . . . . . . . . . 51
4.2. Dark Solitons in Dipolar BEC . . . . . . . . . . . . . . . . . . . . . . . 53
4.2.1. Model of the Problem . . . . . . . . . . . . . . . . . . . . . . . . 53
4.2.2. Lattice Calculations . . . . . . . . . . . . . . . . . . . . . . . . . 54
4.2.3. Effective continuous model - coarse-grained . . . . . . . . . . . . 56
4.2.4. Time-independent Solution . . . . . . . . . . . . . . . . . . . . . 57
4.2.5. Bogoliubov Excitations . . . . . . . . . . . . . . . . . . . . . . . 57
4.2.6. Variational Analysis . . . . . . . . . . . . . . . . . . . . . . . . . 59
4.3. Summary . . . . . . . . . . . . . . . . . . . . . . . . . . . . . . . . . 61

**II. Phonon-instability in Dipolar BEC 63**

**5. Phonon-instability in Dipolar Bose-Einstein Condensates 65**
5.1. Attractive Short-range Interacting Condensates . . . . . . . . . . . . . . 65
5.2. Three-dimensional dipolar BECs . . . . . . . . . . . . . . . . . . . . . . 66
5.3. Two-dimensional Dipolar BECs . . . . . . . . . . . . . . . . . . . . . . 66
5.3.1. Bogoliubov Excitations of a 2D Dipolar BEC . . . . . . . . . . . 67
5.3.2. Dipoles Normal to the Plane . . . . . . . . . . . . . . . . . . . . 68
5.3.3. Dipoles Parallel to the Plane . . . . . . . . . . . . . . . . . . . . 69
5.3.4. Trapped 2D dipolar BECs . . . . . . . . . . . . . . . . . . . . . . 69
5.4. One-dimensional Dipolar BECs . . . . . . . . . . . . . . . . . . . . . . 71
5.5. Summary . . . . . . . . . . . . . . . . . . . . . . . . . . . . . . . . . 72

**III. Faraday Patterns in Dipolar BEC 73**

**6. Faraday Patterns in Dipolar BEC 75**
6.1. Faraday Instability in Short-range Interacting Condensates . . . . . . . 76
6.2. Faraday Instability in Dipolar Condensates . . . . . . . . . . . . . . . . 77
6.2.1. Model of the Problem . . . . . . . . . . . . . . . . . . . . . . . . 77
6.2.2. Bogoliubov Excitations . . . . . . . . . . . . . . . . . . . . . . . 78
6.2.3. Modulation of Short-range Interaction . . . . . . . . . . . . . . . 78
6.3. Modulation of Dipolar Interaction . . . . . . . . . . . . . . . . . . . . . 81
6.4. Experimental Feasibility . . . . . . . . . . . . . . . . . . . . . . . . . . 83
6.5. Summary . . . . . . . . . . . . . . . . . . . . . . . . . . . . . . . . . 84

**7. Summary 85**

**Bibliography** **87**

# List of Figures

1.1. Energy per particle, in units of $\hbar\omega$, as a function of the variational parameter $\lambda$ for an attractive BEC in a spherical trap. The curves are plotted for several values of $N|a|/a_{ho}$. The local minimum disappears at $N = N_{cr}$. 8

1.2. Energy per particle as a function of the variational parameter $\lambda$ for an attractive Gaussian BEC in the absence of a trap. Fig. (1.2(a)) is for 3D case with $N|a| = 0.1$. Fig. (1.2(b)) is for 2D case with $N|a|/l_z = 1$ for upper curve and $N|a|/l_z = 2$ for lower curve. . . . . . . . . . . . . . . . 11

1.3. Energy per particle as a function of the variational parameter $\lambda$ for an attractive 1D Gaussian BEC in the absence of a trap and $\tilde{g}^{(1)} = N|a|/l_\rho^2 = 2$. The stability of a bright soliton is characterized by the minimum in the energy. . . . . . . . . . . . . . . . . . . . . . . . . . . . . . . . 12

1.4. Anisotropy of dipole-dipole interactions. . . . . . . . . . . . . . . . . . . . 16

1.5. Tunability of the magnetic dipole-dipole interaction. . . . . . . . . . . . 17

1.6. Dispersion law $\epsilon_0(q)$ for various values of $\gamma$ and $\mu/\hbar\omega$: (a) $\gamma = 1/2$, $\mu/\hbar\omega = 343$; (b) $\beta = 0.53$, $\mu/\hbar\omega = 46$ (upper curve) and $\beta = 0.47$, $\mu/\hbar\omega = 54$ (lower curve). The solid curves show the numerical results, and the dotted curves the result of Eq. (1.51). . . . . . . . . . . . . . . . 22

2.1. Fig. (2.1(a)): The Gross-Pitaevskii energy functional (2.13) as a function of its variational parameter $L_\rho$, for $\tilde{g} = 200$, and $\beta = -0.20$ (solid line) and $\beta = -0.10$ (dashed line), where $E_s$ is the binding energy of the dipolar soliton. The minium indicates the stability of solitonic solution. Fig. (2.1(b)): The density ($|\psi(x,y)|^2$) plot of the ground state 2D bright soliton in a 2D dipolar BEC with $\tilde{g} = 200$, and $\beta = -0.20$. The ground state is obtained via imaginary time evolution. . . . . . . . . . . . . . . 31

2.2. (2.2(a)): The equilibrium size of the soliton as a function of $\tilde{g}$ for $\beta = -0.2$. Solid line corresponds to results using Eq. (2.13) and empty circles corresponds to numerical results. (2.2(b)): The time evolution of soliton width, for $\tilde{g} = 200$ and $\beta = -0.2$. . . . . . . . . . . . . . . . . . . . . . . 32

2.3. Schematic representation of collective excitations in a cylindrical trap. . 36

2.4. Breathing (bold dashed) and $m = \pm 2$ quadrupole (bold solid) mode for $\tilde{g} = 10$, with $\kappa_0 = L\rho/L_z$. Results from a purely 2D calculation are shown in thin lines. . . . . . . . . . . . . . . . . . . . . . . . . . . . . . . 36

2.5. The Gross-Pitaevskii energy functional (2.37) as a function of its variational parameters $L_x$ and $L_y$, for $\tilde{g} = 10$, and $\beta = 1./0.911$. The minimum (dark region) indicates the stability of solitonic solution. The minimum disappears once $N > N_{cr}$ where the anisotropic soliton is unstable against 2D collapse. . . . . . . . . . . . . . . . . . . . . . . . . . . . . . . . 37
2.6. Stability diagram of an anisotropic soliton as a function of $\beta$ and $\tilde{g}_{cr} = \tilde{g}N_{cr}$, where for $N > N_{cr}$, the soliton is unstable against collapse even for $\beta > 3/4\pi$. . . . . . . . . . . . . . . . . . . . . . . . . . . . . . . . 38
2.7. The ground state anisotropic bright soliton solution of Eq. (2.1). The dipoles are polarized along the $x$ direction and a strong confinement in the $z$ axis. Fig. (2.7(a)): The density $|\Psi|^2$ in the $xy$ planefor $z = 0$, and Fig. (2.1(b)): the density $|\Psi|^2$ in the $xz$ plane for $y = 0$. $\tilde{g} = 10$ and $\beta = 1./0.911$ for both the plots. Since the dipoles are alligned along the $x$ axis, the soliton is more elongated along that direction. . . . . . . . . 38

3.1. Schematic representation of two-dimensional solitons in a single 1D potential. . . . . . . . . . . . . . . . . . . . . . . . . . . . . . . . . . 40
3.2. Density plot of the fusion of two dipolar 2D solitary waves for $\tilde{g} = 20$, $\beta = -0.5$, and $k_0 l_z = 0.01$, where $k_0$ is the intial momentum of the soliton. From top to bottom $\omega_z t/2 = 0, 1000, 2000, 3000, 4000, 5000$. . . . 40
3.3. Schematic representation of the system considered . . . . . . . . . . . 41
3.4. Fig. (3.4(a)): Soliton-Soliton potential for 2D solitons. Dotted line is for point like solitons and solid line for Gaussian shape wavepackets, for a given dipolar strength. Fig. (3.4(b)): Numerical results for the relative distance between two dipolar isotropic solitons as a function of $\tilde{g}$, for $z_0 = 3l_z$,$\beta = -0.20$ . . . . . . . . . . . . . . . . . . . . . . . . . . . 43
3.5. Fig. (3.5(a)): Variational results for low lying excitations: Solid lines are the breathing modes (in and out of phase) and dashed lines are the quadrupole modes (in phase mode greater than out of phase mode for both monopole and quadrupole). The modes for the two solitons $\omega_{TWO}$ are normalized to the corresponding modes ($\omega_{ONE}$) of an independent soliton. The results are for $g/\sqrt{2\pi}\hbar\omega_z l_z^3 = 200, z_0 = 3l_z$. 3.5(b)): the vibrational mode associated with the dynamics of $x_0$. . . . . . . . . . . 44
3.6. Fig. (3.6(a)): Numerical (crosses) and variational (solid) results for $\Delta k/k_0$ ($\Delta k = k_0 - k(t \to \infty)$) as a function of the initial momentum $k_0 l_z$, for $z_0 = 3l_z$, $g/\sqrt{2\pi}\hbar\omega_z l_z^3 = 200$, $\beta = -0.2$. 3.6(b)): Numerical results with $z_0 = 4l_z$ (solid) and $z_0 = 5l_z$ (dotted). . . . . . . . . . . . 46
3.7. Numerical result for the soliton trajectory during spiraling fusion in a 2D soliton scattering, for the case $g/\sqrt{2\pi}\hbar\omega_z l_z^3 = 200$, $\beta = -0.2$, $z_0 = 3l_z$, $\vec{k}_0 l_z = 0.01\hat{x}$, $x_0 = 30l_z$, $y_0 = 10l_z$. . . . . . . . . . . . . . . . . . . . . 47
3.8. Variational results for $\Delta k/k_0$ ($\Delta k = k_0 - k(t \to \infty)$) as a function of the initial momentum $k_0 l_\rho$, for $x_0 = 3l_\rho$, $g/2\pi\hbar\omega_\rho l_\rho^3 = 25$, $\beta = -0.28$. . . . . 48
3.9. Width of a 1D soliton for $x_0 = 3l_\rho$, $g/2\pi\hbar\omega_\rho l_\rho^3 = 25$, $\beta = 0.28$, and $k_0 l_\rho = 0.05$ (solid), 0.168 (dashed), 0.35 (dotted). $\omega_\rho$ ($_\rho$) is the transversal oscillator frequency (length). The time has been re-scaled for comparison. 49

4.1. Numerical results for the imaginary part of the excitation energies of a nodal plane. . . . . . . . . . . . . . . . . . . . . . . . . . . . . . . . 52

4.2. Density plot of the Snake Instability: The Dark Soliton at $t = 0$ starts to oscillate and eventually breaks. . . . . . . . . . . . . . . . . . . . . . . . 53

4.3. Numerical results for the imaginary part of the excitation energies of a DS for $m/m^* = 1$, and $\beta = 0$ (triangles), $-0.5$ (squares) and 1 (circles). Solid lines correspond to the analytical result for low momenta. . . . . . 58

4.4. Numerical results for the imaginary part of the excitation energies of a DS for $\beta = 0$, and $m/m^* = 0.2$ (squares), 0.1 (triangles) and 0.05 (circles). Solid lines correspond to the analytical result for low momenta. . . . . . 58

4.5. Real part of the excitation energies of a DS for $m/m^* = 0.1$, and $\beta = 1.6$. Solid line corresponds to the analytical result for low momenta while empty circles correspond to numerical results. . . . . . . . . . . . . . . . 59

5.1. Series of images for the collapse dynamics of a dipolar BEC in a 3D trap. Upper row shows the experimental results and lower row shows the results of mean-field numerical calculations for the same set of experimental parameters. The picture is taken from the Ref. [1] . . . . . . . . . . . . 67

5.2. 2D soliton gas after phonon instability of an homogeneous dipolar BEC. For both the figures $\mu = -0.2$ and $g/(\sqrt{2\pi}l_z) = 10$. (top) $\perp$-configuration, $\beta = -0.2$, $t = 484/\omega_z$; (bottom) $||$-configuration, $\beta = 0.3$, and $t = 108/\omega_z$. 68

5.3. Trapped BEC in the $\perp$-configuration. In the simulations, $\omega_\rho = 0.001\omega_z$, $g/(\sqrt{2\pi}l_z) = 200$ and $\beta = 0.3$ ($t < 0$) and $-0.3$ ($t > 0$). (left) Formation of ring structures ($t = 810/\omega_z$); (right) Final soliton at the trap center ($t = 7500/\omega_z$). . . . . . . . . . . . . . . . . . . . . . . . . . . . . . . . . 70

5.4. Trapped BEC after tilting at $t = 0$ from $\perp$ to $||$ configuration, with $\omega_\rho = 0.001\omega_z$, $g/(\sqrt{2\pi}l_z) = 200$ and $\beta = 0.3$. (left) Anisotropic ring formation ($t = 1092/\omega_z$); (right) Final formation of an anisotropic soliton ($t = 1281/\omega_z$). . . . . . . . . . . . . . . . . . . . . . . . . . . . . . . . . 70

5.5. Numerical results for the formation of 1D bright solitons as a conseqeunce of the phonon-instability in a homogeneous 1D dipolar BEC. The figure is obtained for $\tilde{\mu} = -0.9$, $\beta = 0.3$ and $g/2\pi l_\rho^2 = 20$. The figure is at a time $t = 3.5/\omega_\rho$. $n(z)$ is the density of the condensate . . . . . . . . . . 71

6.1. Resonant tongues and corresponding Faraday pattern for the parametric instability in short-range interacting condensates. The white domains indicate the instability regions where the homogeneous state is unstable as following from the Floquet analysis of Eq. (6.3). The plot is for $\omega = 0.2$, and $\zeta = \sqrt{\hbar^2/2m\mu}$ with $\mu$ is the chemical potential. . . . . . 77

6.2. Dispersion of a 2D homogeneous BEC of $^{52}$Cr with $a = -0.54$nm ($\beta = -0.375$), a 3D density $\bar{n}_{2d}/\sqrt{2\pi}l_z = 10^{14} cm^{-3}$, $\hbar\omega_z = \mu_{2d}/2$, and $\zeta = \hbar/\sqrt{2m\mu_{2d}} = 0.59\mu$m. . . . . . . . . . . . . . . . . . . . . . . . . 79

6.3. Stability diagram (dark regions are stable) for the parameters of Fig. (6.2) as a function of $\alpha$ and $k$. (6.3(a)) $\hbar\omega/\mu = 0.268$ (regime B). (6.3(b)) $\hbar\omega/\mu = 0.134$ (regime A). The most unstable modes are indicated by a solid line. . . . . . . . . . . . . . . . . . . . . . . . . . . . . . . . . . . . 80
6.4. 6.4(a): Ratio between the Floquet exponent $\sigma_1$ for $\epsilon = \hbar\omega$ and $\sigma_2$ for $\epsilon = 2\hbar\omega$. 6.4(b):Most unstable $k$ as a function of $\omega$ in the regime A. We use the same parameters as for Fig. 6.2. The dashed line indicates the roton frequency or momentum. . . . . . . . . . . . . . . . . . . . . . . . 81
6.5. Faraday patterns for $\hbar\omega/\mu = 0.268$ at $t = 40.6$ ms (Fig. (6.5(a))) and $\hbar\omega/\mu = 0.134$ at $t = 93.2$ ms (Fig. (6.5(b))), and the same parameters as in Fig. (6.2). Figs. (6.5(c)) and (6.5(d)) shows the corresponding Fourier spectrum of Faraday patterns Figs. (6.5(a)) and (6.5(a)) respectively. . 82
6.6. Most unstable $k$ as a function of $\omega$ for modulated $\beta(t)$, $\alpha = 0.12$, and the same parameters as for Fig. 1.6. We indicate the roton and maxon frequencies and momenta. . . . . . . . . . . . . . . . . . . . . . . . . . 83
6.7. Faraday patterns for $\hbar\omega/\mu = 0.32$ at $t = 116.7$ ms (left) and $\hbar\omega/\mu = 0.34$ at $t = 405.1$ ms (right), and the same parameters as in Fig. 5.5. . . . . . 84

# 1. Introduction

For more than a decade now, *ultracold atoms* have been a most active research area in the community of atomic physics. Both experimentally and theoretically, the progress in ultracold atoms is outstanding. New trapping and cooling techniques have been developed since 1970s, which resulted in the discovery of laser based techniques like laser cooling and magneto-optical trapping [2, 3]. These achievements led to several Nobel prizes in this field in the last few years [1].

The growing interest in ultracold atoms is mainly motivated by the existence of direct links to other physics domains like condensed matter, solid-state physics, non-linear physics, quantum optics and quantum information. A close link to condensed matter physics is provided by the physics of ultracold atoms in optical lattices or in low dimensional systems, which helps to experiment and study condensed matter theory in a more controlled way. On the other hand the non-linearity originating from atom-atom interaction in BECs provides an ideal platform to study non-linear physics. So far, the studies on BEC have witnessed several similar phenomena to those appearing in non-linear optics.

Cold atoms have also important applications. Atom interferometry [4] using ultracold atoms can be used, for the precision measurements of various physical constants such as the gravitational constant $G$, the acceleration due to gravity $g$, the Planck constant $h$, the fine structure constant $\alpha$ etc [5, 6, 7]. Atom gyroscopes using the Sagnac effect [8] are used to study the variations in earth's rotation rate, general relativity effects [9], and for navigation and oil exploration. Recently, a lot of interest has been aroused in new directions, as Rydberg atoms, Fermi gases, spinor condensates and ultracold polar-molecules. In this thesis, we study the novel non-linear phenomena induced by the long-range and anisotropic character of the dipole-dipole interaction in dipolar condensates.

## 1.1. Bose-Einstein Condensation

A new state of matter, termed Bose-Einstein condensation, was predicted for bosons in 1925, by Albert Einstein [10] using the photon-statistics developed by Satyendra Nath Bose [11]. BEC is a phenomenon in which, below a critical temperature $T_c$, a macroscopic number of bosons occupy the lowest single particle state with the rest distributed over the excited states [12]. BEC occurs at a very low temperature such that the dimensionless phase-space density, $\rho_{ps} \equiv n\lambda_{db}^3$ is larger than 2.612, where $n$ is the number density of atoms, and $\lambda_{db} = h/(2\pi m k_B T)^{1/2}$ is the thermal de-Broglie wavelength, with $m$ the mass of an atom, $k_B$ the Boltzmann's constant and $T$ the temperature. Nowadays, with novel experimental techniques like laser and evaporative cooling, temperatures of the order of nanokelvins are easily reachable, providing enough phase-space density to observe BEC in atomic systems. BEC was experimentally realized for the first time in 1995 on the atomic vapors of sodium [13] and rubidium [14]. The evidence of condensation is obtained by time-of-flight measurements. A sharp peak in the momentum distribution of condensate density, below the critical temperature, provides a clear evidence, and it becomes the standard way to identify BEC in any kind of system. BEC have been observed in variety of systems such as Chromium atoms [15, 16], excitons [2] [17], microcavity exciton polaritons [3] [18, 19], magnons [4] [20], spin-polarized hydrogen atoms [21] and other alkali atoms.

---

[1] Wolfgang Paul recieved the Nobel prize in 1989 for his studies on ion traps; Steven Chu, Clause Cohen-Tannoudji and William D. Phillips for their work on laser cooling in 1997; Eric A. Cornell, Wolfgang Ketterle and Carl E Wieman got the Nobel prize for the experiments on BEC in 2001.

The discovery of BEC as a realistic achievement of a macroscopic state in a quantum many body system opened many activities from fundamental physics to applied physics. BEC is known to be a fundamental phenomenon, connected to superfluidity in liquid Helium and superconductivity. The macroscopic wavefunction describing a BEC characterizes the off-diagonal long-range behavior of the one-particle density matrix $\rho_1(\vec{r}', \vec{r}, t) = \langle \hat{\Psi}^\dagger(\vec{r}', t)\hat{\Psi}(\vec{r}, t)\rangle$, (where $\hat{\Psi}(\vec{r})$ and $\hat{\Psi}^\dagger(\vec{r}, t)$ are the boson field operators that annihilate and create a particle at the position $\vec{r}$ respectively) and spontaneously broken gauge-symmetry [22], and itself plays the role of an order parameter. Strictly speaking, in a finite sized system neither the concept of broken gauge symmetry, nor the off-diagonal long-range order can be applied. However, in any case the condensate wavefunction can be determined by the diagonalization of the one-body density matrix, $\rho_1(\vec{r}, \vec{r}') = \sum_i N_i \Phi_i^*(\vec{r})\Phi_i(\vec{r}')$ and it corresponds to the eigenfunction $\Phi_i$ with the largest eigen value $N_i$.

Dimensionality plays a crucial role in the concept of BEC. An ideal Bose gas with no external trap exhibits BEC only in 3D, and not in 1D and 2D systems. It can be understood from the concept of the density of states, $\rho(E)$. For an ideal Bose gas with no trap, $\rho(E) \propto E^{(d-2)/2}$, where $d$ is the dimensionality in space. In 3D, the number of excited states close to the ground state ($E = 0$) is zero since $\lim_{E\to 0} \rho(E) = 0$, and as a consequence the thermal fluctuations do not destroy the BEC. On the contrary, in 2D and 1D, the thermal population

$$N_T = \int_0^\infty \frac{\rho(E)dE}{\exp(\beta E) - 1} \tag{1.1}$$

diverges in the thermodynamic limit resulting in the absence of BEC in the thermodynamic limit. However, with an additional harmonic trap the density of states is $\rho(E) \propto E^{d-1}$ and, consequently the integral (1.1) converges in 2D also. In 1D, BEC cannot occur even in the presence of harmonic confinement because of the logarithmic divergence in the integral (1.1) at finite temperature.

---

[2] Electron-hole pair in a semiconductor.

[3] Polaritons are quasiparticles resulting from the coupling of photons with an excitation in the material. Exciton polariton is due to the coupling of visible light with an exciton.

[4] A quantum of a spin wave.

The presence of interactions changes the picture even further. Inter-atomic interactions play a crucial role in the physics of atomic condensates. The physics of short-range interacting condensates are predominantly determined by a single parameter called the $s$-wave scattering length $a$ [23]. The parameter $a$ can be tuned experimentally via Feshbach resonances by sweeping a static magnetic field [24, 25]. The trap geometry, which is most often spherical, pancake or cigar shaped, also play a crucial role in determining the properties of trapped gases. If $a > 0$, the interatomic interaction is purely repulsive and the BEC is stable in all dimensions, for any trap configurations and for any number of atoms. If the interaction is attractive, i.e. $a < 0$, the homogeneous (no trap) BECs are unstable against local collapses in two (2D) and three-dimensions (3D). The presence of a trap guarantees stability below a critical number of atoms, above which the BEC undergoes a global collapse in 2D and 3D [26, 27, 28]. In 1D case with $a < 0$, the stability is confirmed by the formation of bright solitons [29, 30, 31]. If an additional dipole-dipole interaction is present, the stability conditions for a BEC are non-trivial due to its anisotropic nature. A main goal, we have achieved in this thesis, is to provide a clear picture about the stability of dipolar BECs under various circumstances. This has been done mainly using the concept of elementary excitations of the system, which will be one of the main subjects of the subsequent chapters.

### 1.1.1. The Gross-Pitaevskii equation

In the second quantization, the Hamiltonian decsribing $N$ interacting bosons confined by an external potential $V_{ext}$ is given by [23]

$$\begin{aligned}\hat{H} = & \int d\vec{r}\hat{\Psi}^\dagger(\vec{r})\left[-\frac{\hbar^2}{2m}\nabla^2 + V_{ext}(\vec{r})\right]\hat{\Psi}(\vec{r}) \\ & + \frac{1}{2}\int d\vec{r}d\vec{r}'\hat{\Psi}^\dagger(\vec{r})\hat{\Psi}^\dagger(\vec{r}')V(\vec{r}-\vec{r}')\hat{\Psi}(r')\hat{\Psi}(\vec{r}),\end{aligned} \tag{1.2}$$

where $\hat{\Psi}(\vec{r})$ and $\hat{\Psi}^\dagger(\vec{r})$ are the boson field operators that annihilate and create a particle at the position $\vec{r}$, respectively and $V(\vec{r}-\vec{r}')$ is the two-body interatomic potential, with $m$ the mass of an atom. The basic idea of mean-field approach is to separate the condensate contribution from the bosonic field operator. It was first formulated by Bogoliubov in 1947 [32], and is known as the Bogoliubov approximation:

$$\hat{\Psi}(\vec{r},t) = \Psi(\vec{r},t) + \hat{\Psi}'(\vec{r},t), \tag{1.3}$$

where $\Psi(\vec{r},t) \equiv \langle\hat{\Psi}(\vec{r},t)\rangle$, is known as the macroscopic wavefunction of the condensate, while $\Psi'(\vec{r},t)$ describes the non-condensate part. First we write down the time evolution of the field operator using the Heisenberg equation,

$$i\hbar\frac{\partial}{\partial t}\hat{\Psi}(\vec{r},t) = \left[-\frac{\hbar^2}{2m}\nabla^2 + V_{ext}(\vec{r})\hat{\Psi}(\vec{r}) \right.$$
$$\left. + \int d\vec{r}'\hat{\Psi}^\dagger(\vec{r}',t)V(\vec{r}'-\vec{r})\hat{\Psi}(r',t)\right]\hat{\Psi}(\vec{r},t). \tag{1.4}$$

Next, as we are considering the case of a dilute ultracold gas, only binary collisions at low energy are relevant and these collisions are characterized by the $s$-wave scattering length $a$, and hence the interatomic potential can be replaced by an effective delta-function potential [23, 33, 34, 35],

$$V(\vec{r}'-\vec{r}) = g\delta(\vec{r}'-\vec{r}), \tag{1.5}$$

with the coupling constant $g = 4\pi\hbar^2 a/m$. Finally, using the effective interaction potential in Eq. (1.4), and replacing the field operator $\hat{\Psi}$ with the classical field $\Psi$, we obtain,

$$i\hbar\frac{\partial}{\partial t}\Psi(\vec{r},t) = \left[-\frac{\hbar^2}{2m}\nabla^2 + V_{ext}(\vec{r}) + g|\Psi(\vec{r},t)|^2\right]\Psi(\vec{r},t). \tag{1.6}$$

This equation is known as the Gross-Pitaevskii (GP) equation [36, 37, 38]. The validity of the GP Eq. (1.6) is based on the condition that the $s$-wave scattering length $a$ be much smaller than the average distance between the atoms and that the number of atoms in the condensate $N_c$ is much larger than 1, such that the product $N_c a$ is fixed [39]. Using the GP equation to describe the static and the dynamic properties of BECs are well justified recently by the rigorous results obtained in [40]. The complex-valued wavefunction $\Psi$ can be expressed as, $\Psi(\vec{r},t) = \sqrt{n(\vec{r},t)}\exp[i\phi(\vec{r},t)]$, where $n(\vec{r},t)$ is the condensate density, and $\phi$ the phase of the condensate. The $\Psi(\vec{r},t)$ is subjected to the constraint,

$$\int |\Psi(\vec{r},t)|^2 d\vec{r} = N, \tag{1.7}$$

that defines the conservation of total number of particles. The current density, $\vec{j} = (-i\hbar/2m)[\Psi^*\nabla\Psi - \Psi\nabla\Psi^*]$ assumes a hydrodynamic form $\vec{j} = n\vec{v}$, with an atomic velocity $\vec{v}(\vec{r},t) = (\hbar/m)\nabla\phi(\vec{r},t)$. It is straight-forward to see that $\vec{v}$ is irrotational, a crucial point for superfluids. The time-independent GP equation is obtained by writing the wavefunction as $\Psi_0(\vec{r},t) = \Psi_0(\vec{r})\exp(-i\mu t/\hbar)$, then the GP Eq. (1.6),

$$\mu\Psi(\vec{r}) = \left[-\frac{\hbar^2}{2m}\nabla^2 + V_{ext}(\vec{r}) + g|\Psi(\vec{r})|^2\right]\Psi(\vec{r}), \tag{1.8}$$

where the chemical potential $\mu$ is just the Lagrange multiplier associated with the conservation of particle number, and is

$$\mu = \frac{\partial E(N)}{\partial N}, \tag{1.9}$$

when minimizing the energy functional,

$$E = \int d\vec{r} \left[ \frac{\hbar^2}{2m} |\nabla\Psi|^2 + V_{ext}(\vec{r})|\Psi|^2 + \frac{1}{2} g |\Psi(\vec{r})|^4 \right]. \tag{1.10}$$

The three terms in the right-hand side of Eq. (1.10) represents the kinetic energy, the potential energy and the interaction energy, respectively. The GP equation has the form of the famous non-linear Schrödinger (NLS) equation which describes the dynamics of complex fields in non-linear media [41]. NLS equation is a key model appearing in a variety of physical contexts, ranging from optics [42], to fluid dynamics and plasma physics. It is not only limited to the case of conservative systems and the theory of solitons, but also connected to the dissipative models, such as the complex Ginzburg-Landau equation [43], and exploited very much in the context of pattern formation [44]. The GP approach allows to study very important and experimentally relevant nonlinear effects such as the formation of solitons and vortices. In the absence of interaction ($g = 0$), Eq. (1.8) reduces to the usual Schrödinger equation representing single particle, and for harmonic confinement the ground state solution become a Gaussian function with the normalization condition (1.7).

### 1.1.2. The External Potential

The external potential $V_{ext}$ in the GP Eq.(1.6) represents the trap which confines the condensate in real experiments. For charged particles , the strong Coulomb interaction can be used for trapping in electric or electromagnetic fields. For neutral atoms, (as is the case for BEC) the traps are based on three different interactions (i) radiation-pressure traps operating with near resonant field, (ii) magnetic traps by means of magnetic fields [45, 46, 47, 48] and (iii) optical traps by means of laser fields, e.g. an optical dipole trap [49, 50, 51, 52] or optical lattices [53, 54, 55]. The last two kind of traps are conservative and employed at the final stages of typical experiments. At this point we comment just on these conservative traps.

Magnetic traps are based on the state-dependent force on the magnetic dipole moment in an inhomogeneous field, whereas optical traps rely on the electric dipole interaction with far-detuned light. Optical traps work on the principle of ac Stark shift. When an atom is placed in a light field, the electric field $\vec{E}$ induces an atomic dipole moment $\vec{p}$ that oscillates at the driving frequency $\omega$. The interaction between this induced dipole and the electric field leads to an energy shift (known as light shift or ac stark shift) of an atomic energy level, and hence the atom potential energy [49],

$$\Delta E = U_{dip}(\vec{r}) \propto \frac{I(\vec{r})}{\Delta} \tag{1.11}$$

where $I(\vec{r}) = |E(\vec{r})|^2$ is the intensity of the laser field, and $\Delta$ is the detuning of the light field from the atomic resonance $\omega_0$. Two points are clear from Eq. (1.11): (i) for red-detuned light, i.e. $\Delta < 0$, the dipole potential is negative and the interaction attracts atoms into the light field. Therefore the potential minima are found at the maximum of the intensity. For blue-detuned the dipole interaction repels atoms out of the field, and potential minima correspond to the minima of the intensity. Hence, the dipole traps can be classified into two types: red-detuned and blue-detuned traps. A stable optical trap can then realized by simply focusing a laser beam of suitable waist size. Compared to magnetic traps, optical traps may be advantageous since the trapping mechanism is independent of the particular sub-level of the electronic ground state, and in addition it is very flexible for realizing different trapping geometries, e.g. highly anisotropic or multi-well potentials.

A 1D optical lattice is generated by a laser standing wave of the form $E(z,t) = 2E_0 \cos(k_z z)\exp(-i\omega t)$ created by the superposition of the two counterpropagating beams, $E_{\pm}(z,t) = E_0 \exp[i(\pm kz - \omega t)]$, with the same polarization, amplitude $E_0$, wavelength $\lambda = 2\pi/k$, and frequency $\omega$. The dipole potential $V_{dip}$ is proportional to the intensity $I \sim |E(z,t)|^2$ of the light field, and hence

$$V_{dip} \equiv V_{OL}(z) = V_0 \cos^2(kz), \tag{1.12}$$

with a lattice periodicity of $d = \lambda/2$ and the lattice height $V_0 \sim I_0/\Delta$, where $I_0$ is the maximum intensity of the light field. Typically, the lattice depth is measured in units of the recoil energy

$$E_R = \frac{\hbar^2\pi^2}{2md^2} \tag{1.13}$$

and often the dimensionless parameter $s = V_0/E_R$ is used. For a general $3D$ case,

$$V_{OL}(\vec{r}) = V_0[\cos^2(k_x x + \phi_x) + \cos^2(k_y y + \phi_y) + \cos^2(k_z z + \phi_z)], \tag{1.14}$$

where $\phi_i$ are arbitrary phases. The atoms will be trapped in the nodes (anti-nodes) of the optical lattice for the blue- (red-) detuned laser beams. It is also possible to combine both the magnetic and the optical traps, e.g. a double well potential can be realized via combining a harmonic potential with a repulsive localized potential attained by a blue-tuned lasers [56]. An accessibility in achieving a wide variety of trapping potentials has inspired many applications and studies of BECs, which including the realization of strongly correlated systems and low-dimensional systems.

### 1.1.3. Ground State of the GP Equation

The ground state of the GP Eq. (1.6) can be obtained by rewritting the wavefunction as $\Psi(\vec{r},t) = \exp(-i\mu t/\hbar)\Psi_0(\vec{r})$. An important point to be noted is that the evolution of the ground state is not given by the energy but by the chemical potential $\mu$. For a non-interacting gas in a harmonic trap, the ground state of a system of bosons is the occupation of all particles in the lowest single particle state, which refers to a Gaussian wavefunction of the form:

$$\Psi_0(\vec{r}) = \sqrt{N}\left(\frac{m\omega_{ho}}{\pi\hbar}\right)^{3/4} \exp\left[-\frac{m}{2\hbar}(\omega_x x^2 + \omega_y y^2 + \omega_z z^2)\right], \tag{1.15}$$

where $\omega_{ho} = (\omega_x \omega_y \omega_z)^{1/3}$ is the geometric mean of the trapping frequencies. The density distribution then becomes $n(\vec{r}) = |\Psi_0(\vec{r})|^2$ and its value grows with $N$. Eventhough the density grows with $N$, the condensate size is fixed constant by the harmonic oscillator length:

$$a_{ho} = \sqrt{\frac{\hbar}{m\omega_{ho}}} \tag{1.16}$$

which corresponds to the average width of the Gaussian function (1.15). This is the first important length scale of the system and for a typical experiment it is of the order of $1\mu m$. The momentum distribution of the condensate density can be obtained from the Fourier transform of $n(\vec{r})$. It is noted that, a characteristic feature of a BEC in a harmonic trap is the appearance of a peak in both the spatial distribution and in the momentum distribution of the condensate density. On contrary, in a uniform gas, the BEC cant be revealed in coordinate space, since the particles condense into a state of zero momentum. The momentum distribution is measured experimentally via time of flight measurements where the condensate is let to expand freely by switching off the trap, and measures the density of the expanded cloud with light absorption [14]. If the expansion is ballistic, the imaged spatial distribution of the cloud can be directly related to the intial momentum distribution. One can also measure directly the density of atoms in the trap by means of dispersive light scattering [57].

*Thomas-Fermi* (TF) approximation: Atom-atom interactions change the size and shape of the condensates. If $a > 0$, i.e. the interaction is repulsive, and sufficiently large, then the kinetic energy term in Eq. (1.8) is negligible compared to the interaction term, and hence the density of the ground state of a spherically symmetric trap ($\omega_x = \omega_y = \omega_z$) read as

$$n(\vec{r}) = |\Psi_0(\vec{r})|^2 = \frac{\mu}{g}\left(1 - \frac{r^2}{R_{TF}^2}\right), \tag{1.17}$$

where $R_{TF} = (2\mu/m)^{1/2}/\omega_{ho}$ is called the TF radius of the condensate. The Eq. (1.17) is known as the TF approximation. The normalization condition of Eq. (1.17) gives the relation between the chemical potential $\mu$ and the number of particles $N$,

$$\mu = \frac{\hbar\omega_{ho}}{2}\left(\frac{15Na}{a_{ho}}\right)^{2/5}, \tag{1.18}$$

and, hence the TF radius becomes

$$R_{TF} = a_{ho}\left(\frac{15aN}{a_{ho}}\right)^{1/5}. \tag{1.19}$$

As one can see in the TF limit, the size of the condensate proportional to $N^{1/5}$, whereas in the non-interacting case it is fixed by $a_{ho}$. Hence for a repulsive condensates, the size increases with increasing $N$.

If the interaction is attractive, the density tries to peak at the centre of the trap, but the kinetic energy tries to balance this increase. However, if the number of atoms $N$ exceeds

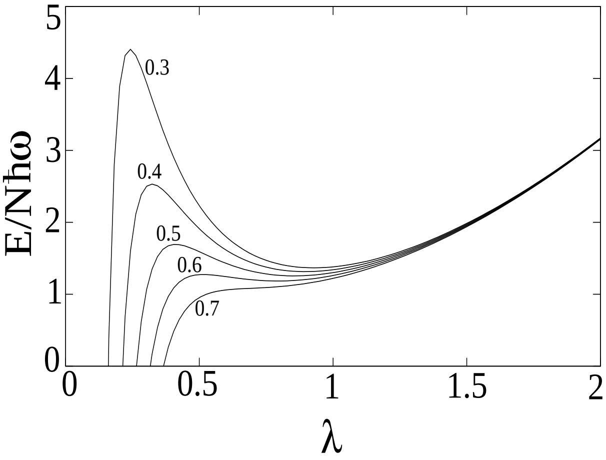

**Figure 1.1.:** Energy per particle, in units of $\hbar\omega$, as a function of the variational parameter $\lambda$ for an attractive BEC in a spherical trap. The curves are plotted for several values of $N|a|/a_{ho}$. The local minimum disappears at $N = N_{cr}$.

a critical value $N_{cr}$, the BEC undergoes a collapse in $2D$ and $3D$ geometries [27, 26]. In experiments, during the collapse, as the density grows and the rate of collisions increases, both the elastic and the inelastic, which results in an explosion which eject atoms from the condensate, and results in a smaller condensate. The two-body and three-body collisions are very important during the collapse of a condensate, and that should be included in the GP Eq. (1.6) to study its dynamics during the collapses. The numerically obtained critical number of atoms necessary for a spherically symmetric BEC to collapse is provided by the equation:

$$N_{cr}|a|/a_{ho} = 0.575, \tag{1.20}$$

where $|a|$ is the absolute value of the scattering length.

The collapse at a critical number of atoms for a spherically symmetric condensate can be understood from a simple variational ansatz. We consider the following Gaussian ansatz

$$\psi(\vec{r}) = \left(\frac{N}{\lambda^3 a_{ho}^3 \pi^{3/2}}\right) e^{-r^2/2\lambda^2 a_{ho}^2}, \tag{1.21}$$

where $\lambda$ fixes the width of the condensate and works as our variational parameter, and calculate the energy using the Eq. (1.10),

$$\frac{E(\lambda)}{N\hbar\omega} = \frac{3}{4}\left(\frac{1}{\lambda^2} + \lambda^2\right) - \frac{N|a|}{\sqrt{2\pi}a_{ho}}\lambda^{-3}, \tag{1.22}$$

where the first term, represents the sum of kinetic energy and the potential energy, is independent of $N$, and the second term represents the interaction energy, its magnitude increases with increase in N. The energy (1.22) as a function of $\lambda$ for different values of $N|a|/a_{ho}$ is shown in the Fig. (1.1). For small values of $N$, $E(\lambda)$ shows a potential barrier which prevents the system to collapse. As $N$ increases, the barrier reduces and disappears at $N = N_{cr}$.

### 1.1.4. Reduced-dimensional GP Equations

Low dimensional systems are an active research area in condensed matter physics and possesses rich physical phenomena. The properties of reduced dimensional BECs have been studied theoretically [58, 59, 60, 61, 62] and experimentally in extremely anisotropic optical and magnetic traps [63], in optical lattice potentials [64, 65, 66] and surface microtraps [67, 68]. For a trapped short-range interacting BECs, assuming cylindrically symmetric, the important length scales are the radii $R_\perp$, $R_z$ and the healing length [5] $\zeta = (4\pi na)^{-1/2}$. These parameters are crucially dependent on the interaction between the atoms. The external confining potential provides the characteristic length scales: $l_{\perp,z} = \sqrt{\hbar/m\omega_{\perp,z}}$. If $R_\perp,\ R_z \ >> \ \zeta >> \ a$, the BEC is said to be 3D in nature and is well described by the Thomas-Fermi approximation (see Eq. (1.17)).

*Quasi-2D GP equation*: If $l_z << \zeta << l_\perp$, the BEC is highly pancake-shaped, and its dynamics is considered to be effectively 2D. The dynamics along the $z$ direction is frozen by the tight harmonic trapping in that direction. Hence one can factorize the condensate wavefunction into: $\Psi(\vec{r},t) = \psi_\perp(x,y,t)\phi_0(z)$, where $\phi_0(z) = 1/(\pi^{1/4}l_z^{1/2})\exp(-z^2/2l_z^2)$ is the ground state of the harmonic trap along the $z$-direction. By employing the above factorization in Eq. (1.6), multiplying on either side by $\phi_0$ and integrating over d$z$, we get the effective 2D GP equation,

$$i\hbar\frac{\partial}{\partial t}\psi(x,y,t) = \left[-\frac{\hbar^2}{2m}\nabla^2_{x,y} + V_{ext}(\vec{\rho}) + g_{2D}|\psi(x,y,t)|^2\right]\psi(x,y,t), \tag{1.23}$$

where $g_{2D} = g/(\sqrt{2\pi}l_z)$ is the effective 2D coupling constant. The above Eq. (1.23) describes a quasi-2D BEC, and is valid only if,

$$g_{2D}|\psi(x,y,t)|^2 << \hbar\omega_z, \tag{1.24}$$

is fulfilled locally at any time $t$. Once the condition (1.24) is violated, the wavefunction along the $z$ axis is no longer the Gaussian ground state and one need to solve the full 3D GP Eq. (1.6) to obtain physically relevant results.

*Quasi-1D GP equation*: If $l_\perp << \zeta << l_z$, then the BEC is highly cigar-shaped and exhibits dynamics only along the $z$ direction. With the similar kind of arguments we made above, and with the following factorization: $\Psi(\vec{r},t) = \psi(z,t)\phi_0(x,y)$ where $\phi_0(x,y) = 1/(\pi^{1/2}l_\perp)\exp(-(x^2+y^2)/2l_\perp^2)$ we obtain the effective 1D GP equation,

$$i\hbar\frac{\partial}{\partial t}\psi(z,t) = \left[-\frac{\hbar^2}{2m}\frac{\partial^2}{\partial z^2} + V_{ext}(z) + g_{1D}|\psi(z,t)|^2\right]\psi(z,t), \tag{1.25}$$

where $g_{1D} = g/(2\pi l_\perp^2)$ is the effective 1D coupling constant. The above dimensionality reductions based on the averaging method are also used in other disciplines, e.g. in nonlinear fiber optics [42]. There are also other sophisticated techniques employed in the dimensionality reduction of the GP equation [69, 70].

---

[5] The name "healing length" came from the fact that it is the distance over which the condensate wavefunction heals over the defects and hence it defines the size of darksolitons or vortices in BEC.

### 1.1.5. Solitons in BEC

Soliton is a characteristic feature of non-linear theory. A soliton or a solitary wave is defined as a spatially confined, non-dispersive, integrable and a non-singular solution of the non-linear theory. The non-linearity can compensate the dispersion in the system, and hence leads to a stable propagating wave preserving its shape. Historically, solitary waves were first observed in a water channel, by John Scott Russel in 1845, and the first mathematical model for solitons was developed by Korteweg and de-Vries known as the KdV equation. Solitons are relevant in disparate field as meteorology, elementary particle physics, plasma theory, laser physics, fiber optics communications and more. Solitons have been also predicted, and observed, in matterwaves. In this section, we briefly introduce two particular types of solitons in BEC, *bright* and *dark* solitons.

*Bright soliton*: It is a self-bounded matter wave, characterized by a density peak with zero background density. The stability of a bright soliton in BEC can be understood from the Gaussian ansatz we introduced in the section (1.1.3). In the absence of a trap, the energy as a function of the variational parameter $\lambda$, in the natural units ($\hbar = 1$, $m = 1$) reads as (see Eq. (1.22)),

$$\tilde{E}(\lambda)^{(d)} = \frac{d}{4\lambda^2} - \frac{\tilde{g}^{(d)}}{\sqrt{2\pi}}\lambda^{-d}, \tag{1.26}$$

where $d$ is the dimensionality of the system and $\tilde{g}^{(d)}$ provides the interaction strength. For $d = 3$, the absence of local minimum (see Fig. (1.2(a))) in the energy $\tilde{E}$ indicates that the system either collapses or expands without limits, for any values of $\tilde{g}^{(3)} = |a|N$. As a consequence there cannot be a self-bound ("bubble-like") solution for the GP equation in a 3D environment. For $d = 2$, both the kinetic energy and the interaction energy scales as $\lambda^{-2}$, and hence depending on the value of $\tilde{g}^{(2)} = |a|N/l_z$ the Gaussian condensate either collapse or expands, where $l_z$ is the fixed width of the Gausian along the $z$ axis, provided by the strong confinement in the $z$ axis. For $N|a|/l_z > \sqrt{\pi/2}$ the interaction energy dominates the kinetic energy and the system minimizes the energy by shrinking and finally the BEC becomes unstable against collapse. If $N|a|/l_z > \sqrt{\pi/2}$ the kinetic energy dominates and the BEC simply expands without limits, see Fig. (1.2(b)). Therefore, similar to 3D, a stable bright soliton is not possible in 2D short-range interacting condensates.

The situation is radically different in a 1D system, where the dispersion balances the attractive inter-atomic interaction and leads to a stable solitonic solution. This is characterized by the appearence of a minimun in the energy (see Fig. (1.3)). These results are verified by the direct numerical simulation of reduced GP equations. When $V_{ext}(z) = 0$, Eq. (1.25) is completely integrable, and possesses an infinite number of integrals of motion [71], in which the lowest order ones are, the number of particles:

$$N = \int |\psi(z)|^2 dz,$$

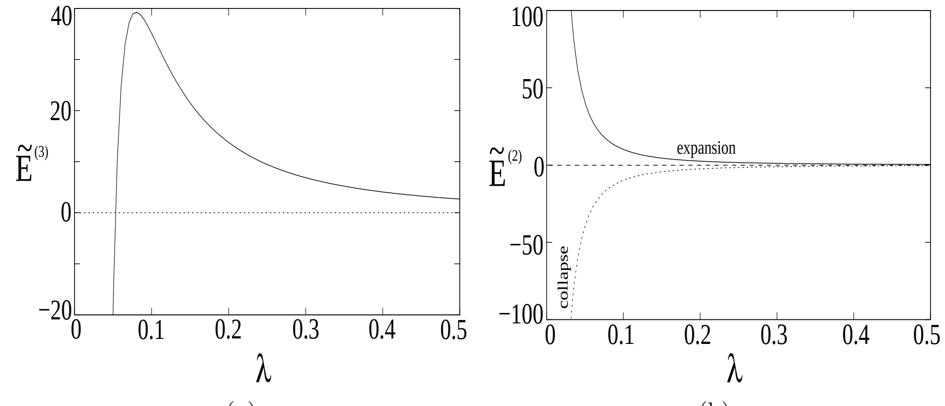

(a)

(b)

**Figure 1.2.:** Energy per particle as a function of the variational parameter $\lambda$ for an attractive Gaussian BEC in the absence of a trap. Fig. (1.2(a)) is for 3D case with $N|a| = 0.1$. Fig. (1.2(b)) is for 2D case with $N|a|/l_z = 1$ for upper curve and $N|a|/l_z = 2$ for lower curve.

the momentum:

$$P = (i/2)\int\left(\psi\frac{\partial\psi^*}{\partial z} - \psi^*\frac{\partial\psi}{\partial z}\right)dz,$$

and the energy:

$$E = (1/2)\int\left(|\partial\psi/\partial z|^2 + g|\psi|^4\right)dz.$$

For attractive BECs (g<0), the NLS Eq. (1.25) possesses a bright solitonic solution of the form [72]:

$$\psi(z,t) = \psi_0\,\mathrm{sech}[(z-vt)/\zeta]\exp[i(kz-\omega t)], \tag{1.27}$$

where $n_0 = |\psi_0|^2$ is the central density, $\zeta = \hbar/\sqrt{m|g|n_0}$ provides the spatial width of the soliton, $k$ is the soliton wavenumber, $\omega$ is the frequency and $v \equiv \partial\omega/\partial k = k$ is the velocity of the soliton. Using the above solitonic solution we obtain the integrals of motion as $N = 2\zeta|\psi_0|^2$, $P = 2|\psi_0|^2 k\eta$ and $E = |\psi_0|^2k^2\eta - |\psi_0|^4\eta/3$. This implies that a bright soliton behaves like a classical particle with an effective mass, $M_b = 2\zeta|\psi_0|^2$, momentum $P_b = M_b v$, and energy $E_b = \frac{1}{2}M_b v^2 - \frac{1}{24}M_b^3$, where $v = k$. In the energy term, the first term is the kinetic energy, whereas the second term describes the binding energy of the soliton [73].

*Dark solitons*: They are density notches (accompanied by phase slips) that propagate without distortion on top of an uniform background. For $g > 0$, the 1D NLS equation admits a dark soliton (DS) solution, and may be written as

$$\psi(z,t) = \psi_0\left(i\frac{v}{c} + \sqrt{1-\frac{v^2}{c^2}}\tanh\left[\frac{z-vt}{\zeta}\sqrt{1-\frac{v^2}{c^2}}\right]\right), \tag{1.28}$$

where in the case of DS $n_0 = |\psi_0|^2$ is the homogeneous background density. DSs are repressented by a suppresion of the density with respect to the bulk value. The density

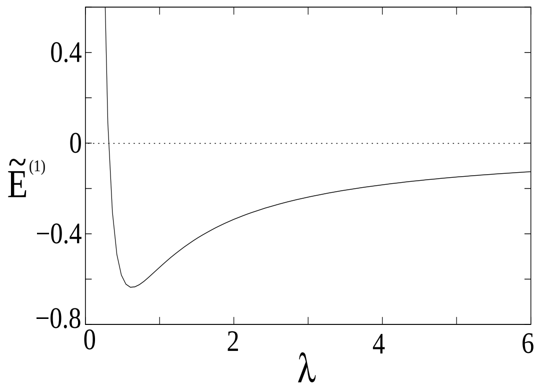

**Figure 1.3.:** Energy per particle as a function of the variational parameter $\lambda$ for an attractive 1D Gaussian BEC in the absence of a trap and $\tilde{g}^{(1)} = N|a|/l_\rho^2 = 2$. The stability of a bright soliton is characterized by the minimum in the energy.

profile $n(z,t) = |\psi(z,t)|^2$ has a minimum in the centre of the soliton corresponding to $n(0) = n_0 v^2/c^2$. This minimum is zero for a DS at rest, and is called a black soliton. Hence, the black soliton is a stationary DS. It is also noted that the width of the soliton is fixed by the healing length $\zeta$, but is amplified by a factor of $1/\sqrt{1 - v^2/c^2}$, which becomes increasingly large as $v \to c$. Another property of a DS is that the phase of the wave function undergoes a finite change

$$\Delta S = 2 \arccos\left(\frac{v}{c}\right) \tag{1.29}$$

when $z$ varies from $-\infty$ to $+\infty$. $\Delta S = \pi$ for a black soliton, with the wavefunction $\psi(z) = \psi_0 \tanh(z/\zeta)$.

As the integrals of motion of the NLS equation refer to both the background and the DS, the integrals of motion of the DS are renormalized so as to extract the contribution of the background [74, 75]. The renormalized energy and the momentum of a DS read respectively as,

$$E_d = \frac{4}{3}\hbar c n_0 \left(1 - \frac{v^2}{c^2}\right) \tag{1.30}$$

and

$$P_d = -2\hbar n_0 \left(\frac{v}{c}\sqrt{1 - \frac{v^2}{c^2}} + \arcsin\left(\frac{v}{c}\right)\right). \tag{1.31}$$

It can be found that $\partial E_d/\partial P_d = v$. It shows the particle nature of a DS. But unlike the bright solitons, the DSs are excited state of the GP Eq. (1.6).

Once the transverse size of the DS exceeds the healing length, then the problem is no longer 1D, and it can be shown that DS in 2D and 3D is dynamically unstable and is known as *snake instability*. A detailed discussion on the dynamics of snake instability is provided in the Chapter 4. As an important result, we show in the chapter 4 that the presence of long range dipole-dipole interaction may prevent the snake instability under proper conditions.

### 1.1.6. Elementary Excitations in BEC

The study of elementary excitations provides an insight into the macroscopic nature of the quantum fluids, as put forward by Lev Landau in the study of Fermi liquids [76]. In analogy, Bogoliubov calculated first the excitation spectrum of a weakly interacting Bose gas, and provide a theoretical description of superfluidity in Helium II [32]. The idea of elementary excitations is the following: any weakly excited state of a macroscopic system may be regarded in quantum mechanics as an assembly of separate elementary excitations. These behave like quasi-particles moving in the volume occupied by the system and possessing definite energies $\epsilon$ and momenta $\vec{p}$. The dispersion relation $\epsilon(\vec{p})$, is a characteristic feature of the macroscopic state and could provide vital information about the system, in particular the collective behavior of the atoms in the system. The dispersion relation of elementary excitations in the case of a BEC can be obtained by linearizing the time dependent GP equation around the ground state. We consider the following type of solutions for Eq. (1.6),

$$\Psi(\vec{r},t) = e^{-i\mu t/\hbar}\left[\Psi_0(\vec{r}) + \sum_j \left(u_j(\vec{r})e^{-i\omega_j t} + v_j^*(\vec{r})e^{i\omega_j t}\right)\right], \tag{1.32}$$

where $u_j$ and $v_j$ are the small complex amplitudes of perturbations and $\pm\omega_j$ are the Bogoliubov frequencies, which are in general complex valued. Using Eq. (1.32) in the GP Eq. (1.6), and up to first order in $u_j$ and $v_j$, we get the following Bogoliubov de-Gennes equations

$$\left[\hat{H}_0 - \mu + 2g|\Psi_0(\vec{r})|^2\right] u_j(\vec{r}) + g\Psi_0(\vec{r})^2 v_j(\vec{r}) = \hbar\omega_j u_j(\vec{r}) \tag{1.33}$$

$$\left[\hat{H}_0 - \mu + 2g|\Psi_0(\vec{r})|^2\right] v_j(\vec{r}) + g\Psi_0(\vec{r})^2 u_j(\vec{r}) = \hbar\omega_j v_j(\vec{r}) \tag{1.34}$$

where $\hat{H}_0 \equiv -(\hbar^2/2m)\nabla^2 + V_{ext}(\vec{r})$, is the single particle Hamiltonian operator. The same approach can be also used for states other than the ground state $\Psi_0$, e.g. in the case of solitons or vortices, which we will see in the subsequent chapters. The Bogoliubov de-Gennes equations can also be derived from a purely quantum mechanical approach [23, 34, 35, 33]. By suitable combinations of Eqs. (1.33) and (1.34), we obtain the condition

$$(\omega_i - \omega_i^*)\int d\vec{r}(|u_j|^2 - |v_j|^2) = 0, \tag{1.35}$$

which means that if $\omega_j - \omega_j^* = 0$, i.e. the eigen frequencies are real for all $j$, then the ground state $\Psi_0$ is stable. In this case, $u_j$ and $v_j$ satisfies the normalization condition:

$$\int d\vec{r}(|u_j|^2 - |v_j|^2) = 1. \tag{1.36}$$

On the other hand, $\mathrm{Im}(\omega_j) \neq 0$ implies the dynamical instability of the state $\Psi_0$, and it is possible only if the orthogonality condition: $\int d\vec{r}(|u_j|^2 - |v_j|^2) = 0$, is satisfied. Furthermore, for each $u_j$ and $v_j$ with frequency $\omega_j$, there exists another solution $u_j^*$ and

$v_j^*$ with frequency $-\omega_j$. From physical point of view, these two solutions with frequencies $\omega_j$ and $\omega_j^*$ represent the same oscillation, as one can see from Eq. (1.32). The $\omega_j = 0$ is always a solution of Eqs. (1.33) and (1.34), with eigenfunctions $u = \alpha\Psi_0$ and $v = \alpha\Psi_0^*$, and hence the order parameter reads $\Psi_0(\vec{r}, t) = \Psi_0(\vec{r})[1 + (\alpha - \alpha^*)] \exp(-i\mu t/\hbar)$. This corresponds to a gauge transformation in which the phase of the order parameter is modified by a quantity $(\alpha - \alpha^*)/i$, which does not result in any physical excitation in the system. In general the Bogoliubov de-Gennes equations are solved numerically, but for homogeneous systems one could obtain an analytic expression for the collective excitations.

*Uniform gas*: For a uniform gas, i.e. $V_{ext} = 0$ and $\Psi_0 = \sqrt{n_0}$ a constant, then the eigenfunctions $u_j$ and $v_j$ are plane waves of the form: $u(\vec{r}) = u_0 e^{i\vec{k}\cdot\vec{r}}$ and $v(\vec{r}) = v_0 e^{i\vec{k}\cdot\vec{r}}$, which leads to the Bogoliubov dispersion relation

$$(\hbar\omega)^2 = \left(\frac{\hbar^2 k^2}{2m}\right)\left(\frac{\hbar^2 k^2}{2m} + 2gn_0\right). \tag{1.37}$$

In the second bracket, first term represents the kinetic energy, whereas the second term is provided by the interaction energy. For sufficiently small $k$, the kinetic energy term can be neglected and Eq. (1.37) provides the phonon dispersion with $\omega = ck$, where $c = \sqrt{gn_0/m}$ is the speed of sound. For large $k$, the dispersion become a free particle spectrum, and the crossover between the two regimes occurs when the dispersion wavelength is of the order of healing length. For $g < 0$, the speed of sound becomes purely imaginary, this indicates an exponential growth in the long-wavelength modes, so called the modulational instability. Since in this case the $k \to 0$ modes become unstable, we term this phenomena as *phonon instability*. Such an instability leads to the collapse of BEC for 2D and 3D geometries, but stabilizes into bright solitons in 1D.

## 1.2. Dipolar Bose-Einstein Condensation

A novel path in cold gases has been opened recently by experiments in which (magnetic or electric) dipole-dipole interaction (DDI) plays a significant or even dominant role. On one side the recent creation of heteronuclear molecules in the lowest ro-vibrational level [77, 78] opens exciting perspectives for the achievement of a quantum degenerate gas of polar molecules, which may possesses large dipole moments (e.g. $\sim 0.5$ Debyes for KRb [77]). On the other side, the magnetic DDI has been shown to lead to exciting novel phenomena in recent experiments on BECs of Chromium, which has a magnetic moment $\mu = 6\mu_B$, with $\mu_B$ being the Bohr magneton [15, 16]. Particularly interesting is the fact that the short-range interactions maybe suppressed by means of Feshbach resonances, leading to a purely dipolar gas [79], and it may influence, or even completely change the properties of Bose gases [80, 81, 82, 83, 84, 85], or the phase diagram for quantum phase transitions in ultracold dipolar gases in optical lattices [86]. The interplay of short-range contact, and long-range dipolar interactions may give rise to phenomena like ferromagnetic order and spin waves [87, 88]. DDI may also lead to novel ground state configurations for dipolar vortex lines in an optical lattice e.g. helicoidal vortex lines [89]. Dipolar particles are also considered to be promising candidates for the implementation of fast and robust quantum-computing schemes [90]. Moreover, despite the small $\mu = 1\mu_B$, the DDI played also a significant role in very recent experiments on spinor Rubidium BECs, since the energy scale of the DDI becomes comparable with the energy scale of spin-changing collisions [91]. Very recent experiments have shown as well that the DDI leads to a observable damping of Bloch oscillations in Potassium BECs in tilted optical lattices [92]. In the following we briefly discuss the mean field theory for a BEC with dipole-dipole interactions.

### 1.2.1. Dipole-dipole Interaction

We consider electric/magnetic dipoles which are polarized along a fixed direction, say along the $z$ axis, by an external electric/magnetic field. The DDI potential between two polarized dipolar particles is given by,

$$V_d(\vec{r}) = \frac{d^2}{|\vec{r}|^3}(1 - 3\cos^2\theta), \tag{1.38}$$

where $d$ characterizes the dipole moment, $\vec{r}$ is the vector between the dipoles and $\theta$ the angle between $\vec{r}$ and the dipole orientation. The two important properties of DDI (1.38) are its anisotropic (partially repulsive and partially attractive) and long-range character. The anisotropic nature of the DDI is illustrated in Fig. (1.5). If the dipoles are alligned parallel to each other ($\theta = \pi/2$), the interaction is purely repulsive, and if the dipoles are on top of eachother, orienting in the same direction ($\theta = 0$), the interaction is purely attractive.

The long-range character of the DDI has important consequences on the scattering properties. Contrary to the short-range interaction, where at very low energies the scattering physics is predominantly determined only by $s$ wave, in the presence of DDI all partial waves contribute to the scattering. A general property of low-energy scattering is that if a potential approaches zero as $r^{-n}$ when $r$ goes to infinity, then in the limit of zero energy the phase shift $\delta_l$ in the scattering channel with an angular momentum $l$ behaves as $k^{2l-1}$ if $l < (n-3)/2$ and as $k^{n-2}$ otherwise. Hence in the case of DDI (n=3) $\delta_l \sim k$ for $l > 0$ and small $k$. On the other hand, due to the anisotropy of DDI the angular momentum is not conserved during the scattering, since the DDI mixes all even (for bosons) and odd (for fermions) angular momenta scattering channels. Hence, a thorough study of scattering with the potential (1.38) requires multichannel scattering theory [93, 94]. The results are summarized as follows: close to the shape resonances [93, 94, 95], due to the coupling between different scattering channels, the potential $V_d$ generates a short-range contribution to the total effective potential in the $s$ wave channel ($l = 0$) that adds to the short-range part of the interparticle interaction: $g\delta(\vec{r})$, and for all other partial waves $l > 0$, the generated contribution is of a long-range ($\sim r^{-3}$) and determines the scattering at low energies. Hence for two dipolar particles, the effective inter-atomic interaction can be replaced by a pseudo potential [80, 96, 97, 98, 99]

$$V(\vec{r}) = g(d)\delta(\vec{r}) + \frac{d^2}{r^3}(1 - 3\cos^2\theta), \tag{1.39}$$

where $g(d) = 4\pi\hbar^2 a(d)/m$ provides the strength of short-range interaction characterized by $a(d)$. The strength of the DDI can be characterized by the quantity $a_d = md^2/\hbar^2$, which has the dimension of length and can be considered as a characteristic radius of the DDI. It can be analogously called “the scattering length for the DDI”.

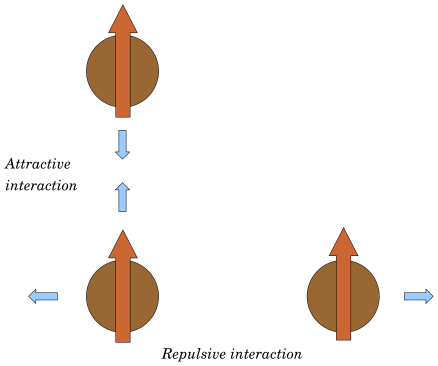

**Figure 1.4.:** Anisotropy of dipole-dipole interactions.

### 1.2.2. Tuning the Dipole-dipole Interaction

The magnitude and sign of the $s$-wave scattering length $a$ can be tuned using the external magnetic fields in the vicinity of Feshbach resonances. Similarly, one can tune also the DDI. For induced electric dipoles, the dipole moment can be tuned by changing the applied external DC electric field. In the case of polar molecules, a external electric field is necessary to create permanent dipole moment. The field induce a coupling between the spherically symmetric rotational ground state of the molecule to the excited rotational state with different parity, hence inducing a non-zero average dipole moment. Hence, the average dipole moment may be tuned by tuning the applied field until reaching the saturation limit where the molecules are completely polarized. Another method is by means of fast rotating magnetic fields [100]. Assume that, the magnetic dipoles are aligned along an external magnetic field (see Fig. (1.5))

$$\vec{B}(t) = B\cos\phi\hat{\mathbf{z}} + B\sin\phi[\cos(\Omega t)\hat{\mathbf{x}} + \sin(\Omega t)\hat{\mathbf{y}}], \tag{1.40}$$

which is a combination of a static magnetic field $B_z$ along the $z$ direction and a fast rotating field $B_\rho$ in the radial plane. $\phi$ is the angle between the dipole orientation and $z$ axis. The frequency $\Omega$ is chosen such that the atoms are not significantly moving during the time $\Omega^{-1}$, while the magnetic moments will follow adiabatically the external field $\vec{B}(t)$. This corrsponds to a situation of $\omega_{Larmor} >> \Omega >> \omega_r, \omega_z$. Hence one obtain a time-averaged effective DDI

$$\bar{V}_d(r,\theta,\phi) = V_d(\vec{r})\left(\frac{3\cos^2\phi - 1}{2}\right). \tag{1.41}$$

The additional multiplication factor $(3\cos^2\phi - 1)/2$ appeared in Eq. (1.41) can be changed continuously from -1/2 to 1, by varying the angle $\phi$. This allows us to change the character of DDI between two dipoles with respect to their allignment. That means, the DDI between two parallel dipoles can be made attractive from repulsive, by means of fast rotating magnetic fields. At a particular angle $\phi_M = 54.7°$ the dipolar interaction averages to zero. This angle, known as the magic angle, is well known in solid-state nuclear magnetic resonance technology. The tuning of DDI has important consequences in the physics of dipolar BEC. In particular, it may lead to the stabilization of multidimensional solitons in dipolar BEC as we discuss in Chapter 2.

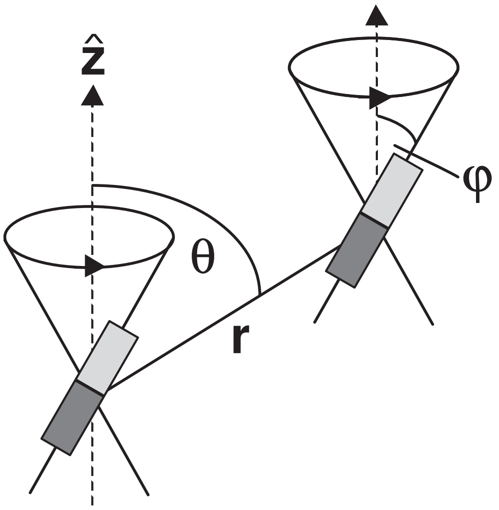

**Figure 1.5.:** Tunability of the magnetic dipole-dipole interaction.

### 1.2.3. Non-local Gross-Pitaevskii Equation

At very low temperatures, and away from the shape resonances, dipolar BECs are described by a non-local non-linear schrödinger equation:

$$i\hbar\frac{\partial}{\partial t}\Psi(\vec{r},t) = \left[-\frac{\hbar^2}{2m}\nabla^2 + V_{ext}(\vec{r}) + g|\Psi(\vec{r},t)|^2 \right.$$
$$\left. + \int d\vec{r}' V_d(\vec{r}-\vec{r}')|\Psi(\vec{r}',t)|^2\right]\Psi(\vec{r},t), \tag{1.42}$$

where the last term is the mean field of DDI and it introduces nonlocal nonlinearity in the system. Using Eq. (1.42) we study the static and dynamical properties of a dipolar BEC. Nonlocality leads to a wealth of novel and interesting phenomena in many areas of nonlinear physics. Nonlocality arises typically due to some sort of transport processes (such as heat conduction in media with thermal response [101, 102, 103], diffusion of charge carriers [104, 105, 106, 107], or atoms or molecules in atomic vapors [108, 109]) or from long-range interaction of molecules or particles such as in nematic liquid crystals [110, 111, 112, 113, 114, 115] or ionization in plasma [116, 117]. Nonlocality is thus a feature of a large number of nonlinear systems leading to novel phenomena of a generic nature. In particular, only in nonlinear optics the nonlocality is found in photrefractive materials [104, 118, 119, 120], in thermal nonlinear media [121, 122, 123, 124, 103], in atomic vapors [109] and in liquid crystals [114, 115]. Remarkably, it may lead to the modification of modulation instability [125, 126, 127, 128], supress collapse of multidimensional beams in self-focusing media [129, 130] and may even represent parametric wave mixing, in both the spatial [131] and spatiotemporal domains [132] where it describes the formation of the so-called $X$ waves. Furthermore, nonlocality significantly affects soliton interactions leading to the formation of bound states of otherwise repelling bright or dark solitons [133, 134, 135, 136], and may also support the formation of stable complex localized structures like multihump [137], azimuthons [138] and vortex ring solitons [139, 140, 103].

### 1.2.4. Properties of Dipolar BEC

A spatially homogeneous dipolar BEC with dominant DDI is unstable against local collapse, similar to the short-range attractively interacting homogeneous BECs. This is a direct consequence of the partially attractive nature of DDI. This instability can be seen directly from the Bogoliubov dispersion relation of a purely dipolar gas (assumed the DDI is completely dominated by the short-range interaction),

$$\epsilon(\vec{k}) = \left[\frac{\hbar^2\vec{k}^2}{2m}\left(\frac{\hbar^2\vec{k}^2}{2m} + 2\tilde{V}_d(\vec{k})n\right)\right]^{1/2}, \tag{1.43}$$

where $\tilde{V}_d(\vec{k}) = (4\pi/3)d^2[3\cos^2\theta_k - 1]$ is the Fourier transform of the DDI, and $n$ is the 3D homogeneous density of the dipolar BEC. Note that $\tilde{V}_d(\vec{k})$ is negative for $\theta_k$ close to $\pi/2$, and for small $\vec{k}$ the Bogoliubov modes become imaginary. These imaginary excitations lead to the collapse of homogeneous dipolar BEC with dominant DDI. Such a collapse could be prevented by a harmonic confinement if the number of particles is below a critical number $N_c$. It is similar to the case of attractive short-range interacting condensates, but in dipolar BEC the trap anisotropy play crucial role in the stability diagram due to the anisotropic nature of DDI [83].

We discuss briefly the properties of the ground state of a trapped dipolar condensate [83], in which the DDI completely dominates the contact interaction, so that we can neglect the term $g|\Psi(\vec{r})|^2$ from Eq. (2.1). We consider a cyllindrically symmetric trap of the form: $V_{ext} = m/2(\omega_\rho^2\rho^2 + \omega_z^2 z^2)$ with the trap aspect ratio $l = (\omega_\rho/\omega_z)^{1/2} = l_z/l_\rho$. The dipole is oriented along the $z$ axis. The ground state properties are governed by the stationary GP equation, in which the l.h.s of Eq. (2.1) is replaced by $\mu\Psi(\vec{r})$. A very relevant parameter is the mean dipole-dipole interaction energy per particle given by the expression $V = (1/N)\int V_d(\vec{r}-\vec{r}')|\Psi(\vec{r})|^2|\Psi(\vec{r}')|^2 d\vec{r}d\vec{r}'$. Note that due to anisotropy of DDI, the energy is minimized by squeezing the atomic cloud in the radial direction and stretching it along the dipolar axis.

For cigar shaped traps with $l \geq 1$ the mean-field DDI is always attractive, and the gas becomes always unstable if the number of particles $N$ exceeds a critical value $N_c$, which depends only on the trap aspect ratio $l$. The quantity $|V|$ increases with $N$ and the shape of the cloud changes. Near $N = N_c$ the shape of the cloud is close to Gaussian with the cloud aspect ratio $L \simeq 2.1$ for a spherical trap ($l = 1$), and $L = 3.0$ for an elongated trap with $l >> 1$. In cigar-shaped traps ($l \gg 1$) especially interesting is the regime where $\hbar\omega_z \ll |V| \ll \hbar\omega_\rho$. In this case the radial shape of the cloud remains the same Gaussian as in a non-interacting gas, but the axial behavior of the condensate will be governed by the DDI which acquires a quasi 1-dimensional (1D) character. Thus, one has a (quasi) 1D gas with attractive interparticle interactions, i.e. a stable (bright) soliton-like condensate, where attractive forces are compensated by the kinetic energy . With increasing $N$, $L_z$ decreases and near $N_c$, |V| is close to $\hbar\omega_\rho$.

The situation is quite different for pancake traps ($l \leq 1$); in particular there exists a critical aspect ratio $l_* \simeq 0.43$, which splits the pancake traps into two different categories: soft pancake traps ($l_* \leq \ < 1$) and hard pancake traps ($l < l_*$). For soft pancake traps the dipole-dipole interaction energy is positive for a small number of particles and increases with $N$. The quantity V reaches its maximum, and the further increase in $N$ reduces $V$ and makes the cloud less pancake. For a critical number of particles $N = N_c$ the BEC becomes unstable. It is found generally that the dipolar condensate is unstable and collapses when $N > N_c$ for $V < 0$ with $|V| > \hbar\omega_\rho$. A detailed study of the stability of dipolar BEC in terms of the excitation modes is contained in [141], and we follow the same approach in the subsequent chapters under various situations.

For hard pancake traps $V$ always remains positive. For small $N$ the shape of the cloud is Gaussian in all directions. With increasing $N$, the quantity $V$ increases and the cloud acquires the Thomas-Fermi profile first in the radial direction and then, for a larger value of $N$, also in the axial direction. Moreover, it is found that the dipolar condensate in a hard pancake trap is also unstable when the number of particles is sufficiently large [142, 143]. Remarkably, there appear regions in parameter space where the condensate obtains its maximum density away from the center of the trap, and it exhibits a biconcave shape. The existence of these regions become more robust by the addition of a small short-range interaction, and the position and size of the region is sensitive to the value of the $s$ wave scattering length $a$. The normal and the biconcave dipolar condensates become unstable in different ways once the instability region is reached. The instability of the condensate with a normal shape is due to the density modulation of condensate in the radial direction, so called the radial roton instability, similar to the case of infinite pancake BEC [144]. In contrast, the biconcave condensates collapse due to density modulations in angular coordinate, which spontaneously break cyllindrical symmetry (the angular roton instability [142]).

### 1.2.5. Roton-maxon Spectrum in Dipolar BEC

One of the most striking features of dipolar BEC is the existence of roton-maxon Bogoliubov spectrum. It resembles the physics of liquid helium, where a roton minimum was first sugested by Landau [145], and later Feynman related the excitation energy to the structure factor of the liquid [146]. We briefly discuss the roton-maxon spectrum obtained in the case of a pancake type BEC [144]. We consider a condensate of dipolar particles harmonically confined in the direction of the dipoles ($z$) and uniform in two other directions ($\vec{\rho} = \{x, y\}$). The dynamics of the condensate wave function $\psi(\vec{r}, t)$ in this infinite pancake trap is described by the time-dependent Gross-Pitaevskii (GP) equation:

$$i\hbar\frac{\partial}{\partial t}\psi(\vec{r},t) = \left\{-\frac{\hbar^2}{2m}\Delta + \frac{m}{2}\omega_z^2 z^2 + g|\psi(\vec{r},t)|^2 \right.$$
$$\left. +d^2\int d\vec{r}' V_d(\vec{r}-\vec{r}')|\psi(\vec{r}',t)|^2\right\}\psi(\vec{r},t), \tag{1.44}$$

where $\omega_z$ is the confinement frequency. The ground state wave function is independent of the in-plane coordinate $\vec{\rho}$ and can be written as $\psi_0(z)\exp(-i\mu t)$, where $\mu$ is the chemical potential. Then, integrating over $d\vec{\rho}'$ in the dipole-dipole term of Eq.(1.44), we obtain a one-dimensional equation similar to the GP equation for short-range interactions:

$$\left\{-\frac{\hbar^2}{2m}\Delta + \frac{m}{2}\omega^2 z^2 + (g+g_d)\psi_0^2(z) - \mu\right\}\psi_0(z) = 0, \tag{1.45}$$

where $g_d = 8\pi d^2/3$. We will discuss the case of $(g+g_d) > 0$, where the chemical potential $\mu$ is always positive. For $\mu \gg \hbar\omega$ the condensate presents a TF density profile in the confined direction: $\psi_0^2(z) = n_0(1 - z^2/L^2)$, with $n_0 = \mu/(g + g_d)$ being the maximum density, and $L = (2\mu/m\omega^2)^{1/2}$ the TF size.

Linearizing Eq.(4.5) around the ground state solution $\psi_0(z)$ we obtain the Bogoliubov-de Gennes (BdG) equations for the excitations. Those are characterized by the momentum $\vec{q}$ of the in-plane free motion and by an integer quantum number ($j \geq 0$) related to the motion in the $z$ direction. The excitation wave functions take the form $f_\pm(z)\exp(i\vec{q}\cdot\vec{\rho})$, where $f_\pm = u \pm v$, and $u, v$ are the Bogoliubov $\{u, v\}$ functions. Then the BdG equations read:

$$\epsilon f_- = \frac{\hbar^2}{2m}\left[-\frac{d^2}{dz^2} + q^2 + \frac{\Delta\psi_0}{\psi_0}\right] f_+ \equiv H_{kin} f_+, \tag{1.46}$$
$$\epsilon f_+ = H_{kin} f_- + H_{int}[f_-], \tag{1.47}$$

where $H_{kin}$ is the sum of kinetic energy operators, and

$$H_{int}[f_-] = 2(g_d+g)f_-(z)\psi_0^2(z) - (3/2)g_d\, q\, \psi_0(z) \times$$
$$\times \int_{-\infty}^{\infty} dz'\, f_-(z')\psi_0(z')\exp(-q|z-z'|). \tag{1.48}$$

For each $j$ we get the excitation energy $\epsilon_j$ as a function of $q$. We will be mostly interested in the lowest excitation branch $\epsilon_0(q)$ for which the confined motion is not excited in the limit $q \to 0$.

The second term in the rhs of Eq.(1.48) originates from the non-local character of the DDI and gives rise to the momentum dependence of an effective coupling strength. In the limit of low in-plane momenta $qL \ll 1$, this term can be omitted. In this case, excitations of the lowest branch are essentially 2D and the effective coupling strength corresponds to repulsion. Equations (1.46) and (1.47) become identical to the BdG equations for the excitations of a trapped condensate with a short-range interaction characterized by a coupling constant $(g + g_d) > 0$. In the TF regime for the confined motion, the spectrum of low-energy excitations for this case has been found by Stringari [147]. The lowest branch represents phonons propagating in the $x, y$-plane. The dispersion law and the sound velocity $c_s$ are given by

$$\epsilon_0(q) = \hbar c_s q; \quad c_s = (2\mu/3m)^{1/2}. \tag{1.49}$$

For $qL \gg 1$, the excitations become 3D and the effective coupling strength decreases. The interaction term is then reduced to $H_{int}[f_-] = (2g - g_d)\psi_0^2(z) f_-(z)$ as in the integrand of Eq. (1.48) one can put $z' = z$ in the arguments of $f_-$ and $\psi_0$. In this case, Eqs. (1.46) and (1.47) are similar to the BdG equations for the excitations of a condensate with short-range interactions characterized by a coupling constant $(2g - g_d)$. If the parameter $\gamma = g/g_d > 1/2$, this coupling constant is positive and one has excitation energies which are real and positive for any momentum $q$ and condensate density $n_0$. For $\gamma < 1/2$, the coupling constant is negative and one easily shows that at sufficiently large density the condensate becomes dynamically unstable with respect to the creation of high momentum excitations.

We thus see that the most interesting behavior of the excitation spectrum in the TF regime is expected for $qL \gg 1$ and $\gamma$ close to the critical value 1/2. The analytical results of Eqs. (1.46) and (1.47) are summarized as follows [144]. For the critical value $\gamma = 1/2$ the dispersion law is characterized by a plateau and for the $j$-th branch of the spectrum it is given by

$$\epsilon_j^2(q) = E_q^2 + \hbar^2\omega^2(1 + j(j+3)/2); \; qL \gg 1, \tag{1.50}$$

where $E_q = \hbar^2 q^2/2m$. For $\beta \neq 1/2$, assuming that the coupling term $\mu E_q |2\beta - 1|/(1 + \beta) << \hbar^2\omega_z^2$, the lowest branch of the spectrum is found as

$$\epsilon^2(q) = E_q^2 + \frac{(2\gamma - 1)(5 + 2\gamma)}{3(1+\gamma)(2+\gamma)} E_q \mu + \hbar^2\omega_z^2; \quad qL \gg 1. \tag{1.51}$$

From Eq.(1.51) one sees two types of behavior of the spectrum. For $\gamma > 1/2$ the excitation energy monotonously increases with $q$ (see Fig.1b). If $\gamma < 1/2$, then the dispersion law (1.51) is characterized by the presence of a minimum. Since in the limit of $qL \ll 1$ the energy $\epsilon_0$ grows with $q$, the existence of this minimum indicates that the spectrum as a whole should have a roton-maxon character. As discussed above, the appearance of roton-maxon spectrum is related to the reduction in the coupling strength with an increase of momentum, resulting from the transformation of the character of excitations from 2D to 3D.

The dipolar condensate is the first example of a weakly interacting gas offering a possibility of obtaining a roton-maxon dispersion, up to now only observed in the relatively

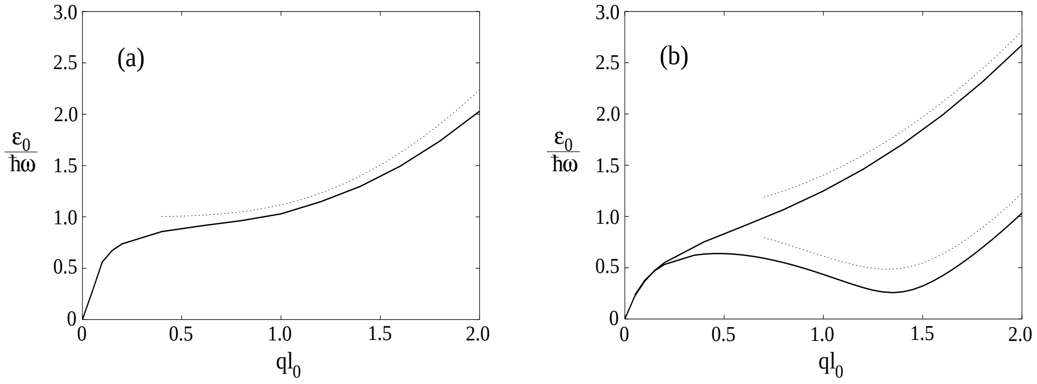

**Figure 1.6.:** Dispersion law $\epsilon_0(q)$ for various values of $\gamma$ and $\mu/\hbar\omega$: (a) $\gamma = 1/2$, $\mu/\hbar\omega = 343$; (b) $\beta = 0.53$, $\mu/\hbar\omega = 46$ (upper curve) and $\beta = 0.47$, $\mu/\hbar\omega = 54$ (lower curve). The solid curves show the numerical results, and the dotted curves the result of Eq. (1.51).

more complicated physics of liquid He. In contrast to the helium case, the rotonization in dipolar condensates is easily *tunable*. By varying the density, the frequency of the tight confinement, and the short-range coupling one can manipulate and control the spectrum, making the roton minimum deeper or shallower. One can also eliminate it completely and get the Bogoliubov-type spectrum or, on the opposite, reach the point of instability.

The instability of dipolar condensates with regard to short-wave excitations is fundamentally different from the well-known instability of condensates with attractive short-range interaction (negative scattering length). In the latter case the chemical potential is negative and the ground state does not exist. The unstable excitations are long-wave and an infinitely large cloud undergoes local collapses. For the dipolar BEC the chemical potential is positive and the instability is related to the momentum dependence of the DDI. The unstable excitations become the ones with high momenta at which the coupling is attractive. The existence of the roton minimum at a given $\gamma < 1/2$ for $\mu/\hbar\omega$ just below the point of instability, is likely to indicate that there is a new ground state in the region of the condensate instability, probably with a periodic density modulation. In the strongly correlated regime, in the rotonic regime there may be a liquid to solid quantum phase transition is possible [86]. Hence, to study roton excitations is fundamentally important. The roton excitations is also predicted for dipolar BECs in 2D geometries [148] and 1D geometries [149, 150]. Although the roton instability could suggest supersolid, supersolid in bulk dipolar BEC (quasi-2D) has been shown as unstable [151]. In Chapter 6, we will discuss how to probe rotonic excitations by means of Faraday patterns.

## 1.3. Overview

This thesis is organized as follows:

In chapter 2, we discuss the stability of 2D dipolar bright solitons in dipolar BECs as shown in Refs. [152, 153]. We introduce a variational Gaussian ansatz in the energy functional, and obtain the stability domain for the interaction parameters. We also calculate the low-lying excitations in 2D isotropic solitons by means of variational calculations, which provide a better understanding on the behavior of solitons. At the end of the chapter, we discuss a crucial point concerning the stability of anisotropic 2D solitons, that they exhibit a 2D collapse if the number of particles in the soliton exceeds a critical number.

In Chapter 3, we discuss the scattering dynamics of 2D bright solitons in dipolar BECs placed at unconnected layers of a 1D optical lattice. We study the scattering of 2D solitons by means of direct numerical simulations of dimensionally reduced GP equations, and also using a variational formalism. Both the approaches show an excellent agreement with each other. We show that the dipolar solitons scatter inelastically, and show different scattering scenarios includes resonant scattering, formation of soltion molecule, and spiraling motion with a non-zero relative angular momentum which provides a fascinating link to the physics of photorrefractive materials. In the final session of the chapter, we show that similar effects should be observable in 1D geometries, where the experimental requirements may be easily fulfilled in on-going Chromium experiments.

In Chapter 4, we analyze the stability of a stationary dark soliton in a 3D dipolar BEC by means of Bogoliubov theory and variational calculations. Both the approaches show an excellent agreement with each other. We show that on contrary to short-range interacting BECs, where snake instability is just prevented by a sufficiently strong transverse confinement, dipolar BECs allow for stable dark solitons of arbitrarily large transversal sizes, opening a qualitatively novel scenario in nonlinear atom optics. We obtain the stability conditions, which requires a sufficiently large DDI and a sufficiently deep optical lattice in the nodal plane.

In Chapter 5, we study the post-phonon-instability (post-PI) dynamics of 2D dipolar BECs with and without an external confinement by direct numerical simulations of 2D GP equations with DDI. We show that the post-PI dynamics of a 2D dipolar BEC differs qualitatively from 2D and 3D short-range interacting gases, and 3D dipolar BECs. Contrary to these cases, the PI is not necessarily followed by the collapse of the gas, but on the contrary leads to a transient regime characterized by the formation of a gas of attractive inelastic 2D bright solitons, which eventually undergo fusion, leading to the creation of a single excited stable bright soliton. If the dipoles are normal to the trap plane these solitons are stable as long as the gas remains 2D, whereas if the dipoles are parallel to the trap plane the (anisotropic) solitons may become unstable even in 2D for a critical number of particles per soliton. We study also the phonon-like instability in the presence of an harmonic confinement, and we show that it is followed by the creation of transient ring-like and anisotropic patterns, which eventually lead to the creation of a single excited 2D soliton. In the final part of the chapter, we analyze the post-PI dynamics in 1D dipolar BECs. On contrary to the repulsive soliton train in non-dipolar BECs, the formed 1D dipolar solitons attract each other and finally merge into a single one.

In Chapter 6, we study the formation of Faraday patterns in 2D dipolar BECs exhibiting a roton-maxon Bogoliubov spectrum. The linear stability analysis of GP equation gives a Mathieu equation. We analyze the solutions of Mathieu equation by a method so-called Floquet analysis, and the nature of Floquet exponent determines the characteristic behavior of Faraday patterns. We show that even a shallow roton largely modifies the physics of Faraday patterns in dipolar BECs. Whereas in non-dipolar BECs the Faraday pattern size decreases monotonously with the driving frequency $2\omega$, in dipolar BECs the patterns show a $\omega$-dependence characterized by abrupt changes in the pattern size, which are especially remarkable when the dipole itself is modulated. Faraday patterns constitute hence an excellent tool to probe the onset of rotonization in ongoing experiments with dipolar condensates.

# Part I.

# Solitons in Dipolar BEC

# 2. Two-dimensional Bright Solitons in Dipolar BEC

Multidimensional solitons have profound interest in nonlinear optics and matter waves. Multidimensional solitons have been experimentally observed in nematic liquid crystals [154] and in photorrefractive screening solitons [155]. In optics, quasi-2D spatiotemporal solitons in crystals is realized with quadratic nonlinearity [156, 157]. So far in matter waves, only quasi-1D bright solitons were experimentally observed in self-attracting BECs of $^7$Li [29, 30] and $^{85}$Rb atoms [31], and gap bright solitons were created in a repulsive $^{87}$Rb condensate confined in an optical lattice [158]. 2D/3D bright solitons are unstable against collapse in BECs with attractive cubic nonlinearity. Theoretically proposed stabilization techniques for 2D bright solitons involve the use of optical lattices [159], but with limited mobility, or the periodic time modulation of the nonlinearity by means of a Feshbach resonance [160]. Another idea is to create gap bright solitons in 2D or 3D optical lattices with repulsive nonlinearity. But so far no experimental realization of 2D or 3D matter wave soliton has been reported. A promising possibility is provided by the nonlocal nonlinearity of dipolar BECs, as we have discussed in the introduction of this thesis. We show that indeed the nonlocality induced by the DDI may stabilize 2D bright solitons in matter waves. In this chapter we show in detail the requirements, and the stability conditions of a 2D bright solitons in dipolar BEC, by means of numerical and variational calculations [152].

## 2.1. Two-dimensional Nonlocal GP Equation

In the following, we consider a BEC of $N$ particles with electric dipole moment $d$ (the results are equivalently valid for magnetic dipoles) oriented in the $z$ direction by a sufficiently large external field and that, hence, interact via a dipole-dipole potential: $V_d(\vec{r}) = g_d(1-3\cos^2\theta)/r^3$, where $g_d = \alpha d^2$, $\theta$ the angle formed by the vector joining the interacting particles and the dipole direction, and $-1/2 \leq \alpha \leq 1$ a tunable parameter by means of rotating orienting fields [100]. The tunability of DDI by means of fast rotating fields is discussed in the section (1.2.2). As we will see later in this chapter that dipolar tuning is necessary for the stabilization of 2D bright solitons in dipolar BEC with dipoles oriented perpendicular to the plane. In the discussion of this case we follow closely [152]. At very low temperatures, a dipolar BEC is described by a non-local non-linear schrödinger equation:

$$i\hbar\frac{\partial}{\partial t}\Psi(\vec{r},t) = \left[-\frac{\hbar^2}{2m}\nabla^2 + V_{ext}(\vec{r}) + g|\Psi(\vec{r},t)|^2 \right.$$
$$\left. + \int d\vec{r}' V_d(\vec{r}-\vec{r}')|\Psi(\vec{r}',t)|^2\right]\Psi(\vec{r},t), \tag{2.1}$$

where $\int|\Psi(\vec{r},t)|^2 d\vec{r} = N$, and $g = 4\pi\hbar^2 a/m$ is the coupling constant characterizes the contact interaction, with $a$ the $s$-wave scattering length. In the following we consider $a > 0$, i.e., repulsive short-range interactions. We assume an external trapping potential $V_{ext}(\vec{r}) = m\omega_z^2 z^2/2$, with no trapping in the $xy$ plane. Since we are interested in 2D bright solitons, we assume a sufficiently tight trap along the $z$ direction, so that we can consider the system as a quasi-2D BEC extended in the $xy$ plane. The quasi-2D GP equation from 3D GP Eq. (2.1) can be obtained via averaging method introduced in the section (1.1.4). Hence, we assume that the condensate is frozen in the ground state $\phi_0(z) = (1/\sqrt{\pi^{1/2}l_z})\exp(-z^2/2l_z^2)$, of the harmonic oscillator in the $z$ direction. Thus, the BEC wave function factorizes as $\Psi(\vec{r},t) = \psi(\rho,t)\phi_0(z)$. Employing this factorization, the convolution theorem [161], the Fourier transform of the dipolar potential, $\tilde{V}_d(\vec{k}) = (4\pi/3)g_d(3k_z^2/k^2 - 1)$, multiplying on either side by $\phi_0(z)$, and integrating over the $z$ direction in Eq. (2.1), we arrive at the 2D nonlocal nonlinear Schrödinger equation: [1]

$$i\hbar\frac{\partial}{\partial t}\psi(\vec{\rho},t) = \left[-\frac{\hbar^2}{2m}\nabla_\rho^2 + \frac{g}{\sqrt{2\pi}l_z}|\psi(\vec{\rho},t)|^2 + \frac{4\sqrt{\pi}g_d}{3\sqrt{2}l_z}\right.$$
$$\left. + \int\frac{d\vec{k}_\rho}{(2\pi)^2}e^{i\vec{k}_\rho\cdot\vec{\rho}}\tilde{n}(\vec{k}_\rho)h_{2D}\left(\frac{k_\rho l_z}{\sqrt{2}}\right)\right]\psi(\vec{\rho},t), \tag{2.2}$$

where $\tilde{n}$ is the Fourier transform of $n(\rho) = |\psi(\vec{\rho})|^2$, and $h_{2D}(k) = 2 - 3\sqrt{\pi}ke^{k^2}\mathrm{erfc}(k)$, with $\mathrm{erfc}(k)$ is the complementary error function. Using Eq. (2.2), we numerically study the formation and the dynamics of 2D bright solitons in dipolar BEC. Unlike dark solitons, bright solitons are ground states of the GP equations. Hence, we can write the solitonic ground state solution as $\psi(\vec{\rho},t) = \exp(-i\mu_{2d}t)\psi(\vec{\rho})$, where $\mu_{2d}$ is the 2D-chemical potential. To ensure the 2D character of the problem, and hence the validity of Eq. (2.2), the condition $\mu_{2d} << \hbar\omega_z$ should be satisfied locally at any time $t$.

## 2.2. Gaussian Ansatz

As we discussed in Chapter 1, a suitable Gaussian ansatz provide a good insight into the physics of bright solitons, especially, it could provide good estimation of stability domain for relevant parametric in the system. We consider the following Gaussian solution:

$$\Psi_0(\vec{r}) = \frac{N}{\pi^{3/4}l_z^{3/2}L_\rho L_z^{1/2}}\exp\left(-\frac{x^2+y^2}{2l_z^2L_\rho^2} - \frac{z^2}{2l_z^2L_z^2}\right), \tag{2.3}$$

---

[1] To derive Eq.(2.2) from Eq.(2.1), one may need the following integral: $\int dx\left(\frac{3x^2}{a^2+x^2} - 1\right)\exp(-x^2b^2/2) = \frac{2\sqrt{2\pi}}{b} - 3\pi a\exp(a^2b^2/2)\mathrm{erfc}(ab/\sqrt{2})$ [162]

where $l_z = \sqrt{\hbar/m\omega_z}$ is the width of the ground state of the strong harmonic trap along the $z$ axis, and $L_\rho$ and $L_z$ are dimensionless variational parameters related with the widths of the the condensate in the $xy$ plane and the $z$ direction respectively. We have numerically checked that this ansatz is indeed a very good approximation of the exact solutions of Eq. (2.1) for the situations under considerations.

### 2.2.1. Energy of the System

We calculate the energy of the system by inserting the Gaussian ansatz (2.3) in the following energy functional:

$$\begin{aligned} E = \int d\vec{r} \Bigg[ &\frac{\hbar^2}{2m}|\nabla\Psi_0|^2 + V_{ext}(z)|\Psi_0|^2 + \frac{1}{2}g|\Psi_0(\vec{r})|^4 \\ &+ \int d\vec{r}' V_d(\vec{r}-\vec{r}')|\Psi_0(\vec{r}',t)|^2|\Psi_0(\vec{r},t)|^2 \Bigg], \end{aligned} \tag{2.4}$$

where the last term provides the dipolar contribution to the energy, and it can be trivially calculated by using the convolution theorem, and is simplified to

$$\int d\vec{r} \int d\vec{r}' V_d(\vec{r}-\vec{r}')|\Psi_0(\vec{r}',t)|^2|\Psi_0(\vec{r},t)|^2 = \int \frac{d\vec{k}}{(2\pi)^3}\tilde{V}_d(\vec{k})\tilde{n}_0(\vec{k})^2, \tag{2.5}$$

where $\tilde{V}_d(\vec{k})$ and $\tilde{n}_0(\vec{k}) = \exp(-k_\rho^2 l_z^2 L_\rho^2/4 - k_z^2 l_z^2 L_z^2/4)$ are the Fourier transforms of the DDI and the density $n_0(\vec{r}) = |\Psi_0|^2$ respectively. Finally, one obtains the energy of a dipolar Gaussian BEC as a function of its widths $L_\rho$ and $L_z$ as

$$\frac{E}{N\hbar\omega_z} = \frac{1}{2L_\rho^2} + \frac{1}{4L_z^2} + \frac{L_z^2}{4} + \frac{1}{L_\rho^2 L_z}\left[\frac{\tilde{g}}{4\pi} + \frac{\tilde{g}_d}{3}f\left(\frac{L_\rho}{L_z}\right)\right] \tag{2.6}$$

where $\tilde{g} = Ng/(\sqrt{2\pi}\hbar\omega_z l_z^3) = 2\sqrt{2\pi}Na/l_z$ and $\tilde{g}_d = Ng_d/(\sqrt{2\pi}\hbar\omega_z l_z^3)$, and $f(\kappa) = (\kappa^2 - 1)^{-1}\left[2\kappa^2 + 1 - 3\kappa^2 H(\kappa)\right]$, with $H(\kappa) = \arctan(\sqrt{\kappa^2-1})/\sqrt{\kappa^2-1})$, and $\kappa = L_\rho/L_z$. In order to see whether a 2D solitonic solution exists or not, one has to look for the minimum of the energy as a function of the radial width $L_\rho$ for a fixed $L_z$. The appearance of a local minimum indicates soliton stability and then it can be identified as its equilibrium widths.

### 2.2.2. Stability Conditions for a 2D Soliton

The minimization of $E$ with respect to $L_\rho$ and $L_z$ leads to the equations:

$$1 + \frac{\tilde{g}}{4\pi L_z}\left[1 - \frac{2\pi}{3}\beta F\left(\frac{L_\rho}{L_z}\right)\right] = 0, \tag{2.7}$$

$$L_z = \frac{1}{L_z^3} + \frac{\tilde{g}}{4\pi L_\rho^2 L_z^2}\left[1 - \frac{4\pi}{3}\beta G\left(\frac{L_\rho}{L_z}\right)\right] \tag{2.8}$$

where

$$F(\kappa) = (1-\kappa^2)^{-2}\left[-4\kappa^4 - 7\kappa^2 + 2 + 9\kappa^4 H(\kappa)\right] \tag{2.9}$$

and

$$G(\kappa) = (1-\kappa^2)^{-2}\left[-2\kappa^4 + 10\kappa^2 + 1 - 9\kappa^2 H(\kappa)\right], \tag{2.10}$$

with $\beta = \tilde{g}_d/\tilde{g}$. Eqs. (2.7) and (2.8) admit a solution, and hence a localized wave, only under certain conditions. A simplified picture may be achieved by considering the fully 2D situation in which the confinement along the $z$ axis is strong enough to guarantee $L_z = 1$. In that case, both the kinetic and the short-range part in the energy scale as $1/L_\rho^2$. In the absence of DDI ($\tilde{g}_d = 0$), and irrespective of the value of $L_\rho$, $E(L_\rho)$ is always either growing with $L_\rho$ (collapse instability) or decreasing with $L_\rho$ (expansion instability) [see Fig.(1.2(b))]. This reflects the well-known fact that 2D solitons are not stable in NLSE with contact interactions. In the case of a dipolar BEC, the situation is remarkably different, since the function $f$ depends explicitly on $L_\rho$. This allows for the appearance of a minimum in $E(L_\rho)$, which from the asymptotic values of $f$ ($f(0) = -1$ and $f(\kappa \to \infty) = 2$) should occur if:

$$\frac{\tilde{g}_d}{3} < 1 + \frac{\tilde{g}}{4\pi} < \frac{-2\tilde{g}_d}{3}. \tag{2.11}$$

A simple inspection shows that this condition can be fulfilled only if $\tilde{g}_d < 0$, i.e. only if the dipole is tuned, as discussed in the section (1.2.2) of Chapter 1, with $\phi > 54.7^\circ$ (this is true also for $L_z \neq 1$). In that case, the tuning of the DDI may allow for the observation of a stable 2D solitary wave, characterized by an internal energy $E_S < 0$, [see Fig. (2.1(a))]. Note that if $Na/l_z \gg 1$, i.e. for large short-range repulsive interactions, from Eq.(2.11) we arrive at the stability condition for the 2D dipolar bright solitons

$$|\beta| > 3/8\pi \simeq 0.12. \tag{2.12}$$

If $|\beta| < 0.12$, the repulsive short-range interaction dominates the attractive DDI in the $xy$ plane, and hence the soliton is unstable against expansion, [see Fig. (2.1(a))]. We have compared this value with the results obtained from the direct numerical simulation of Eq. (2.2) for the case of large $\tilde{g}$. We obtained stable 2D solitary waves for $|\beta| > 0.12$, showed an excellent agreement with the results obtained via Gaussian ansatz. The ground state solitonic solution of Eq. (2.2) is obtained numerically via imaginary time evolution, and is shown in the Fig. (2.1(b)). Using it as an initial condition, we confirmed the stability of the soliton by a real time evolution [see Fig. (2.2(b))]. Since the soliton is isotropic in the $xy$ plane, here onwards we call it as *isotropic* bright soliton. In the numerics, we employed split-operator method, and the momentum contribution in the Hamiltonian is simulated using the fast Fourier transform technique. The equilibrium width of the bright soliton as a function of $\tilde{g}$ is shown in the Fig. (2.2(a)). $\tilde{g}$ can be increased by increasing $N$. The numerical results are slightly different from the energy calculations, but qualitatively they are in excellent agreement. As expected, by increasing $N$ the size of the soliton decreases. But it reaches a minimum value and becoming quasi-independent of $\tilde{g}$ for large values of $\tilde{g}$. It can be explained using the expression of the energy (2.13): for small values of $\tilde{g}$, the increase in $N$ increases the attractive DDI in the $xy$ plane, and hence the system reduces energy by compressing the soliton size. As $N$ increases and for large values of $\tilde{g}$, the kinetic energy is negligible compared to the interaction energy and hence the energy of the soliton can be approximated as,

$$\frac{2E}{\hbar\omega_z} \sim \frac{\tilde{g}}{\sqrt{2\pi}L_\rho^2 L_z}\left[14\pi + \frac{\beta}{3}f(L_\rho)\right], \tag{2.13}$$

and as a consequence, the minimun of $E(L_\rho)$ just depend only on $\beta$ and not on any particular values of $\tilde{g}$ or $\tilde{g_d}$.

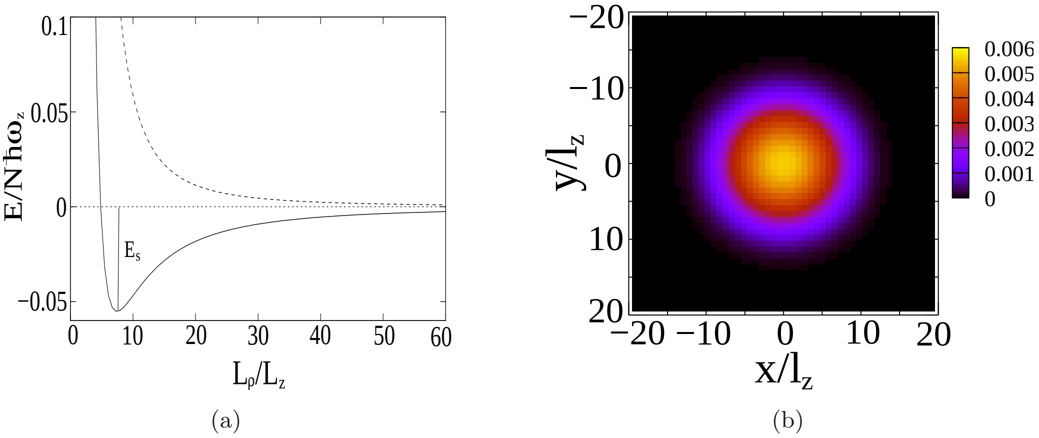

(a)

(b)

**Figure 2.1.:** Fig. (2.1(a)): The Gross-Pitaevskii energy functional (2.13) as a function of its variational parameter $L_\rho$, for $\tilde{g} = 200$, and $\beta = -0.20$ (solid line) and $\beta = -0.10$ (dashed line), where $E_s$ is the binding energy of the dipolar soliton. The minium indicates the stability of solitonic solution. Fig. (2.1(b)): The density ($|\psi(x, y)|^2$) plot of the ground state 2D bright soliton in a 2D dipolar BEC with $\tilde{g} = 200$, and $\beta = -0.20$. The ground state is obtained via imaginary time evolution.

## 2.3. Time Dependent Variational Analysis

### 2.3.1. Model of the System

In this section, we introduce a variational formalism [80] which helps us to gain more understanding on the stability and the dynamics of the 2D dipolar solitory waves. We follow the approach pioneered by Perez-Garcia *et al* [163, 164], which has been used successfully for many studies on trapped condensates, and also attemted to explain the anomalous behavior in the finite temperature excitation experiment [165, 166]. Basically, the idea is to treat the problem of solving Eq. (2.1) as a variational problem,

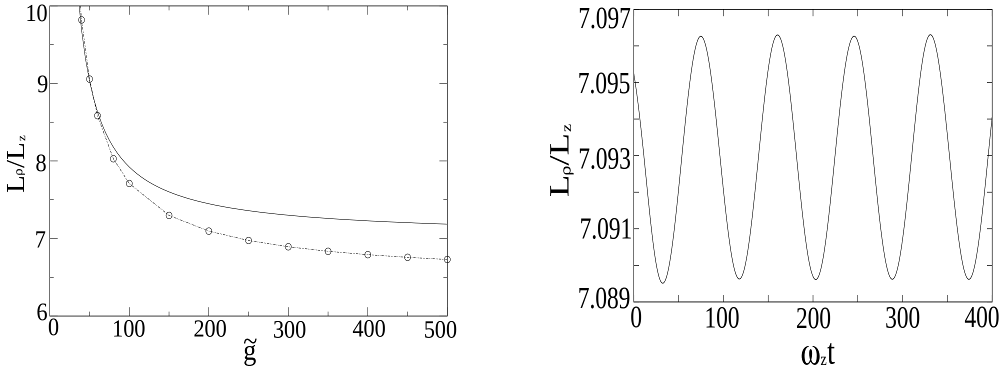

(a)

(b)

**Figure 2.2.:** (2.2(a)): The equilibrium size of the soliton as a function of $\tilde{g}$ for $\beta = -0.2$. Solid line corresponds to results using Eq. (2.13) and empty circles corresponds to numerical results. (2.2(b)): The time evolution of soliton width, for $\tilde{g} = 200$ and $\beta = -0.2$.

corresponding to a stationary point of the action related to the Lagrangian Density $\mathcal{L}$:

$$\begin{aligned}\mathcal{L} &= \frac{i\hbar}{2}(\Psi\dot{\Psi}^* - \dot{\Psi}\Psi^*) + \frac{\hbar^2}{2m}|\nabla\Psi|^2 + \frac{1}{2}m\omega_z^2 z^2|\Psi(\vec{r},t)|^2 + \\ & \frac{g}{2}|\Psi(\vec{r},t)|^4 + \frac{1}{2}|\Psi(\vec{r},t)|^2\int d\vec{r}' V_d(\vec{r}-\vec{r}')|\Psi(\vec{r}',t)|^2. \end{aligned} \tag{2.14}$$

where the asterik denotes the complex conjugation. Hence, one has to find $\Psi$, such that the action

$$S = \int \mathcal{L} d\vec{r} dt \tag{2.15}$$

is extreme. We consider the following Gaussian ansatz as a trial function,

$$\Psi(\vec{r},t) = A(t) \prod_{\eta=x,y,z} e^{-[\eta-\eta_0(t)]^2/2w_\eta^2 + i\eta\alpha_\eta(t) + i\eta^2\beta_\eta(t)}, \tag{2.16}$$

where $A$ is the complex amplitude, $w_\eta$ the width, $\alpha_\eta$ the slope, $\beta_\eta$ the (curvature radius)$^{-1/2}$, and $\eta_0$ the center of the dipolar BEC are the variational parameters. Our aim is to find the equations governing the evolution of the above variational parameters. So, inserting Eq. (2.15) into Eq. (2.14) and then calculate an effective Langrangian $L$ by integrating the Lagrangian density over all space coordinates

$$L = \langle \mathcal{L} \rangle = \int d\vec{r} \mathcal{L}, \tag{2.17}$$

we arrive at

$$\begin{aligned} L &= N\hbar \sum_{\eta=x,y,z} \left[ \dot{\alpha}_\eta \eta_0 + \dot{\beta}_\eta \left( \frac{w_\eta^2}{2} + \eta_0^2 \right) \right] + \frac{N\hbar^2}{2m} \sum_{\eta=x,y,z} \left[ \frac{1}{2w_\eta^2} + \alpha_\eta^2 \right. \\ & \left. + 4\beta_\eta^2 \left( \frac{w_\eta^2}{2} + \eta_0^2 \right) + 4\alpha_\eta \beta_\eta \eta_0 \right] + \frac{N^2 g}{2(2\pi)^{3/2} w_x w_y w_z} + \frac{N m \omega_z^2 w_z^2}{4} \\ & + \frac{N^2 g_d}{12\pi^2} \int d\vec{k} (3\cos^2\theta_k - 1) \prod_{\eta=x,y,z} e^{-\frac{k_\eta^2 w_\eta^2}{2}} \end{aligned} \tag{2.18}$$

where we have used the atom number conservation

$$N = \pi^{3/2} |A(t)|^2 w_x(t) w_y(t) w_z(t) = \text{const.} \tag{2.19}$$

At this point we have reduced the problem of solving the Eq. (2.1) to a finite dimensional problem, i.e., solving the following Lagrange equations

$$\frac{d}{dt}\left( \frac{\partial L}{\partial \dot{q}_j} \right) - \frac{\partial L}{\partial q_j} = 0, \tag{2.20}$$

with the notation

$$q_j \equiv (w_x, w_y, w_z, x_0, y_0, z_0, \alpha_x, \alpha_y, \alpha_z, \beta_x, \beta_y, \beta_z).$$

### 2.3.2. Evolution Equations for the Parameters

For the parameters $\alpha$ and $\beta$ we get,

$$\beta_\eta = \frac{m \dot{w}_\eta}{2\hbar w_\eta} \tag{2.21}$$

and

$$\alpha_\eta = \frac{m}{\hbar} \left( \dot{\eta}_0 - \frac{\dot{w}_\eta \eta_0}{w_\eta} \right) \tag{2.22}$$

The problem can be further simplified by eliminating the parameters $\alpha$ and $\beta$ from the Lagrangian $L$. This can be done by the *gauge transformation* of Lagrangian, i.e., by transforming the Lagrangian $L$ to $L'$ by keeping the action $S$ invariant, which preserves the equations of motion. We define,

$$L' = L - \frac{dg}{dt}, \tag{2.23}$$

with

$$g = \hbar \sum_\eta \left[ \alpha_\eta \eta_0 + \beta_\eta \left( \frac{w_\eta^2}{2} + \eta_0^2 \right) \right]. \tag{2.24}$$

Hence

$$\begin{aligned} L' &= -\frac{Nm}{2}\sum_{\eta}\left[\dot{\eta}_0^2+\frac{\dot{w}_\eta^2}{2}-\frac{\hbar^2}{2m^2w_\eta^2}\right]+\frac{N^2g}{2(2\pi)^{3/2}w_xw_yw_z} \\ &+\frac{Nm\omega_z^2w_z^2}{4}+\frac{N^2g_d}{12\pi^2}\int d\vec{k}(3\cos^2\theta_k-1)\prod_{\eta=x,y,z}e^{-\frac{k_\eta^2w_\eta^2}{2}} \end{aligned} \tag{2.25}$$

The Lagrangian $L'$ describes the physics of a 3D Gaussian BEC with DDI, and a harmonic confinment along the $z$ axis. The widths of the condensate satisfy the following equations:

$$m\ddot{w}_x=\frac{\hbar^2}{mw_x^3}+\frac{Ng}{(2\pi)^{3/2}w_x^2w_yw_z}-2\frac{\partial V}{\partial w_x}, \tag{2.26}$$

$$m\ddot{w}_y=\frac{\hbar^2}{mw_y^3}+\frac{Ng}{(2\pi)^{3/2}w_y^2w_xw_z}-2\frac{\partial V}{\partial w_y}, \tag{2.27}$$

$$m\ddot{w}_z=\frac{\hbar^2}{mw_z^3}+\frac{Ng}{(2\pi)^{3/2}w_y^2w_xw_z}-m\omega_z^2w_z-2\frac{\partial V}{\partial w_z}, \tag{2.28}$$

where

$$V(w_x,w_y,w_z)=Ng_d/(12\pi^2)\int d\vec{k}(3\cos^2\theta_k-1)\prod_{\eta=x,y,z}e^{-k_\eta^2w_\eta^2/2}. \tag{2.29}$$

The Eqs. (2.26), (2.27) and (2.28) describe the motion of a particle with coordinates $(w_x,w_y,w_z)$ in an effective potential [80, 167]

$$U(w_x,w_y,w_z)=\frac{\hbar^2}{2m}\left(\frac{1}{w_x^2}+\frac{1}{w_y^2}+\frac{1}{w_z^2}\right)+\frac{m\omega_z^2w_z^2}{2}+\frac{Ng}{(2\pi)^{3/2}w_xw_yw_z}+V(w_x,w_y,w_z). \tag{2.30}$$

The equilibrium widths of the condensate are then obtained by minimizing the effective potential $U$, and the evolution of the condensate widths are found by numerically integrating the above equation of motions for the corresponding widths along $x$, $y$ and $z$ axes.

### 2.3.3. Small Amplitude Shape Oscillations

Once the equilibrium widths are found, the frequencies of small amplitude oscillations are obtained by evaluating the second order derivatives of the effective potential $U$, and it takes the following symmetric form:

$$\begin{pmatrix} U_{11} & U_{12} & U_{13} \\ U_{12} & U_{11} & U_{13} \\ U_{13} & U_{13} & U_{33} \end{pmatrix}, \tag{2.31}$$

where $U_{ij}=U_{ji}$ due to the commuting property of derivative operations with different coordinates, and $U_{11}=U_{22}$ and $U_{13}=U_{23}$ due to the cylindrical symmetry. The diagonalization of the above symmetric matrix gives the three-mode frequencies $\nu_1 = \sqrt{U_{11} - U_{12}}$ and

$$\nu_{3,2} = \frac{\sqrt{U_{11} + U_{12} + U_{33} \pm \sqrt{(U_{11} + U_{12} - U_{33})^2 + 8U_{13}^2}}}{\sqrt{2}}. \tag{2.32}$$

The schematic representation of the modes are shown in the Fig. (2.3). Mode 1 is purely radial due to the cylindrical symmetry. Its angular momentum projection along the $z$ axis is $m = 2$. Modes 2 and 3 are the quadrupole and the monopole oscillations respectively, and are customarily called the low and the high $m = 0$ modes.

Also, a 2D version of above equations can be obtained by taking into account the two following facts: (i) the trap along the $z$ axis is so strong that there is no dynamics along the $z$ direction, hence $w_z$ is independent of time, (ii) we assume a 2D soliton which is not moving and, is placed at the origin of the cordinate system, hence $\eta_0(t) = 0$ for all $x, y$ and $z$. Now we end up with two time dependent variables, $q_j = w_x, w_y$. The corresponding equations of motion are

$$m\ddot{w}_x = \frac{\hbar^2}{m w_x^3} + \frac{g}{(2\pi)^{3/2} w_x^2 w_y w_z} - 2\frac{\partial V}{\partial w_x}, \tag{2.33}$$

$$m\ddot{w}_y = \frac{\hbar^2}{m w_y^3} + \frac{g}{(2\pi)^{3/2} w_y^2 w_x w_z} - 2\frac{\partial V}{\partial w_y}, \tag{2.34}$$

The Eqs. (2.34) and (2.34) describe the motion of a particle with coordinates $(w_x, w_y)$ in an effective potential

$$U^{(2D)}(w_x, w_y) = \frac{\hbar^2}{2m}\left(\frac{1}{w_x^2} + \frac{1}{w_y^2}\right) + \frac{g}{(2\pi)^{3/2} w_x w_y w_z} + V(w_x, w_y). \tag{2.35}$$

The modes are again obtained by diagonalizing the second derivative matrix of the effective potential $U^{(2D)}$. We get two eigen frequencies corresponding to the modes 1 and 2: $\nu_{2,1} = \sqrt{U_{11} \pm U_{12}}$. Due to the strong trapping along the $z$ diection, mode 3 becomes highly energetic, and hence we are no longer interested in mode 3. The lowest lying modes of a 2D dipolar bright soliton are shown in the Fig. (2.4). The lowest-lying mode has for any value of $\beta$ a breathing character. For sufficiently small values of $|\beta|$, the breathing mode tends to zero, and eventually the system becomes unstable against expansion. This corresponds to the disappearance of the minimum in the energy. In this regime, the 2D picture provides a good description of the physics of the problem, as shown in Fig. (2.4). For sufficiently large values of $|\beta|$, the 3D character of the system becomes crucial, leading to a different sort of instability, in this case against 3D collapse. This is reflected in the decrease of the frequency of the breathing mode. Hence, as expected from general arguments for nonlocal nonlinearity [130], the DDI can stabilize the 2D solitary waves. However, a new crucial feature is introduced by the anisotropic character of the dipolar interaction, since too large DDI can destabilize the solitary waves.

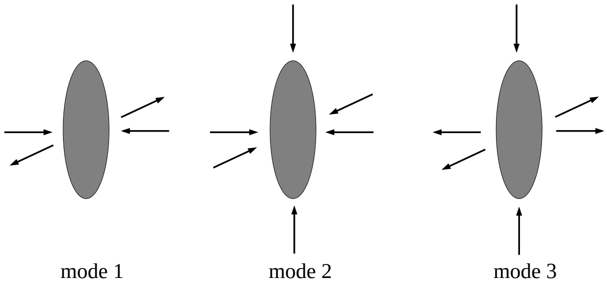

**Figure 2.3.:** Schematic representation of collective excitations in a cylindrical trap.

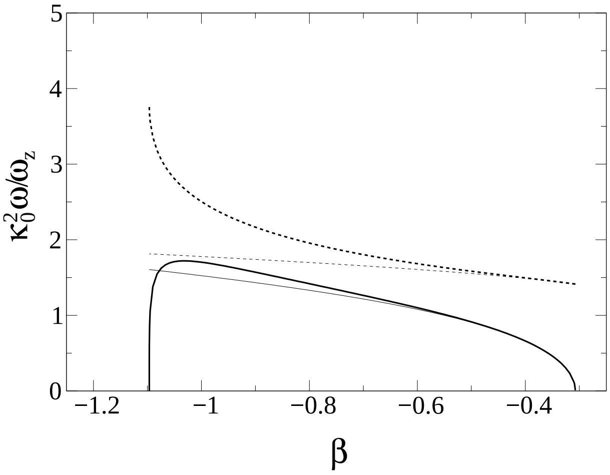

**Figure 2.4.:** Breathing (bold dashed) and $m = \pm 2$ quadrupole (bold solid) mode for $\tilde{g} = 10$, with $\kappa_0 = L\rho/L_z$. Results from a purely 2D calculation are shown in thin lines.

## 2.4. Anisotropic Solitons

Two dimensional solitonic solutions are also possible if the dipoles are aligned parallel to the *xy* plane, as recently proposed in [153]. In this section we briefly discuss the stability conditions and some particular characteristics of such solitons. Since the dipoles are alligned parallel to the plane, say along the *x* axis, the DDI in the *xy* plane is anisotropic becoming partially attractive and partially repulsive. Hence the soliton is more elongated along the *x* axis. Since the shape of the soliton has an anisotropic character, it is called *anisotropic* solitons. The stability conditions for an anisotropic soliton can be estimated using the Gaussian trial function in the corresponding energy functional (2.4). We assume an anisotropic ansatz of the form:

$$\Psi_{ani} = \frac{N}{\pi^{3/4} l_z^{3/2} \sqrt{L_x^{1/2} L_y^{1/2} L_z^{1/2}}} \exp\left[-\frac{1}{2l_z^2}\left(\frac{x^2}{L_x^2} + \frac{y^2}{L_y^2} + \frac{z^2}{L_z^2}\right)\right], \qquad (2.36)$$

where $L_x$, $L_y$ and $L_z$ are the dimensionless variational parameters related with the widths along the $x$, $y$ and $z$ directions respectively. We obtain the energy

$$\frac{E}{N\hbar\omega_z} = \frac{1}{4}\left(\frac{1}{L_x^2} + \frac{1}{L_y^2} + \frac{1}{L_z^2}\right) + \frac{L_z^2}{4} + \frac{1}{L_x L_y L_z}\left[\frac{\tilde{g}}{4\pi} + \frac{\tilde{g}_d}{3} h(L_x, L_y, L_z)\right] \tag{2.37}$$

with

$$h(L_x, L_y, L_z) \equiv \int_0^1 \frac{3 L_y L_z x^2 dx}{L_x^2 \sqrt{1 + \left(L_y^2/L_x^2 - 1\right) x^2}\sqrt{1 + \left(L_z^2/L_x^2 - 1\right) x^2}} - 1 \tag{2.38}$$

It is found that the energy $E$ exhibits a minimum for $\tilde{g} > 0$ when $\beta > 3/4\pi \approx 0.24$ (see Fig. (2.5)). Noted that, eventhough one needs a sufficiently large DDI to stabilize the 2D anisotropic solitons, the tuning of DDI is not required. Hence anisotropic solitons are more feasible experimentally compared to the isotropic ones where the tuning of DDI is unavoidable. However, one may show that for a given $\beta > 3/4\pi$, there is a critical universal value $\tilde{g}_{cr}(\beta) \equiv gN_{cr}/\sqrt{2\pi} l_z$ (see Fig. 3.7) such that for $N > N_{cr}$ the minimum of $E(L_x, L_y)$ disappears [168]. As a consequence, contrary to the case of isotropic solitons, which are always stable as long as the soliton is 2D, there is a critical number of particles per soliton, $N_{cr}$, which decreases for larger $\beta$ (see Fig. (2.6)). Beyond this number the 2D soliton collapses. This result is also verified by a direct simulation of the 3D NLSE (2.1). Note that this result was not discussed in [153] and constitutes a novel result of this thesis.

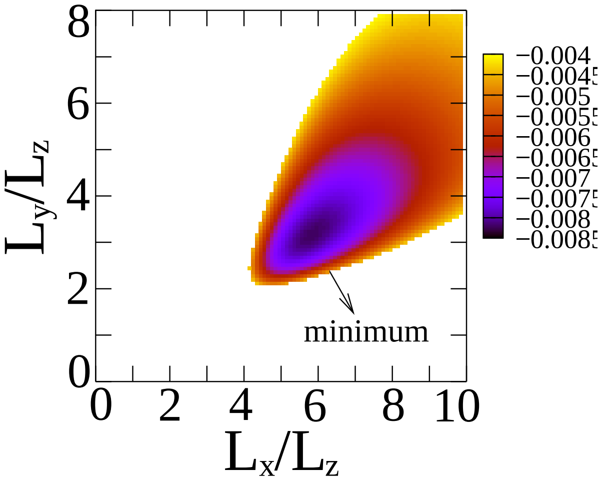

**Figure 2.5.:** The Gross-Pitaevskii energy functional (2.37) as a function of its variational parameters $L_x$ and $L_y$, for $\tilde{g} = 10$, and $\beta = 1./0.911$. The minimum (dark region) indicates the stability of solitonic solution. The minimum disappears once $N > N_{cr}$ where the anisotropic soliton is unstable against 2D collapse.

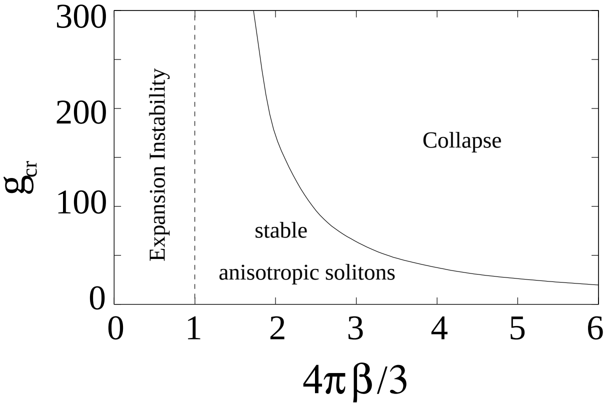

**Figure 2.6.:** Stability diagram of an anisotropic soliton as a function of $\beta$ and $\tilde{g}_{cr} = \tilde{g}N_{cr}$, where for $N > N_{cr}$, the soliton is unstable against collapse even for $\beta > 3/4\pi$.

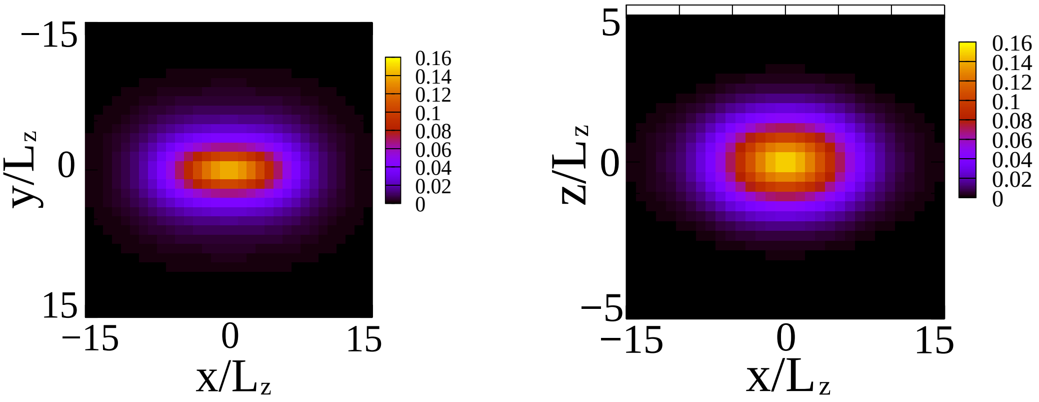

(a)

(b)

**Figure 2.7.:** The ground state anisotropic bright soliton solution of Eq. (2.1). The dipoles are polarized along the $x$ direction and a strong confinement in the $z$ axis. Fig. (2.7(a)): The density $|\Psi|^2$ in the $xy$ planefor $z = 0$, and Fig. (2.1(b)): the density $|\Psi|^2$ in the $xz$ plane for $y = 0$. $\tilde{g} = 10$ and $\beta = 1./0.911$ for both the plots. Since the dipoles are alligned along the $x$ axis, the soliton is more elongated along that direction.

# 3. Soliton-soliton Scattering in Dipolar BECs

In order to deepen our understanding of the 2D isotropic solutions we found in the Chapter 2 , and their comparison with the solitonic solutions of the 1D NLSE, we have analyzed the scattering of these solitons. In nonlinear optics, the soliton-soliton interactions in one dimension have been described completely and analytically by Gordon [169]. They are perfectly elastic. In short-range interacting condensates but trapped by a confining potential, the soliton dynamics may be chaotic with three or more solitons even in one dimension [170], and higher dimensional effects can lead to inelastic collisions [171, 172]. In this chapter we discuss the scattering of 1D and 2D dipolar bright solitons without any harmonic confinement in the radial direction. As we will discuss, the non-local character of the DDI provides unusual scattering scenarios in matter waves[173].

## 3.1. Scattering of 2D Bright Solitons in a Single Plane

First we analyze the scattering of 2D dipolar bright isotropic solitons in a single plane, where the spatial overlapping of solitons is possible (we follow here the discussion of [152]). We consider two solitons along a line, which are well separated such that the interaction between them is negligible. We let them collide with different values of their initial center-of-mass kinetic energy, $E_{kin}$ and study the collisional properties. The schematic diagram of situation under consideration is shown in the Fig. (3.1). Since $\beta < 0$ for isotropic solitons, they attract each other in the $xy$ plane. As a result they gain kinetic energy when approaching each other. Direct numerical simulations of the 2D nonlocal NLSE show that the scattering of dipolar 2D solitary waves is *inelastic*. In particular, as shown in Fig. (3.7), for sufficiently slow localized waves (for the case considered in Fig. (3.7)), when $E_{kin} \leq 2.9|E_S|$, where $E_s$ is the binding energy of the soliton, two solitary waves merge when colliding. As observed in Fig. ( 3.7), the solitary waves, when overlapping they transfer their center-of-mass kinetic energy into the internal energy, transforming into a single localized structure. This structure, although localized, is in an excited state, and clear oscillations may be observed. For larger initial kinetic energies, the waves move apart from each other after the collision, but the transfer of kinetic energy into internal energy is enough to unbind the solitary wave, and the solitary waves are destroyed. This inelastic character of the scattering of dipolar 2D solitary waves, clearly differs these solutions from the solitonic solutions of the 1D NLSE [72].

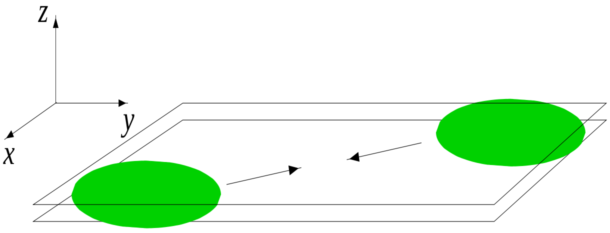

**Figure 3.1.:** Schematic representation of two-dimensional solitons in a single 1D potential.

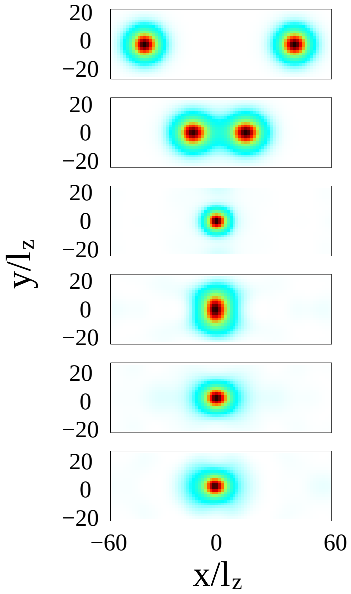

**Figure 3.2.:** Density plot of the fusion of two dipolar 2D solitary waves for $\tilde{g} = 20$, $\beta = -0.5$, and $k_0 l_z = 0.01$, where $k_0$ is the intial momentum of the soliton. From top to bottom $\omega_z t/2 = 0, 1000, 2000, 3000, 4000, 5000$.

## 3.2. Two-dimensional Bright Solitons in Double-well Potential

### 3.2.1. Model of the Problem

Now we consider two isotropic bright solitons in a 1D double-well potential with suppressed tunneling. Such a setup can be realised as two adjacent sites in an 1D optical lattices with a sufficiently large lattice depth. Contrary to the short-range interacting gases in a deep double-well potential, the 2D dipolar gases interact with each other through DDI. This inter-site interaction introduces novel and rich phenomena in the context of dipolar BECs. The schematic diagram of the double well potential with 2D dipolar solitons is shown in the Fig. (3.3). At sufficiently low temperatures, our system is described by the following two coupled dimensionally reduced 2D NLSE with nonlocal nonlinearity:

$$
\begin{aligned}
i\hbar\frac{\partial}{\partial t}\psi_j = \Bigg[-\frac{\hbar^2}{2m}\nabla_\rho^2 + \frac{g|\psi_j|^2}{\sqrt{2\pi}l_z} + \frac{4\sqrt{\pi}g_d}{3\sqrt{2}l_z}\int\frac{d\vec{k}_\rho}{(2\pi)^2}e^{i\vec{k}_\rho\vec{\rho}} \\
\Big(\tilde{n}_j(\vec{k}_\rho)F\left(k_\rho l_z,0\right)+\tilde{n}_{-j}(\vec{k}_\rho)F\left(k_\rho l_z,2z_0/l_z\right)\Big)\Bigg]\psi_j \qquad (3.1)
\end{aligned}
$$

where $j=\pm1$ is the layer-index, $\Psi_j$ are the wavefunctions at each well, $U_j(z)=m\omega_z^2(z+jz_0)^2/2$, $\int|\Psi_j(\vec{r},t)|^2d\vec{r}=N$, and $g=4\pi\hbar^2a/m$ characterizes the contact interaction with $a$ the $s$-wave scattering length, $l_z^2=\hbar/m\omega_z$ is the onsite harmonic-oscillator length, $\tilde{n}_j$ is the Fourier transform of $|\psi_j(\vec{\rho})|^2$ and $F(\sqrt{2}k,\sqrt{2}\lambda)=2e^{-\lambda^2}-(3\sqrt{\pi}ke^{k^2}/2)[e^{-2k\lambda}\,\mathrm{erfc}(k-\lambda)+e^{2k\lambda}\mathrm{erfc}(k+\lambda)]$, with $\mathrm{erfc}(x)$ the complementary error function. Eq. (3.1) is an extension of Eq. (2.2) by including the dipolar coupling between the solitons. Using Eqs. (3.1), we study numerically the equilibrium properties and the dynamics of the unconnected 2D dipolar solitons.

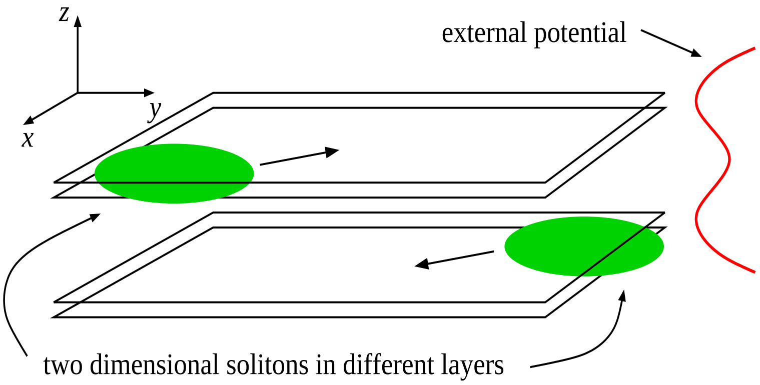

**Figure 3.3.:** Schematic representation of the system considered

### 3.2.2. Variational Method

Using the variational approach we employed in the Chapter 2 to study the stability of the soliton, we study the dynamics of two solitons in the double-well potential. We consider a 2D Gaussian Ansatz:

$$
\begin{aligned}
\psi_j(\vec{\rho},t) &= A\prod_{\eta=x,y}\exp\left[-\frac{(\eta-j\eta_0)^2}{4w_\eta^2}\right]\times \\
&\quad\times\exp\left[i\frac{m}{\hbar}\left(j\eta\dot{\eta}_0+(\eta-j\eta_0)^2\frac{\dot{w}_\eta}{w_\eta}\right)\right], \qquad (3.2)
\end{aligned}
$$

where $A$ is the normalization factor, $\{x_0,y_0\}$ is the soliton center, $w_{x,y}$ the soliton widths. The variables $x_0,y_0,w_x,w_y$ are time-dependent. The center of mass motion is an independent degree of freedom and it can be decoupled. Without loss of generality, it has not been included in the variational Ansatz. Introducing Eq. (3.2) into the corresponding Lagrangian:

$$\begin{aligned}\mathcal{L}_j &= \frac{i\hbar}{2}(\Psi_j\dot{\Psi}_j^* - \dot{\Psi}_j\Psi_j^*) + \frac{\hbar^2}{2m}|\nabla\Psi_j|^2 + \frac{1}{2}m\omega_z^2 z^2|\Psi_j(\vec{r},t)|^2 + \\ &\frac{g}{2}|\Psi_j(\vec{r},t)|^4 + \frac{1}{2}|\Psi_j(\vec{r},t)|^2\int d\vec{r}' V_d(\vec{r}-\vec{r}')(|\Psi_1(\vec{r}',t)|^2 + |\Psi_{-1}(\vec{r}',t)|^2), \quad (3.3)\end{aligned}$$

we obtain the effective Lagrangian:

$$\begin{aligned}L_j &= -\frac{Nm}{2}\sum_{\eta=x,y}\left[\dot{\eta}_0^2 + \frac{\dot{w}_\eta^2}{2} - \frac{\hbar^2}{2m^2w_\eta^2}\right] + \frac{N^2g}{2(2\pi)^{3/2}w_xw_yw_z} \\ &+\frac{Nm\omega_z^2w_z^2}{4} + \frac{N^2g_d}{12\pi^2}\int d\vec{k}(3\cos^2\theta_k - 1)\prod_{\eta=x,y,z}e^{-\frac{k_\eta^2w_\eta^2}{2}}(e^{2ik_\eta\eta_0}+1). \quad (3.4)\end{aligned}$$

Using the Lagrangian (3.4) we obtain the following set of equations of motion

$$m\ddot{q}_i = -\frac{\partial}{\partial q_i}U, \quad (3.5)$$

where $q_{\{i\}} = x_0, y_0, w_x, w_y$ are the dynamical variables. The problem then reduces to the analysis of an effective particle in a potential

$$U = \frac{\hbar^2}{8m}\left(\frac{1}{w_x^2} + \frac{1}{w_y^2}\right) + \frac{g}{\sqrt{2\pi}8\pi w_xw_yl_z} + V, \quad (3.6)$$

that includes the dipolar interaction term

$$\begin{aligned}V &= \frac{g_d}{12\pi^2}\int d\vec{k}\left(3\frac{k_z^2}{k^2} - 1\right)e^{-k_z^2l_z^2/4 - k_x^2w_x^2/2 - k_y^2w_y^2/2} \\ &(1 + \cos(2k_xx_0)\cos(2k_yy_0)\cos(2k_zz_0)), \quad (3.7)\end{aligned}$$

that couples the unconnected solitons. This coupling gives rise to interesting interlayer effects which will be analyzed in the following sections.

### 3.2.3. Stationary Solution of the Two-coupled Solitons

In this section we analyze the stationary state of the coupled 2D isotropic bright solitons. Since the stabilization of the 2D solitons demands $g_d < 0$, the soliton-soliton potential is maximally repulsive for solitons when they are aligned exactly on top of each other. However, due to the angular dependence of the DDI, the potential becomes attractive at a given distance between the solitons, vanishing at long separations between them. As a consequence, the soliton-soliton potential presents a minimum (see Fig. (3.4(a))), and hence the soliton pair can form a soliton-molecule. The equilibrium separation between the solitons in the molecule, and the corresponding equilibrium widths of the solitons can be obtained by calculating the minimum of potential $U$. We have performed this

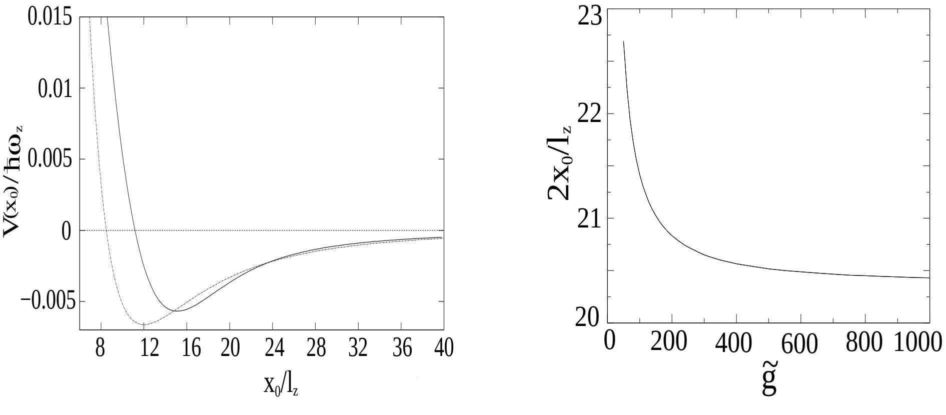

(a) (b)

**Figure 3.4.:** Fig. (3.4(a)): Soliton-Soliton potential for 2D solitons. Dotted line is for point like solitons and solid line for Gaussian shape wavepackets, for a given dipolar strength. Fig. (3.4(b)): Numerical results for the relative distance between two dipolar isotropic solitons as a function of $\tilde{g}$, for $z_0 = 3l_z$,$\beta = -0.20$

task for different parameter regimes by means of a Powell-minimization procedure, and compared our results with those obtained from the direct numerical simulation of the coupled GPEs in imaginary time. Note that due to symmetry on the $xy$-plane, we can fix without loss of generality $y_0 = 0$ i.e. the solitons are assumed aligned along the $x$ axis with $y_0 = 0$. In such a situation, the equilibrium widths of the solitons along the y direction, i.e. the direction perpendicular to the line joining the solitons, are larger than that along $x$. This elongation in widths along the $x$ axis is due to the attractive pull between the solitons.

The equilibrium position is by no means that expected from approximating the solitons as point-like objects. When the solitons approach each other, their structure becomes more relevant and that shifts the minimum of the molecular potential, but assymptotically both the potentials are same. In the case of point like solitons, the interaction potential between the solitons would be provided by $V_{point} \propto -(x_0^2 - 2z_0^2)/(x_0^2 + z_0^2)^{5/2}$, which presents a minimum at $x_0 = 2z_0$. This value is certainly smaller than the results obtained from our variational or numerical calculations (see Fig. 3.4(b)). Note that for growing $g$ the equilibrium separation between the solitons in the molecule is as expected reduced, becoming quasi independent of $g$ for large $g$. This is explained since for large $g$ and fixed $\beta$ (i.e. increasing the number of atoms) the kinetic energy term becomes negligible compared to the interaction terms, and hence the minimum of $U$ just depends on $\beta$ and not on the particular values of $g$ and $g_d$.

### 3.2.4. Lowest-lying excitations

In section (2.3.3) we calculated the lowest lying excitations of a single isotropic bright soliton. The excitations of a single soliton are significantly modified by the presence of an additional soliton due to the dipolar coupling between them. In the following we analyze the small amplitude oscillations of a bound state of two solitons. We estimate the frequencies of the lowest-lying excitations $\omega_j$ of the soliton molecule by means of our variational approach. This is done by calculating the eigenvalues of the Hessian of the potential $U$ at the equilibrium point. In order to address the excitation in which the soliton widths of one soliton can oscillate in phase and out of phase with the widths of the other soliton, we have extended our variational calculation to the case in which the soliton widths of both solitons are not necessarily the same. Hence, we consider five variational parameters $(x_0, w_{x1}, w_{y1}, w_{x2}, w_{y2})$ and evaluate the corresponding five frequencies and the eigen modes.

The frequency of the vibrational mode (see Fig. (3.5(b))) associated with the dynamics of $x_0$ is much smaller than the monopole and quadrupole modes. In Fig. (3.5(a)) we depict the frequencies of the internal modes, associated with the dynamics of the soliton widths, normalized by their values for independent solitons. A significant shift as well as a splitting of the frequencies of the internal modes is observed due to the presence of the second soliton. Additionally, the mode geometry is significantly modified. For independent solitons the modes have a perfect monopole and quadrupole symmetry for any value of $\beta$. For interacting solitons the lowest energy mode becomes more pronounced along the $y$ direction. For values of $\beta$ approaching the instability threshold at which no stable soliton is possible (around $\beta = -0.15$ in Fig. (3.5(a))), the internal modes of a single soliton transform in the presence of the second soliton into modes purely associated with oscillations of the $w_y$ and $w_x$ widths, respectively.

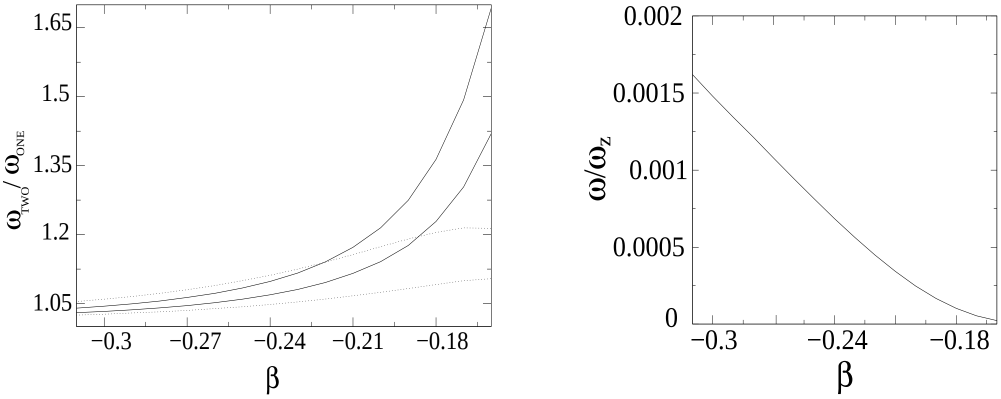

(a)

(b)

**Figure 3.5.:** Fig. (3.5(a)): Variational results for low lying excitations: Solid lines are the breathing modes (in and out of phase) and dashed lines are the quadrupole modes (in phase mode greater than out of phase mode for both monopole and quadrupole). The modes for the two solitons $\omega_{TWO}$ are normalized to the corresponding modes ($\omega_{ONE}$) of an independent soliton. The results are for $g/\sqrt{2\pi}\hbar\omega_z l_z^3 = 200, z_0 = 3l_z$. 3.5(b)): the vibrational mode associated with the dynamics of $x_0$.

### 3.2.5. Scattering of Two-dimensional Solitons

In the following, we consider the scattering of two 2D isotropic solitons in a double well potential. We first discuss the case where the relative velocity is parallel to the vector connecting the centers of mass of the two solitons and hence assuming $y_0 = 0$. We shall denote this case as the 1D scattering scenario since the soliton just moves along the $x$ direction with no velocity component along the $y$ direction. We have studied the scattering for different initial relative velocities both by direct numerical simulations of Eqs. (3.1) and by determining the evolution of $\{x_0, w_x, w_y\}$ for each soliton in our variational calculation. Fig. (3.6) shows the variation of the soliton momentum as a function of the initial momentum. During the scattering process the total energy of the system is conserved but the coupling between the external degree of freedom (relative distance of the two centers of mass) and the internal degree of freedom (modes of the single solitons) leads to a dissipation in the dynamics of the external variables. It should be stressed that this dissipation is due to the extended structure of the dipolar solitons, and would be absent for point like solitons due to the absence of internal degrees of freedom.

As expected, for sufficiently large initial velocities the scattering may be considered as elastic. For sufficiently low velocities, the initial kinetic energy of the solitons is fully transformed during the inelastic scattering into internal soliton energy, and the initially independent solitons become bounded into an excited molecular state (fusion, $|\Delta k|/k_0 = 1$). For all the other cases (including the resonance discussed below) the two solitons have a relative momentum after the collision and the relative distance between the two centers of mass increases with time after the collision.

Interestingly, the inelastic losses do not increase monotonically for decreasing velocities, but on the contrary show pronounced resonant peaks at intermediate velocities (see Fig. (3.6)). This effect is motivated by a coupling to internal soliton modes, which leads after the collision to a dramatic enhancement of the soliton widths that eventually may increase without limits leading to the destruction of the scattered solitons. We stress that this resonance behavior is only possible because internal modes of the 2D soliton are at rather low energies, well within the inelastic regime. However, a direct comparison between the internal modes discussed in the previous section, and the position of the resonance just provides a qualitative understanding of the regime of velocities for which the resonance occurs. A more quantitative analysis is largely prevented, because the internal modes of the solitons vary dynamically when the solitons approach each other. For higher momenta (right part of the resonance) the two solitons cross each other, but the interaction time is not large enough to excite the internal modes of the solitons. For low momenta (left part of the resonance) the relative kinetic energy is too small to allow the solitons to cross the potential barrier. They can either form a molecule or reflect off each other. If the interlayer distance is increased, the inelastic losses are as expected reduced, but an even more complicated structure of resonances is then resolved (see Fig. (3.6(b))).

The possibility of generating stable 2D solitons in dipolar gases allows for a novel soliton

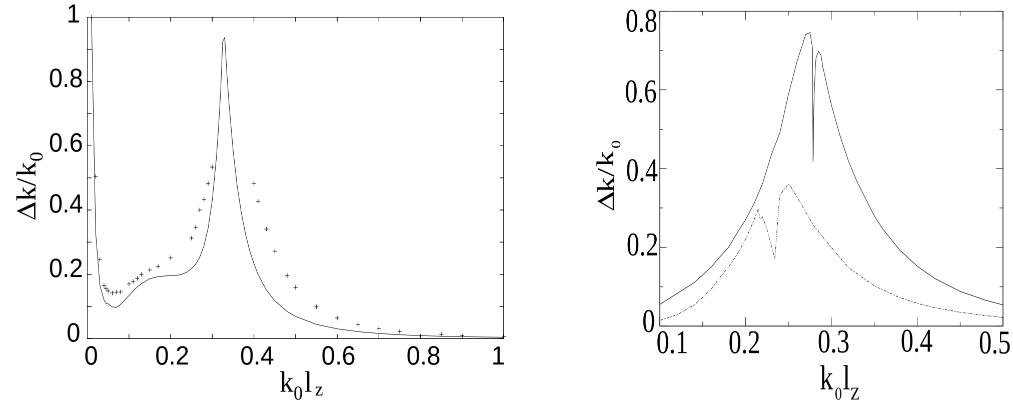

(a)

(b)

**Figure 3.6.:** Fig. (3.6(a)): Numerical (crosses) and variational (solid) results for $\Delta k/k_0$ ($\Delta k = k_0 - k(t \to \infty)$) as a function of the initial momentum $k_0 l_z$, for $z_0 = 3l_z$, $g/\sqrt{2\pi}\hbar\omega_z l_z^3 = 200$, $\beta = -0.2$. 3.6(b)): Numerical results with $z_0 = 4l_z$ (solid) and $z_0 = 5l_z$ (dotted).

scattering scenario in cold gases, that we denote as the 2D scattering scenario. Contrary to the case discussed above, in this scenario the relative velocity is not parallel to the vector connecting the centers of mass of the two solitons, hence $y_0 \neq 0$, leading to a non-vanishing angular momentum. This scattering scenario obviously demands stable 2D solitons, and hence it is not possible in short-range interacting condensates where the freely moving 2D solitons are not stable. The non-vanishing angular momentum is conserved after the collision, and as a consequence, for the case of soliton-fusion at low velocities a spiraling motion of the solitons is observed during the inelastic fusion. The solitons eventually stabilize into a rosetta-like orbit around each other (Fig. (3.7)). The spiraling motion of the solitons links the physics of dipolar BEC to that of photorrefractive materials, where soliton spiraling has been proposed [174] and experimentally observed [155].

## 3.3. One-dimensional Bright Solitons in Dipolar BEC

1D bright solitons are stable in BEC even without DDI. However, the presence of DDI add new characteristics to 1D matter-wave solitons especially on collision dynamics. Utilizing the attractive part of the DDI, it is possible to have a stable 1D bright soliton with positive $s$ wave scattering length in dipolar BEC. We consider a dipolar BEC in an external potential: $V_{ext}(\rho) = m\omega_\rho^2\rho^2/2$ with dipoles are polarized along the $z$ direction. The external confinement is sufficiently strong such that the dipolar BEC is 1D in nature. Using the energy functional (2.4) with an associated external potential, it is possible to show that for $\tilde{g} > 0$ we obtain a stable bright soliton if $\beta > 3/4\pi$. Note that since $\beta > 0$ no tuning of DDI is required and hence the situation is less

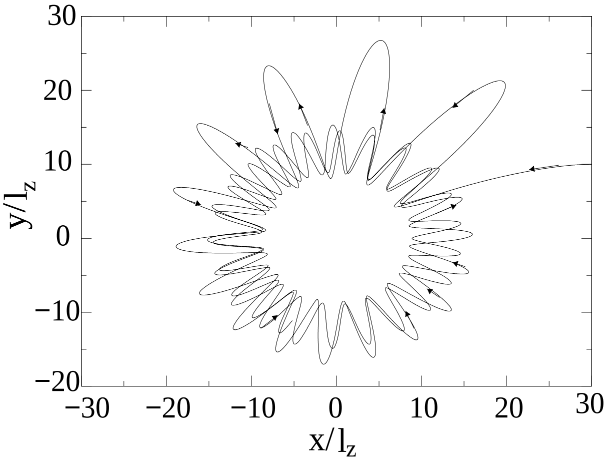

**Figure 3.7.:** Numerical result for the soliton trajectory during spiraling fusion in a 2D soliton scattering, for the case $g/\sqrt{2\pi}\hbar\omega_z l_z^3 = 200$, $\beta = -0.2$, $z_0 = 3l_z$, $\vec{k}_0 l_z = 0.01\hat{x}$, $x_0 = 30l_z$, $y_0 = 10l_z$.

experimentally demanding. For $^{52}$Cr a Feshbach resonance is necessary to satisfy the previous condition, but Feshbach resonances are well characterized and accessible [175]. The results obtained from energy calculations are verified using the reduced 1D GP equation with DDI,

$$\begin{aligned} i\hbar\frac{\partial}{\partial t}\psi(z,t) = \Bigg[ & -\frac{\hbar^2}{2m}\frac{\partial^2}{\partial z^2} + \frac{g}{2\pi l_\rho^2}|\psi(z,t)|^2 + \frac{2g_d}{3l_\rho^2} \\ & + \int \frac{dk_z}{2\pi} e^{ik_z z}\tilde{n}(k_z) h_{1D}(k_z)\Bigg] \psi(z,t), \end{aligned} \tag{3.8}$$

where

$$h_{1D}(k_z) = \int_0^\infty dx \left( \frac{2k_z^2 - x}{k_z^2 + x} \right) e^{-x/2}. \tag{3.9}$$

In order to study the scattering, we consider 1D BECs placed at neighboring 1D-sites. We consider two neighboring wires realized by means of a two dimensional optical lattice (placed in the $x-y$ plane), and the dipoles are oriented along the wire axis ($z$ direction). At each wire, the transversal confinement is approximated by an harmonic potential $m\omega_\rho^2[(x \pm x_0)^2 + y^2]/2$. As for the 2D case, we analyze the scattering of the coupled 1D solitons by means of a variational wavefunction:

$$\begin{aligned} \Psi_j(\vec{r},t) &= A \exp\left[ -\frac{(z-jz_0)^2}{2w_z^2} - \frac{(x-jx_0)^2 + y^2}{2l_\rho^2} \right] \times \\ & \times \exp\left[ i\frac{m}{\hbar}\left( jz\dot{z}_0 + (z-jz_0)^2 \frac{\dot{w}_z}{w_z} \right) \right], \end{aligned} \tag{3.10}$$

where $j = \pm 1$, $l_\rho = \sqrt{\hbar/m\omega_\rho}$ is the transversal harmonic oscillator length, and $\omega_z$ and $z_0$ are variational parameters that describe the width of both solitons and their positions, respectively. After substituting the ansatz in the corresponding Lagrangian, we obtain the following Euler-Lagrange equations:

$$m\ddot{z}_0 = -\frac{\partial}{\partial z_0}\mathcal{U}, \qquad m\ddot{w}_z = -\frac{\partial}{\partial w_z}\mathcal{U}, \tag{3.11}$$

where again the problem reduces to an effective particle in a potential

$$\mathcal{U} = \frac{\hbar^2}{8m}\frac{1}{w_z^2} + \frac{g}{2(2\pi)^{3/2} w_z l_\rho^2} + \mathcal{V}, \tag{3.12}$$

with $\mathcal{V}$ being the dipolar interaction

$$\begin{aligned} \mathcal{V} \;=\; & \frac{g_d}{12\pi^2}\int d\vec{k}\left(3\frac{k_z^2}{k^2}-1\right)e^{-k_z^2 w_z^2/2 - k_x^2 l_\rho^2/2 - k_y^2 l_\rho^2/2} \\ & (1+\cos(2k_x x_0)\cos(2k_z z_0)), \end{aligned} \tag{3.13}$$

As for the 2D solitons, we have calculated the change of the soliton momentum as a function of the initial momentum, obtaining similar results as in 2D (see Fig. (3.8)), i.e. three main scattering regimes, soliton-fusion, resonant scattering and elastic interaction. In Fig. (3.9) we depict an example of the dynamics of the soliton width in and out of resonance, which clearly shows a resonant (although non-destructive) behavior of the soliton widths for intermediate velocities.

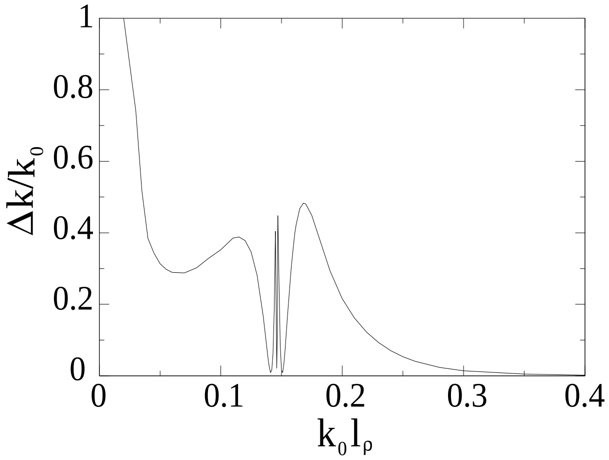

**Figure 3.8.:** Variational results for $\Delta k/k_0$ ($\Delta k = k_0 - k(t \to \infty)$) as a function of the initial momentum $k_0 l_\rho$, for $x_0 = 3l_\rho$, $g/2\pi\hbar\omega_\rho l_\rho^3 = 25$, $\beta = -0.28$.

## 3.4. Summary

Summarizing, interlayer effects are a fundamentally new feature introduced by the DDI in dipolar gases placed in unconnected layers of an optical lattice. These effects may

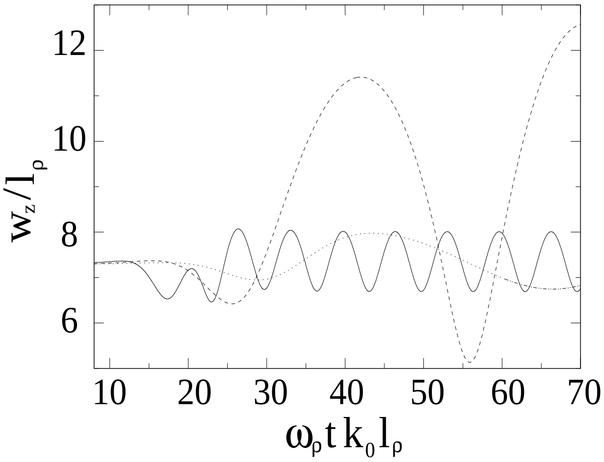

**Figure 3.9.:** Width of a 1D soliton for $x_0 = 3l_\rho$, $g/2\pi\hbar\omega_\rho l_\rho^3 = 25$, $\beta = 0.28$, and $k_0 l_\rho = 0.05$ (solid), 0.168 (dashed), 0.35 (dotted). $\omega_\rho$ ($_\rho$) is the transversal oscillator frequency (length). The time has been re-scaled for comparison.

have remarkable consequences, as e.g. the formation of a BEC of filaments [176]. In this chapter we analyzed by means of numerical methods the rich physics introduced by interlayer effects in the nonlinear properties of dipolar BECs, and in particular in the scattering of unconnected solitons. The DDI induces an inelastic soliton-soliton scattering, that for low relative velocities, leads to the inelastic fusion into a soliton molecule. Interestingly, the inelastic losses do not increase monotonically for decreasing relative velocities, but on the contrary show strong resonances at intermediate velocities, at which, after interacting, the soliton widths are strongly modified, eventually leading to soliton destruction. This effect appears, because, due to the relatively low excitation frequencies of the solitons, a resonant coupling between incoming kinetic energy and internal soliton modes is possible for low relative velocities well within the inelastic regime. We have shown that a similar effect should be observable in 1D geometries, where the experimental requirements may be easily fulfilled in on-going Chromium experiments. Finally, we have considered the 2D scattering of dipolar solitons, a unique possibility offered by the dipolar interactions in cold gases. We have shown that due to the combination of inelastic trapping and initial angular momentum a spiraling motion is possible, offering fascinating links to similar physics in photorrefractive materials.

# 4. Dark Solitons in Three Dimensional Dipolar Bose-Einstein Condensates

A dark soliton is a localized wavepacket consisting of a notch in the ambient density and a phase slip across its centre. It is supported in repulsive/defocusing nonlinear media where the shape of the wavepacket is preserved by a balance between dispersive kinetic energy and the nonlinearity in the system. It has been thoroughly studied both experimentally and theoretically in the context of non-linear optics [177]. As we have mentioned in Chapter. 1 DSs are dynamically stable only in 1D and are unstable in higher dimensions. DSs poses other instabilities like thermal instability, arising from the interaction with a thermal cloud, that leads to dissipation causing the DS to accelerate to the edge of the BEC and disappear [178]. Slow solitons are sensitive to quantum fluctuations aswell [179].

We are particularly interested in the dynamical instability of DSs. In 2D and 3D they are prone to transverse instabilities [180, 181, 182], and bend like a snake, finally decaying into vortices in both BECs [183] and nonlinear optics [184]. In the context of BEC this is used as a way to produce both vortices and anti-vortices [183], which is not possible with the usual stirring techniques. A sufficiently tight transverse confinement could prevent this dynamical instability [185]. Another kind of dynamical instability arises from the fact that DSs are solutions of a homogeneous system, and hence the presence of external confinement breaks the integrability. This leads to instability of soliton via sound emission while moving through the inhomogeneous background density [186, 187].

In this chapter we focus on stationary DSs in dipolar BECs. In a 3D system a standing DS has the form of a planar node, and in 2D it is a line or a band. Another way to create higher dimensional DSs is to wrap a 3D or a 2D DS around on itself. In 2D it takes the form of a nodal ring, termed as dark ring soliton, and in 3D it is a nodal spherical shell, termed as spherical shell soliton [188, 189]. These objects are always unstable in harmonic traps, but can have lifetimes larger than that of BEC experiments. In this chapter we show that a long-range DDI could stabilize a 3D stationary DS in the presence of a sufficiently strong optical lattices [190].

## 4.1. Dark Solitons in 3D BEC

In this section we briefly discuss the stability of a standing DS in a uniform short-range interacting condensates [185]. Consider a homogeneous BEC, with repulsive inter-atomic interaction ($g > 0$) and a condensate homogeneous density of $n_0$. The chemical potential

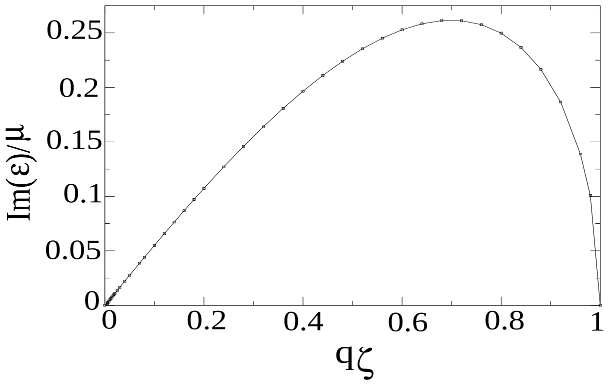

**Figure 4.1.:** Numerical results for the imaginary part of the excitation energies of a nodal plane.

of the system, $\mu = gn_0$, and we define the healing length $\zeta = \hbar/\sqrt{m\mu}$. Now, we assume a stationary DS along the $z$ direction, or in other words a nodal $xy$ plane at the centre of the condensate. The stationary solution of such a system is provided by the following time-independent GP equation:

$$\mu\Psi_0(z) = \left[-\frac{\hbar^2}{2m}\frac{\partial^2}{\partial z^2} + g|\Psi_0(z)|^2\right]\Psi_0(z), \tag{4.1}$$

where $g = 4\pi\hbar^2 a/m$. The Eq. (4.1) exhibits a simple solution describing the DS in the $z$ direction as

$$\Psi_0(z) = \sqrt{n_0}\tanh(z/\zeta). \tag{4.2}$$

The stability of the solution (4.2) is analyzed by means of Bogoliubov theory. We consider the small amplitude modulations in nodal plane in the form: $\chi(\vec{r},t) = u(z)\exp[i(\vec{q}\cdot\vec{\rho} - \epsilon t/\hbar)] + v(z)^*\exp[-i(\vec{q}\cdot\vec{\rho} - \epsilon^* t/\hbar)]$, where $q$ is the momentum of the transverse mode with energy $\epsilon$ and the eigen wavefunctions $u$ and $v$. Introducing this ansatz into (4.1) and linearizing in $\chi$, one obtains the Bogoliubov-de Gennes (BdG) equations for the excitation energies $\epsilon$ and the corresponding eigenfunctions $f_\pm = u \pm v$:

$$\epsilon f_-(z) = \left[-\frac{\hbar^2}{2m}\left(\frac{\partial^2}{\partial z^2} - q^2\right) + g|\Psi_0(z)|^2 - \mu\right] f_+(z) \tag{4.3}$$

$$\epsilon f_+(z) = \left[-\frac{\hbar^2}{2m}\left(\frac{\partial^2}{\partial z^2} - q^2\right) + 3g|\Psi_0(z)|^2 - \mu\right] f_-(z) \tag{4.4}$$

The lowest eigenvalue $\epsilon(q)$ for each $q$ provides the dispersion law. It is found that the excitation spectrum $\epsilon(q)$ is purely imaginary for $q\zeta < 1$, as shown in the Fig. (4.1). The presence of imaginary modes, which grows exponentially in the systems, indicates the dynamical instability of the DS. Because of this instability, the nodal plane acquires a characteristic snake-like bending, known as *snake instability* (see Fig. (4.2)). A subsequent decay of the DS into more stable structures as vortex rings and sound excitations has been observed experimentally [183].

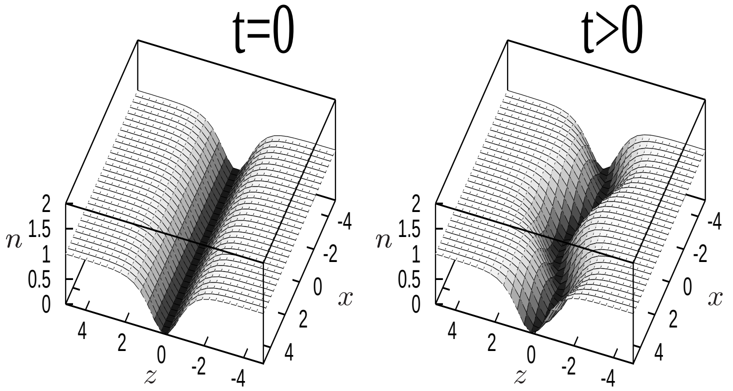

**Figure 4.2.:** Density plot of the Snake Instability: The Dark Soliton at $t = 0$ starts to oscillate and eventually breaks.

## 4.2. Dark Solitons in Dipolar BEC

In the following, we study the dynamical stability of DSs in a three-dimensional dipolar BEC. We show that the long-range character of the DDI may have striking consequences for the stability of DSs in dipolar BECs. Contrary to usual BECs, for which, as mentioned above, DSs become unstable when departing from the 1D condition, the DDI may stabilize DSs in a 3D environement. This stabilization is purely due to the long-range and anisotropic characters of the DDI. We study in detail the conditions for this stabilization, and the stabilization regimes.

### 4.2.1. Model of the Problem

In the following, we consider a dipolar BEC in a 2D optical lattice, and with no other external confinements. At sufficiently low temperatures the system is described by the non-local non-linear Schrödinger equation (NLSE):

$$\begin{aligned} i\hbar\frac{\partial}{\partial t}\Psi(\vec{r},t) = &\left[-\frac{\hbar^2}{2m}\nabla^2 + V_{ol}(x,y) + g|\Psi(\vec{r},t)|^2\right.\\ &\left.+\int d\vec{r}' V_d(\vec{r}-\vec{r}')|\Psi(\vec{r}',t)|^2\right]\Psi(\vec{r},t), \end{aligned} \tag{4.5}$$

where $g = 4\pi\hbar^2 a/m$, with $a$ the $s$-wave scattering length and $m$ the particle mass. For reasons that will become clear below, the BEC is assumed to be in a 2D optical lattice,

$$V_{ol}(x,y) = sE_R\left[\sin^2(q_l x) + \sin^2(q_l y)\right], \tag{4.6}$$

where $E_R = \hbar^2 q_l^2/2m$ is the recoil energy, $q_l$ is the laser wave vector and $s$ is the dimensionless parameter providing the lattice depth.

### 4.2.2. Lattice Calculations

In the tight-binding regime (i.e. for a sufficiently strong lattice but still maintaining the coherence), we may write

$$\Psi(\vec{r},t) = \Sigma_{i,j} w_{ij}(x,y)\psi_{i,j}(z,t), \tag{4.7}$$

where $w_{ij}(x,y)$ are the Wannier functions associated to the lowest energy band in the 2D periodic potential and the site located at $(bi, bj)$, with $b = \pi/q_l$. Hence, the discrete GP equation reads as [191]

$$\begin{aligned} i\hbar\frac{\partial\psi_{ij}(z,t)}{\partial t} &= -J(\psi_{i+1,j}(z,t) + \psi_{i-1,j}(z,t) + \psi_{i,j+1}(z,t) + \psi_{i,j-1}(z,t)) \\ &-\frac{\hbar^2}{2m}\frac{\partial^2}{\partial z^2}\psi_{ij}(z,t) + \bar{g}|\psi_{ij}(z,t)|^2\psi_{ij}(z,t) + V_{dd}(z,i,j,t)\psi_{ij}(z,t) \end{aligned} \tag{4.8}$$

where

$$J = -\int w(x+b)^* w(y)^* \left[-\frac{\hbar^2}{2m}\left(\frac{\partial^2}{\partial x^2} + \frac{\partial^2}{\partial y^2}\right) + V_{\text{ext}}(x,y)\right] w(x)w(y)dxdy,$$

$$n_{ij}(z,t) = |\psi_{ij}(z,t)|^2,$$

$$f_{ij}(x,y) = f(x-bi, x-bj) = [w(x-bi)w(y-bj)]^2,$$

$$\bar{g} = g\int |f(x,y)|^2 dxdy,$$

and

$$V_{dd}(z,i,j,t) = \int V_d(\vec{r}-\vec{r}')\sum_{i'j'} n_{i'j'}(z',t) f_{i'j'}(x',y') d^3r' f_{ij}(x,y)dxdy \tag{4.9}$$

In deriving the interaction term we made the following approximation: $w(x+bi)w(x+bi')w(y+bj)w(y+bj') \approx \delta_{ii'}\delta_{jj'}f(x+bi, y+bj)$. Using the convolution theorem the DDI term can be written as

$$\begin{aligned} V_{dd}(z,i,j,t) &= \frac{1}{(2\pi)^3}\int d^3k \tilde{V}_d(\vec{k})|\tilde{f}(k_x,k_y)|^2 \times \\ &\times \sum_{i,'j'} \tilde{n}_{i'j'}(k_z)\exp\left[ik_x b(i-i') + ik_y b(j-j') + ik_z z\right], \end{aligned} \tag{4.10}$$

where $\tilde{V}(\vec{k})$, $\tilde{f}(k_x,k_y)$, and $\tilde{n}_{ij}(k_z)$ denote the the Fourier transform of $V(\vec{r})$, $f(x,y)$, and $n_{ij}(z)$, respectively. We define the discrete Fourier transform

$$\tilde{\mathtt{n}}(\vec{k}) = \sum_{ij}\exp\left[-ik_x bi - ik_y bj\right]\tilde{n}_{ij}(k_z) \tag{4.11}$$

which fulfills

1. $\tilde{\mathtt{n}}(k_x + 2\pi n/b, k_y + 2\pi m/b, k_z) = \tilde{\mathtt{n}}(k_x, k_y, k_z)$ with $n, m = 0, \pm1, \pm2, ...$

2. $\left(\frac{b}{2\pi}\right)^2 \int_{IBZ} \tilde{\mathtt{n}}(\vec{k}) \exp\left[ik_x bi + ik_y bj\right] dk_x dk_y = \tilde{n}_{ij}(k_z)$

where $IBZ$ is the first Brillouin zone $[(-\pi/b, \pi/b) \times (-\pi/b, \pi/b)]$. In the dipolar term (4.11), we split the integral of $k_x$ and $k_y$ in the following way

$$\int_{-\infty}^{+\infty} F(k_x, k_y) \exp\left[ik_x bi + ik_y bj\right] dk_x dk_y = \tag{4.12}$$

$$\sum_{nm} \int_{IBZ} F(k_x + 2\pi n/b, k_y + 2\pi m/b) \exp\left[ik_x bi + ik_y bj\right] dk_x dk_y$$

and we obtain

$$V_{dd}(z, j) = \int_{IBZ} \tilde{\mathcal{V}}(k) \tilde{\mathtt{n}}(k) \exp\left[ik_x bi + ik_y bj + ik_z z\right] d^3k \tag{4.13}$$

with

$$\tilde{\mathcal{V}}(k) = \sum_{nm} \tilde{V}(k_x + 2\pi n/b, k_y + 2\pi m/b, k_z) |\tilde{f}(k_x + 2\pi n/b, k_y + 2\pi m/b)|^2 \tag{4.14}$$

We assume that $b$ is the smallest scale of distance. Since the soliton core has a size of the order of the healing length, then the dominant contribution is provided by $k_z \sim 1/\xi$, where $\xi$ is the healing length. We assume $b \ll \xi$. In addition, we will be interested in $k_x, k_y$ momenta $q$ such that $q \sim 1/\xi$. Hence for $n, m \neq 0$, $\tilde{V}(k_x + 2\pi n/b, k_y + 2\pi m/b, k_z) \simeq \tilde{V}(2\pi n/b, 2\pi m/b, 0) = -g_d/2$. Then

$$\tilde{\mathcal{V}}(k) = \tilde{V}(k) |\tilde{f}(k_x, k_y)|^2 + \mathcal{C}_{dd}(k_x, k_y) \tag{4.15}$$

$$\begin{aligned}
\mathcal{C}_{dd}(k_x, k_y) &= g_d \sum_{m \neq 0} |\tilde{f}(k_x + 2\pi n/b, k_y + 2\pi m/b)|^2 \\
&\approx g_d \sum_{n,m \neq 0} \exp\left[-(k_x + 2\pi n/b)^2 \sigma^2/2\right] \exp\left[-(k_y + 2\pi m/b)^2 \sigma^2/2\right] \approx \\
&\approx g_d \sum_{n,m \neq 0} \exp\left[-(2\pi n/b)^2 \sigma^2/2\right] \exp\left[-(2\pi m/b)^2 \sigma^2/2\right] = \\
&= g_d (\Theta_3\left(0, \exp\left[-2\pi^2 \sigma^2/b^2\right]\right) - 1)^2 \equiv \mathcal{G}_d. 
\end{aligned} \tag{4.16}$$

where $\Theta$ is the elliptic theta function. In the previous expressions we have assumed a Gaussian form (with width $\sigma \simeq b/\pi s^{1/4}$ with $s = V_0/E_R$ (see Chapter 1)) for the function $f$; it is known that it gives good results for the interaction term. The final form of the discrete GPE reads

$$\begin{aligned}
i\hbar \frac{\partial \psi_{ij}(z,t)}{\partial t} &= -J(\psi_{i+1,j}(z,t) + \psi_{i-1,j}(z,t) + \psi_{i,j+1}(z,t) + \psi_{i,j-1}(z,t)) \\
&\quad - \frac{\hbar^2}{2m} \frac{\partial^2}{\partial z^2} \psi_{ij}(\rho, t) + \tilde{g} |\psi_{ij}(z,t)|^2 \psi_{ij}(z,t) \\
&\quad + \int_{IBZ} \tilde{V}(\vec{k}) |\tilde{f}(k_x, k_y)|^2 \tilde{\mathtt{n}}(\vec{k}, t) \exp\left[ik_x bi + ik_y bj + ik_z z\right] \frac{d^3k}{(2\pi)^3} \psi_{ij}(z,t)
\end{aligned}$$

where we redefine the contact interaction

$$\tilde{g} = \bar{g} + \frac{\mathcal{G}_d}{b^2} \tag{4.17}$$

### 4.2.3. Effective continuous model - coarse-grained

Since we will consider (in our Bogoliubov analysis) $k_z \ll \pi/b$, then we can actually re-write an effective continuous model. To this aim we rewrite the tunneling part as [192]

$$\begin{aligned} -J(\psi_{i+1,j} + \psi_{i-1,j} + \psi_{i,j+1} + \psi_{i,j-1} - 4\psi_{i,j}) &\to -Jb^2\left(\partial_x^2 + \partial_y^2\right)\psi \\ &= -\frac{\hbar^2}{2m^*}\left(\partial_x^2 + \partial_y^2\right)\psi, \end{aligned} \tag{4.18}$$

where we have employed the effective mass associated to the lowest band $E(\kappa) = -2J(\cos\kappa_x b + \cos\kappa_y b)$ at quasi-momentum $\kappa = 0$, namely $\hbar^2/2m^* = Jb^2$. We added the term $4J\psi_{i,j}$ which it only shifts the chemical potential. We redefine

$$\frac{1}{b}\psi_{ij}(\rho) \to \psi(\vec{r}), \tag{4.19}$$

where now $\psi(\vec{r})$ is the new coarse-grained wave function. As a consequence

$$\tilde{g}n_{i,j}(z) \to \tilde{g}n(\vec{r}) \tag{4.20}$$

where $b^2\tilde{g} \to \tilde{g}$ and $n_{i,j}(z)/b^2 \to n(\vec{r})$ and

$$\int_{IBZ} \tilde{V}(\vec{k})|\tilde{f}(k_x,k_y)|^2\tilde{\mathrm{n}}(\vec{k})\exp\left[ik_xbi + ik_ybj + k_zz\right]d^3k \to \int \tilde{V}(\vec{k})\tilde{n}(\vec{k})\exp\left[i\vec{k}\vec{r}\right]d^3k. \tag{4.21}$$

In this expression we have employed that since, as discussed above, we will consider that at most $k_z \sim 1/\xi$, and $\xi \gg \sigma$, then $|\tilde{f}(k_x,k_y)| \simeq 1$. In conclusion, the effective continuous GPE (which we employ in the following) reads:

$$\begin{aligned} i\hbar\frac{\partial\Psi(\vec{r},t)}{\partial t} &= \left[-\frac{\hbar^2}{2m^*}\left(\frac{\partial^2}{\partial x^2} + \frac{\partial^2}{\partial y^2}\right) - \frac{\hbar^2}{2m}\frac{\partial^2}{\partial z^2} + \tilde{g}n(\vec{r},t)\right]\Psi(\vec{r},t) + \\ &+ \frac{1}{(2\pi)^3}\int \tilde{V}(\vec{k})\tilde{n}(\vec{k},t)\exp(i\vec{k}\cdot\vec{r})d^3k\Psi(\vec{r},t) \end{aligned} \tag{4.22}$$

where

$$\tilde{g} = gb^2\int |f(x,y)|^2dxdy + \mathcal{G}_d \approx \frac{g}{2\pi}\left(\frac{b}{\sigma}\right)^2 + g_d(\Theta_3\left(0, \exp\left[-2\pi^2\sigma^2/b^2\right]\right) - 1)^2, \tag{4.23}$$

where in the latest equation we assumed, as above, a Gaussian approximation for the Wannier function.

### 4.2.4. Time-independent Solution

We assume that the DS lies on the $xy$ plane, hence the solution can be written as: $\Psi_0(\vec{r},t) = \psi_0(z)\exp[-i\mu t/\hbar]$, where $\mu$ is the chemical potential. Introducing this expression into Eq. (4.22) we obtain a 1D time-independent NLSE in $z$ of the form:

$$\mu\psi_0(z) = \left[-\frac{\hbar^2}{2m}\frac{\partial^2}{\partial z^2} + \bar{g}|\psi_0(z)|^2\right]\psi_0(z). \tag{4.24}$$

Since $\psi_0$ is independent of $x$ and $y$, in Eq. (1.8) the DDI just regularizes the value of the local coupling constant $\bar{g} = \tilde{g} + g_d$. Eq. (1.8) allows for a simple solution describing a DS, $\psi_0 = \sqrt{n_0}\tanh(z/\zeta)$, where $\zeta = \hbar/\sqrt{m\bar{g}n_0}$ is the corresponding healing length and $n_0$ is the bulk density. In the following we use the dimensionless parameter $\beta = g_d/\tilde{g}$.

### 4.2.5. Bogoliubov Excitations

In order to study the dynamical stability of the DS, we do the Bogoliubov analysis by considering a transversal perturbation in the nodal plane of the form: $\Psi(\vec{r},t) = \Psi_0(\vec{r},t) + \chi(\vec{r},t)\exp(-i\mu t/\hbar)$, where $\chi(\vec{r},t) = u(z)\exp[i(\vec{q}\cdot\vec{\rho} - \epsilon t/\hbar)] + v(z)^*\exp[-i(\vec{q}\cdot\vec{\rho} - \epsilon^* t/\hbar)]$, where $q$ is the momentum of the transverse modes with energy $\epsilon$. Introducing this ansatz into (4.5) and linearizing in $\chi$, one obtains the Bogoliubov-de Gennes (BdG) equations for the excitation energies $\epsilon$ and the corresponding eigenfunctions $f_\pm = u \pm v$:

$$\begin{aligned}\epsilon f_-(z) &= \left[-\frac{\hbar^2}{2m}\left(\frac{\partial^2}{\partial z^2} - \frac{m}{m^*}q^2\right) - \mu + 3\bar{g}\psi_0(z)^2\right]f_+(z)\\ &\quad -\frac{3}{2}g_d q\psi_0(z)\int_{-\infty}^{\infty}dz'\exp(-q|z-z'|)\psi_0(z')f_+(z'), \qquad (4.25)\\ \epsilon f_+(z) &= \left[-\frac{\hbar^2}{2m}\left(\frac{\partial^2}{\partial z^2} - \frac{m}{m^*}q^2\right) - \mu + \bar{g}\psi_0(z)^2\right]f_-(z) \qquad (4.26)\end{aligned}$$

The lowest eigenvalue $\epsilon(q)$ for each $q$ provides the dispersion law. Note that the DDI has two main effects: (i) it leads to a regularized $\bar{g}$, and (ii) it introduces a qualitatively new term in the second line of Eq. (4.25). Whereas the first effect leads to a quantitative modification of the DS width since it modifies the healing length $\zeta$, the second effect is a purely dipole-induced non local effect, which, as we show below, may lead to remarkable consequences for the DS stability.

When $\beta = 0$ (no DDI) and $m/m^* = 1$ (no lattice), we recover the BdG equations: (4.3) and (4.4), obtained in the case of standard short-range interacting BECs. It has been shown [185] that in that case the dispersion law $\epsilon(q)$ is purely imaginary for $q\zeta < 1$ (Fig. 4.1). Hence DSs in homogeneous 3D short-range interacting BECs, are dynamically unstable against transverse modulations. Due to this instability the nodal plane acquires a characteristic snake-like bending. As we discussed before it is called the *snake instability* (see Fig. 4.2) and has been experimentally observed in non linear optics [193, 184] and recently in the context of BEC [183]. In the latter case,

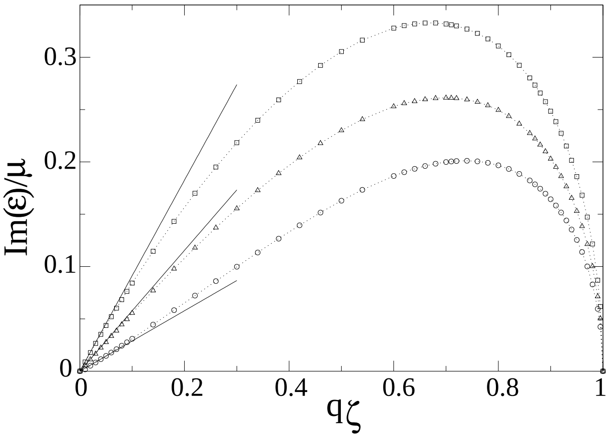

**Figure 4.3.:** Numerical results for the imaginary part of the excitation energies of a DS for $m/m^* = 1$, and $\beta = 0$ (triangles), $-0.5$ (squares) and 1 (circles). Solid lines correspond to the analytical result for low momenta.

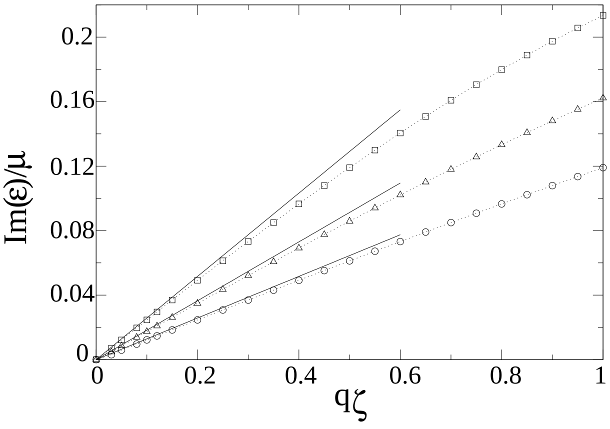

**Figure 4.4.:** Numerical results for the imaginary part of the excitation energies of a DS for $\beta = 0$, and $m/m^* = 0.2$ (squares), 0.1 (triangles) and 0.05 (circles). Solid lines correspond to the analytical result for low momenta.

the bending results in the decay of a DS into vortex rings and sound excitations [180]. In the presence of a 2D lattice, we found that the DS remains dynamically unstable [see Fig. (4.4)]. The lattice is taken into account through the effective mass. We have obtained the Bogoliubov excitation spectrum for different lattice strengths as shown in Fig. (4.4). It is found that the imaginary modes still remain in the system even in the presence of an optical lattice, hence conveying the message that a lattice alone cannot stabilize a stationary DS.

In the presence of DDI ($\beta \neq 0$) but without lattice ($m/m^* = 1$), the transverse instability persists, since $\epsilon(q)$ remains imaginary for $q\zeta < 1$. For $\beta > 0$ ($\beta < 0$), $|\epsilon(q)|$ decreases (increases) when $|\beta|$ grows [Fig. (4.3)]. The situation can change dramatically in the presence of both the DDI and an optical lattice in the $xy$ plane. Surprisingly, for sufficiently large dipoles and small $m/m^*$, $\epsilon(q)$ becomes real and hence the dark soliton

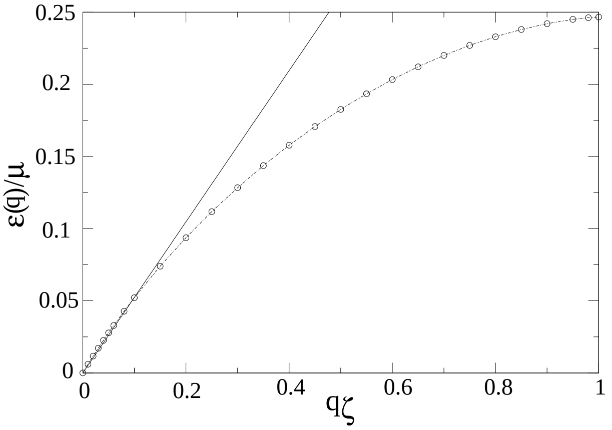

**Figure 4.5.:** Real part of the excitation energies of a DS for $m/m^* = 0.1$, and $\beta = 1.6$. Solid line corresponds to the analytical result for low momenta while empty circles correspond to numerical results.

becomes dynamically stable [see Fig. (4.5)]. This remarkable fact can be understood by analyzing the surface tension of the nodal plane.

### 4.2.6. Variational Analysis

In this section we introduce a variational approach to calculate the lowest modes of a dark soliton. We notice that for low momenta, the Bogoliubov excitations $\epsilon(q)$ is always linear in $q$, suggesting the idea that for low momenta, the nodal plane may be described by an elastic model with Lagrangian density:

$$\mathcal{L}(\partial\phi/\partial t, \vec{\nabla}\phi) = (M/2)\,(\partial\phi/\partial t)^2 - (\sigma/2)|\vec{\nabla}\phi|^2, \tag{4.27}$$

where $\phi$ is the displacement field of the nodal plane from the ground state, $M$ is the mass per unit area and $\sigma$ plays the role of a surface tension of the nodal plane. The eigen frequencies of the Lagrangian (4.27) are,

$$\omega = \sqrt{\frac{\sigma}{M}}\; q. \tag{4.28}$$

Hence by analyzing the nature of term $\sqrt{\sigma/M}$, one could study the stability of the lowest phonon modes in the nodal plane. By expanding the energy of a moving soliton up to second order in the velocity, we obtain the soliton mass $M = -4\hbar n_0/c$, where $c = \sqrt{\bar{g}n_0/m}$ is the sound velocity. Note that $M < 0$. Since the mass is negative, the stability of the phonon modes require $\sigma > 0$, otherwise the modes (4.28) become purely imaginary. We calculate $\sigma$ by inserting a variational ansatz of the form:

$$\Psi_{\text{var}}(\vec{r}) = \sqrt{n_0}\tanh[(z - \sqrt{2}\alpha\cos(qx))/\zeta], \tag{4.29}$$

in the energy functional of a dark soliton with DDI,

$$E = \int d\vec{r} \left[ \frac{\hbar^2}{2m} |\nabla \Psi_{var}|^2 + \frac{\bar{g}}{2} \left( |\Psi_{var}(\vec{r})|^2 - n_0 \right)^2 \right.$$
$$\left. + \int d\vec{r}' V_d(\vec{r} - \vec{r}') \left( |\Psi_{var}(\vec{r}', t)|^2| - n_0 \right) \left( \Psi_{var}(\vec{r}, t)|^2 - n_0 \right) \right]. \tag{4.30}$$

Eq. (4.29) represents a transverse modulation of the nodal plane with amplitude $\alpha$ and momentum $q$. The dipolar part of the energy is again calculated by employing the convolution theorem and hence the Fourier transform of the DDI, and for small amplitude $\alpha$ one obtain the energy of a dark soliton with modulation:

$$E = E_0 + E_1 \tag{4.31}$$

with

$$E_0 = \frac{2\hbar^2 n_0}{3\zeta m} + \frac{2\bar{g} n_0^2 \zeta}{3} \tag{4.32}$$

and

$$E_1 = \frac{2\hbar^2 \alpha^2 n_0}{3\zeta m} q^2 - \frac{3\pi}{8} g_d n_0^2 \zeta^2 \alpha^2 q^2 \int dk_z \frac{k_z^4}{(q^2 + k_z^2)\sinh(k_z \zeta \pi/2)}, \tag{4.33}$$

where $E_0$ is the energy of a dark soliton without the modulation in the nodal plane and $E_1$ provides the energy associated with the small amplitude modulations in the nodal plane. Since we are interested in the energy associated with the modes $q \to 0$, the integral in the Eq. (4.33) is estimated upto the second order in $q$, and also taking into account the optical lattice in the $xy$ plane, which replaces $m$ by $m^*$ in Eq. (4.33), we finally obtain

$$E_1 \approx \left( \frac{2\hbar^2 \alpha^2 n_0}{3\zeta m^*} - g_d n_0^2 \zeta \right) \alpha^2 q^2. \tag{4.34}$$

By assuming the ansatz (4.29) in the Lagrangian (4.27), one obtains the energy associated with linear excitations,

$$E_L = \frac{\sigma}{2} \alpha^2 q^2. \tag{4.35}$$

By equating Eqs. (4.34) and (4.35), we obtain the expression for the surface tension of the nodal plane,

$$\sigma = \frac{4 n_0 \hbar^2}{3\zeta m^*} - 2 g_d n_0^2 \zeta \tag{4.36}$$

Then the eigenmodes:

$$\epsilon^2/\hbar^2 = \omega^2 = (\sigma/M) q^2, \tag{4.37}$$

which provide the low energy linear excitations of the dark soliton, can be either purely real or purely imaginary, crucially depending on the sign of $\sigma/M$. In the absence of DDI ($\beta = 0$), $\sigma$ is always positive, the modes are purely imaginary, and hence the DS shows snake instability for any value of $m/m^*$ (see Fig. (4.4)). The stabilization hence is a characteristic feature introduced by the DDI. Note that for $\beta = 0$ and $m/m^* = 1$ our analytical result coincides with the one found in Ref. [185], where the linear excitations are found to be $\epsilon(q \to 0) = q\zeta/3$. In the absence of an additional optical lattice, the dynamical instability of the DS at low $q$ dissapears for $\beta > 2$, i.e. for situations for which the homogeneous dipolar BEC as a whole is itself unstable against local collapses. Such instability, which we termed as the phonon-instability, will be discussed in detail in Chapter. 5. Increasing the depth of the lattice potential reduces the role of the kinetic energy term $(m/m^*)q^2$ in Eqs. (4.25) and (4.26) (or equivalently reduces the first term in Eq. (4.36)) and hence enhances the role of DDI. A sufficiently large DDI or small $m/m^* < (m/m^*)_{cr} = 3\beta/2(1+\beta)$ leads to stable low-energy($q \to 0$) linear excitations. We have confirmed that this analytical result coincides with our results obtained from BdG Eqs. (4.25) and (4.26). When $m/m^*$ decreases further or $\beta$ grows, a wider regime of momenta up to $q\sqrt{m/m^*}\zeta \sim 1$ is stabilized [Fig. (4.5)]. Indeed, direct numerical simulations of 3D GP equation show that the dark nodal plane becomes completely stable against snake instability, whereas under the same conditions the DS is unstable in the absence of DDI. Instabilities may appear for momenta $q\sqrt{m/m^*}\zeta \sim 1$, but this large-momentum instability is typically irrelevant, since for sufficiently small $m/m^*$ it concerns momenta much larger than the lattice momentum. Although our effective mass theory breaks down for such momenta, it becomes clear that such high momentum instabilities are physically prevented by the zero point oscillations at each lattice site [1]

## 4.3. Summary

Summarizing, contrary to short-range interacting BECs, where snake instability is just prevented by a sufficiently strong transverse confinement, dipolar BECs allow for stable dark solitons of arbitrarily large transversal sizes. Dissipation would eventually lead to thermodynamical instability [182] whose detailed analysis, as well as that of quantum instabilities [194], demands a separate work. We have obtained the stability conditions, which demand a sufficiently large dipole and a sufficiently deep optical lattice in the nodal plane. We stress, that the stabilization of nodal planes against snake instability is purely linked to the long-range nature of the DDI, opening a qualitatively new scenario in non linear atom optics.

---

[1] The lattice-induced large-momentum cut-off is introduced in our simulations of 3D GP equation is by the numerical grid in the $xy$ plane.

# Part II.

# Phonon-instability in Dipolar BEC

# 5. Phonon-instability in Dipolar Bose-Einstein Condensates

The stability of dipolar BEC is an issue of obvious concern due to the partially attractive character of the DDI. We have discussed the stability of a purely dipolar trapped condensates in Chapter 1. It was shown that the properties of the trapped dipolar BECs crucially depend on the trap geometry [83]. In this chapter, we extend our study to the stability of dipolar BECs by means of Bogoliubov theory and direct numerical simulations, in particular in the case of 2D dipolar BECs [168].

## 5.1. Attractive Short-range Interacting Condensates

Bogoliubov spectrum for the elementary excitations of an attractive short-range interacting homogeneous BECs reads as ,

$$\epsilon(k) = [E_k(E_k + 2g^{(d)}n_0)]^{1/2}, \tag{5.1}$$

where $E_k = \hbar^2k^2/2m$ is the kinetic energy and $g^{(d)}$ provides the interaction for a $d$ dimensional BEC. Since $g^{(d)} < 0$ for an attractive BEC, the linear Bogoliubov excitations ($\epsilon(k \to 0)$) are purely imaginary. Such imaginary modes grow exponentially in time, and lead to the instability of the homogeneous BEC. Since the phonon modes are unstable, we term such instability as phonon-instability (PI). A direct numerical analysis of the GP Eq. (1.6) shows that a homogeneous BEC with short-range attractive interaction is unstable against local collapses in 2D and 3D situations. But in the case of 1D attractive BECs, the low momenta excitations are also purely imaginary, but show a qualitatively different post-instability dynamics. Instead of collapse, the homogeneous BEC is stabilized due to the formation of bright solitons [29, 30, 31].

A 3D attractive BEC may get stabilized in an external trap if the number of atoms in the BEC is below a critical number [195, 196, 28, 197] as we discussed in Chapter 1. The zero-point energy due to confinement act as a barrier against collapse, following the formation of a metastable BEC. Just below the critical number, the atoms tunnel through the barrier and the system collapses spontaneously [198]. The collapse in an attractive BEC can be controlled by means of Feshbach resonances, which are used to tune the interaction from repulsive to attractive [26, 197, 199]. After the tuning of interaction the cloud shrinks and eventually disappeares because the cloud becomes too small. It is observed that a burst of atoms emanates from the remanant BEC during the collapse [26] resembling supernova explosion. It is also found that the collapse is partial

[200, 201], rather than complete. As an interesting feature, numerical simulations of trapped attractive condensates revealed pattern formation once BEC becomes unstable against collapse [202].

## 5.2. Three-dimensional dipolar BECs

We have shown in Chapter 1 that purely dipolar homogeneous BECs are unstable against low momentum excitations similar to the case of short-range attractively interacting condensates. The competition between repulsive short-range interaction and the anisotropic DDI would provide a stability window for the parameter $\beta = g_d/g$ in the case of dipolar BECs, which we discuss below. The 3D homogeneous ($V_{ext}(\vec{r}) = 0$) solution of Eq. (2.1) is $\Psi(\vec{r}, t) = \sqrt{\bar{n}_{3d}} \exp\left[-i\mu_{3d}t/\hbar\right]$, where $\bar{n}_{3d}$ denotes the 3D density, and $\mu_{3d} = (g + \tilde{V}_d(0))\bar{n}_{3d}$ is the chemical potential, with $\tilde{V}_d(\vec{q}) = (4\pi/3)\alpha d^2[3q_z^2/|\vec{q}|^2 - 1]$ the Fourier transform of the DDI for dipoles oriented along the $z$-direction. In the following we assume $g > 0$. A Bogoliubov analysis of the 3D homogeneous BEC provides the dispersion relation for quasiparticles:

$$\epsilon(\vec{q}) = [E_{kin}(\vec{q})[E_{kin}(\vec{q}) + E_{int}(\vec{q})]]^{1/2}, \tag{5.2}$$

where $E_{kin}(\vec{q}) = (\hbar^2 q_\rho^2 + \hbar^2 q_z^2)/2m$ is the kinetic energy, and $E_{int}(\vec{q}) = 2(g + \tilde{V}_d(\vec{q}))\bar{n}_{3d}$ is the interaction energy, which includes both short-range and dipolar parts. Note that $\tilde{V}_d(\vec{q})$ may become negative for some particular directions, and hence for low momenta phonon instability is just prevented if $-3/8\pi < \beta < 3/4\pi$. If $\alpha > 0$, phonons with $\vec{q}$ lying on the $xy$ plane are unstable if $\beta > 3/4\pi$, while for $\alpha < 0$ phonons with $\vec{q}$ along $z$ are unstable if $\beta < -3/8\pi$. In both cases, the dipolar BEC is unstable against local collapses. In the presence of trapping, this instability leads to a global collapse of the BEC, and may be geometrically prevented in sufficiently pancake-shaped traps, as shown recently in [1]. The complex collapse dynamics involves an anisotropic $d$-wave explosion resembling the $d$- wave symmetry of the DDI (see Fig. (5.1)), and an abrupt atom number loss is observed. The experimental results show an excellent agreement with mean-field calculations involving three-body losses.

## 5.3. Two-dimensional Dipolar BECs

Now we study the stability of 2D dipolar BECs with and without the external confinement. In the following we show that the PI is crucially different in 2D. We first consider an homogeneous dipolar BEC in the $xy$ plane, which is strongly confined by an harmonic potential $V(z) = m\omega_z^2 z^2/2$ along the transversal $z$-direction. If the chemical potential $\mu_{2d} \ll \hbar\omega_z$, the system can be considered "frozen" into the ground state $\phi_0(z)$ of $V$ and hence the BEC wave function factorizes as $\Psi(\vec{r}) = \psi(\vec{\rho})\phi_0(z)$. The dipole orientation with respect to the $xy$ plane plays a crucial role in the dynamics of 2D dipolar BECs. In the following we discuss two extremal configurations, in which the dipoles are normal to the $xy$ plane ($\perp$-configuration) and parallel to it (along $x$) ($||$-configuration). In order to

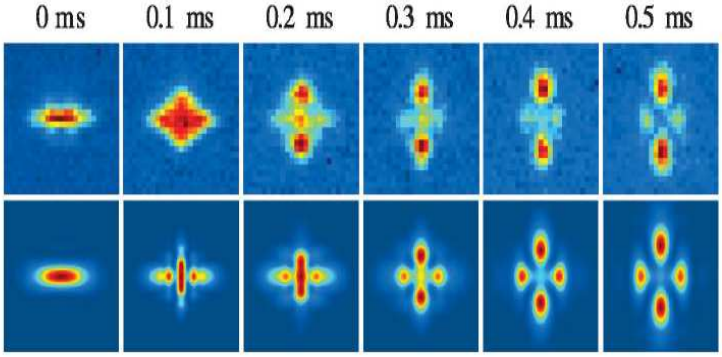

**Figure 5.1.:** Series of images for the collapse dynamics of a dipolar BEC in a 3D trap. Upper row shows the experimental results and lower row shows the results of mean-field numerical calculations for the same set of experimental parameters. The picture is taken from the Ref. [1]

study the dynamics of 2D dipolar BECs we use the reduced 2D GP Eq. (2.2) obtained in Chapter 2:

$$
\begin{aligned}
i\hbar\frac{\partial}{\partial t}\psi(\vec{\rho}) = \Bigg[ & -\frac{\hbar^2}{2m}\nabla_\rho^2 + \frac{g}{\sqrt{2\pi}l_z}|\psi(\vec{\rho})|^2 \\
+ \quad \frac{4\sqrt{\pi}g\beta}{3\sqrt{2}l_z} & \int \frac{d\vec{k}}{(2\pi)^2} e^{i\vec{k}\cdot\vec{\rho}}\tilde{n}(\vec{k})h_{2D}\left(\frac{\vec{k}l_z}{\sqrt{2}}\right)\Bigg]\psi(\vec{\rho}),
\end{aligned}
\tag{5.3}
$$

where $\vec{k}$ is the $xy$-momentum, $\tilde{n}$ the Fourier transform of $|\psi(\vec{\rho})|^2$, $h_{2D}(\vec{\kappa}) = 2-3\sqrt{\pi}\kappa e^{\kappa^2}\mathrm{erfc}(\kappa)$ for $\perp$-configuration, and $h_{2D}(\vec{\kappa}) = -1+3\sqrt{\pi/2}(\kappa_x^2/k)e^{\kappa^2}\mathrm{erfc}(\kappa)$ for $||$-configuration, with $\mathrm{erfc}(\kappa)$ the complementary error function and $l_z = \sqrt{\hbar/m\omega_z}$.

### 5.3.1. Bogoliubov Excitations of a 2D Dipolar BEC

The homogeneous solution of (5.3) is $\psi(\vec{\rho}, t) = \sqrt{\bar{n}_{2d}}\exp[-i\mu_{2d}t/\hbar]$, where $\bar{n}_{2d}$ denotes the homogeneous 2D density, and $\mu_{2d} = g\bar{n}_{2d}(1+8\pi\beta/3)/\sqrt{2\pi}l_z$ is the chemical potential for $\perp$-configuration and $\mu_{2d} = g\bar{n}_{2d}(1-4\pi\beta/3)/\sqrt{2\pi}l_z$ for $||$-configuration. The corresponding Bogoliubov equations provide the dispersion relation for elementary excitations of 2D BEC [203, 204]:

$$
\epsilon(\vec{k})^2 = E_{kin}^2 + \frac{2gn_0E_{kin}}{\sqrt{2\pi}l_z}\left[1 + \frac{4\pi\beta}{3}h_{2D}\left(\frac{kl_z}{\sqrt{2}}\right)\right] \tag{5.4}
$$

where $E_{kin} = \hbar^2|\vec{k}|^2/2m$ is the kinetic energy. In the following we study in detail the stability of 2D dipolar BEC based on the Bogoliubov excitations (5.4).

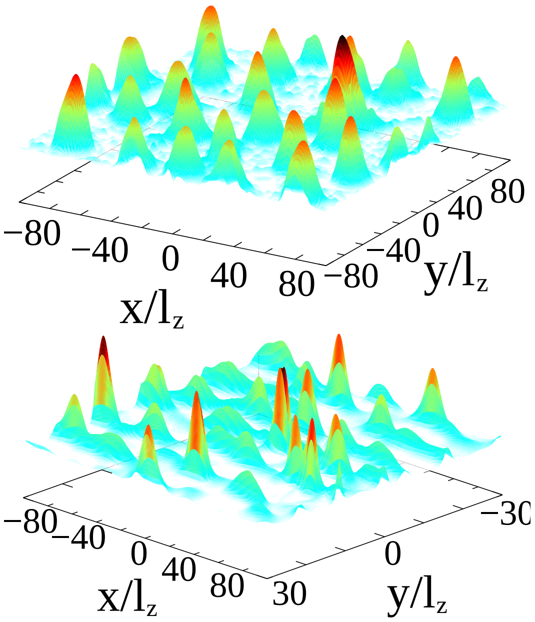

**Figure 5.2.:** 2D soliton gas after phonon instability of an homogeneous dipolar BEC. For both the figures $\mu = -0.2$ and $g/(\sqrt{2\pi} l_z) = 10$. (top) $\perp$-configuration, $\beta = -0.2$, $t = 484/\omega_z$; (bottom) $||$-configuration, $\beta = 0.3$, and $t = 108/\omega_z$.

### 5.3.2. Dipoles Normal to the Plane

We discuss first the $\perp$-configuration where the dipoles are oriented perpendicular to the $xy$ plane. From (5.4) we see that the excitations with $\vec{k} \to 0$ become purely imaginary if $\beta < -3/8\pi$, i.e. phonon-instability demands the tuning of the DDI using the rotating-orienting fields [100]. We recall from Chapter. 2 that the stable 2D isotropic bright solitons are possible for $g > 0$ if $\beta < -3/8\pi$ [152]. That means that the conditions for phonon-instability and soliton stability are exactly identical. This fact, far from being accidental, shows that PI and 2D soliton formation are intrinsically linked.

Using Eq. (5.3), we have numerically studied the post-PI dynamics by employing periodic boundary conditions. In all our simulations, we check that $\tilde{\mu}_{2d} = \mu_{2d}/\hbar\omega_z \ll 1$ to ensure the 2D character of the problem. Starting from an homogeneous solution with an overimposed random noise provided by a tiny random local phase ($< 10^{-4}\pi$), our real time simulations show the dynamical formation of a soliton gas, Fig. (5.2) (top). The long-range character of the DDI leads to an attractive soliton-soliton interaction (since $\beta < 0$). As discussed in Ref. [173] the soliton-soliton scattering is inelastic, and for low relative velocities (as it is the case in the soliton gas) soliton fusion is expected. This is indeed observed, and hence the number of solitons decreases in time, whereas the number of particles per soliton increases. As long as the problem remains 2D, the isotropic solitons remain stable (contrary to the anisotropic solitons discussed below). However, the density within a given soliton may eventually become large enough to violate the 2D condition $\tilde{\mu}_{2d} \ll 1$. In that case the soliton becomes unstable against 3D collapse [152] as we discussed in Chapter. 2.

### 5.3.3. Dipoles Parallel to the Plane

The $||$-configuration shows a relatively similar physics. From Eq. (5.4) we see that the Bogoliubov excitations $\epsilon(\vec{k} \to 0)$ becomes unstable if $\beta > 3/4\pi$. This condition is exactly that found recently in Ref. [153] for the stability of 2D anisotropic bright solitons, whose properties were discussed in Chapter 2. Unlike isotropic solitons, anisotropic solitons undergo collapse once the number of atoms surpasses a critical number [168], a crucial point concerning possible experiments which we discuss below.

Using Eq. (6.4), and starting once more from an homogeneous gas, we have observed the dynamical formation of a gas of anisotropic solitons, after the initial formation of stripes along the dipole axis (Fig. (5.2), bottom). Due to the anisotropic nature of DDI in the plane, the inelastic dynamics of anisotropic solitons is relatively more complicated. Solitons along the $x$ axis attract each other, fuse together and become unstable against 2D collapse once they surpass the critical number of particles per soliton.

### 5.3.4. Trapped 2D dipolar BECs

Now we consider an harmonic trap on the $xy$-plane of the form $V(\rho) = m\omega_\rho^2\rho^2/2$. As an initial condition for our time evolution, we employed a dipolar BEC in the Thomas-Fermi regime (sufficiently large $g$), obtained for the $\perp$-configuration with $\beta > 0$ (no phonon-instability) by imaginary time evolution of Eq. (5.3). As above we multiply the wavefunction by a tiny random phase. In order to trigger the phonon-like instability in our real time evolutions, at time $t = 0$ we may either switch to $\beta < 0$ (which keeps the polar symmetry) or tilt the dipole switching into the $||$-configuration (hence violating the polar symmetry). We call these two cases, cases (i) and (ii).

Figs. (5.3) illustrate the case (i). The phonon-like instability leads to transient ring-shaped structures. The formed ring structures resemble to those found in pre-collapse dynamics of an attractive short-range interacting BEC [202]. The harmonic trap leads to successive shrinkings and expansions of the rings, which oscillate in the trap. This process continues until the rings merge into a single excited soliton. We have observed that for sufficiently shallow traps the ring structures develop azimuthal instability, which again leads to the formation of 2D bright solitons, recovering, as expected, the homogeneous case. The case (ii) is illustrated in Figs. (5.4). An initial anisotropic ring-like structure breaks into a pair of anisotropic clouds, which eventually merge into the trap center forming a single stable bright soliton, which as expected is anisotropic, being more elongated in the dipole $x$-direction. Note that for both (i) and (ii) the non-dissipative character of the problem implies that the solitons are produced in an excited internal state.

Now, we comment on possible experimental realizations. PI for dipoles lying on the trap plane (and hence anisotropic solitons [153]) does not require tuning, which may be experimentally demanding. Hence, 2D post-PI dynamics should be relatively easy to observe in on-going experiments. A possible path would be to prepare a 2D stable

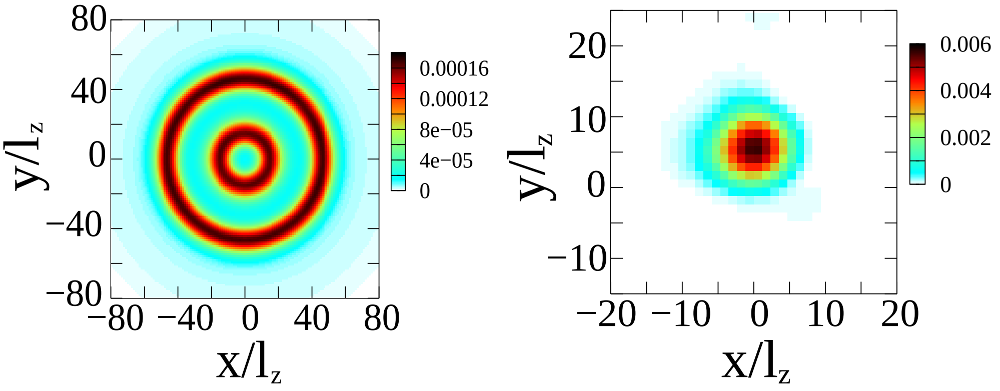

**Figure 5.3.:** Trapped BEC in the ⊥-configuration. In the simulations, $\omega_\rho = 0.001\omega_z$, $g/(\sqrt{2\pi}l_z) = 200$ and $\beta = 0.3$ $(t < 0)$ and $-0.3$ $(t > 0)$. (left) Formation of ring structures $(t = 810/\omega_z)$; (right) Final soliton at the trap center $(t = 7500/\omega_z)$.

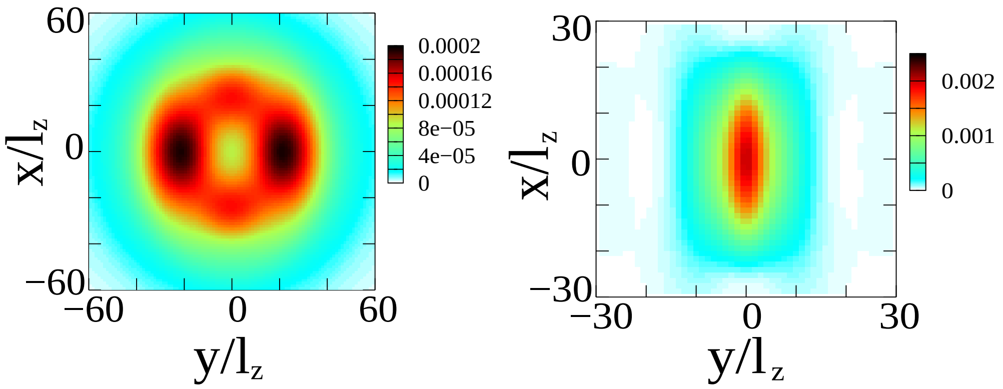

**Figure 5.4.:** Trapped BEC after tilting at $t = 0$ from ⊥ to $||$ configuration, with $\omega_\rho = 0.001\omega_z$, $g/(\sqrt{2\pi}l_z) = 200$ and $\beta = 0.3$. (left) Anisotropic ring formation $(t = 1092/\omega_z)$; (right) Final formation of an anisotropic soliton $(t = 1281/\omega_z)$.

BEC orienting the dipoles perpendicular to the trap plane, and then suddenly re-orient the dipoles on the plane. An equivalent alternative, more feasible experimentally, would be to maintain at any time the dipole on the trap plane, but drive the instability by increasing $\beta$ using Feshbach resonances as in Ref. [1]. As we have shown, the 2D post-PI dynamics should lead to the creation of 2D bright solitons for the first time ever in quantum gases, since they are fundamentally impossible in absence of DDI. 2D solitons would offer new scenarios for the matter-wave soliton scattering (see Chapter 3), as e.g. 2D inelastic scattering and spiraling, similar to that in photorrefractive materials [155].

## 5.4. One-dimensional Dipolar BECs

To complete the discussion on PI in dipolar BECs we briefly mention the post-PI dynamics in 1D dipolar BEC. We consider a dipolar BEC with dipoles polarized along

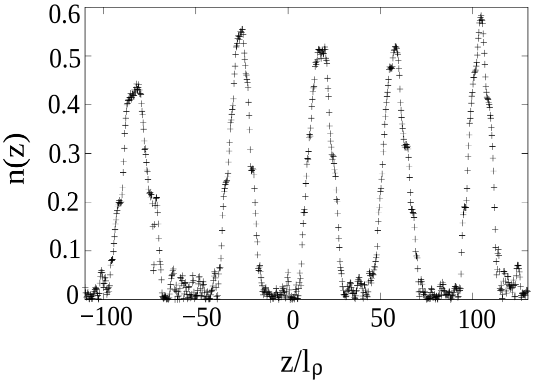

**Figure 5.5.:** Numerical results for the formation of 1D bright solitons as a conseqeunce of the phonon-instability in a homogeneous 1D dipolar BEC. The figure is obtained for $\tilde{\mu} = -0.9$, $\beta = 0.3$ and $g/2\pi l_\rho^2 = 20$. The figure is at a time $t = 3.5/\omega_\rho$. $n(z)$ is the density of the condensate

the $z$ axis and a strong confinement in the $xy$ plane provided by an external potential: $V_{ext}(\rho) = m\omega_\rho^2\rho^2/2$. Bogoliubov analysis provides the following dispersion relation for an 1D homogeneous dipolar BEC:

$$\epsilon(\vec{k}_z)^2 = E_{kin}^2 + \frac{gn_0E_{kin}}{\pi l_\rho^2}\left[1 - \frac{4\pi\beta}{3}h_{1D}\left(k_z l_\rho\right)\right], \tag{5.5}$$

where $l_\rho = \sqrt{\hbar/m\omega_\rho}$, and $h_{1D}(x) = 1 - 2\pi x^2 e^{x^2}\Gamma(0, x^2/2)$ with $\Gamma$ the upper incomplete gamma function. As one can see from Eq. (5.5) the low-momenta modes $\epsilon(k_z \to 0)$ become purely imaginary for $\beta > 3/4\pi$ if $g > 0$. Noted that, as we discussed in Chapter 3, the condition for phonon-instability coincide with the stability of 1D bright solitons in dipolar BECs. Eventhough, the phonon-instability leads to soliton formation both in dipolar and short-range attractive 1D BECs, the soliton dynamics is qualitatively different in both the cases. In the short-range case, the solitons are formed with a relative phase difference of $\pi$, and hence the solitons repel each other leading to the formation of a stable soliton train [30, 31]. On the contrary, in dipolar BECs the solitons are formed with attractive interactions between the solitons due to the attractive nature of DDI along the polarized $z$ axis. As a consequence, the formed 1D dipolar solitons attract each other, and fuse together. Since we are not assuming any dissipation in the system the formed solitons will be in an excited state. After sufficiently large time, the solitons will emerge into a single excited soliton. The soliton may be unstable against 3D collapse if the density in a single soliton is large enough such that the soliton looses its 1D character.

## 5.5. Summary

Summarizing, we have shown that the post-PI dynamics of a 2D dipolar BEC differs qualitatively from 2D and 3D short-range interacting gases, and 3D dipolar BECs.

Contrary to these cases, the PI is not necessarily followed by the collapse of the gas, but on the contrary leads to a transient regime characterized by the formation of a gas of attractive inelastic 2D bright solitons, which eventually undergo fusion, leading to the creation of a single excited stable bright soliton. If the dipoles are normal to the trap plane these solitons are stable as long as the gas remains 2D, whereas if the dipoles are parallel to the trap plane the (anisotropic) solitons may become unstable even in 2D for a critical number of particles per soliton. We have shown that the phonon-like instability in the presence of an harmonic confinement is followed by the creation of transient ring-like and anisotropic patterns, which eventually lead to the creation of a single excited 2D soliton. Finally, we have analyzed the post-PI dynamics in 1D dipolar BECs characterized by the formation of attractive solitons which merge into a single one, differing from the usual repulsive soliton train in non-dipolar BECs.

# Part III.

# Faraday Patterns in Dipolar BEC

# 6. Faraday Patterns in Dipolar BEC

Pattern formation may occur naturally or in driven systems when the non-linearity in the system is modulated. Externally driven or Faraday patterns have been observed in many systems including those in hydrodynamics, non-linear optics, liquid crystals, chemical reactions and biological media [44, 205]. Recently it has been predicted theoretically [206, 207, 208] and also observed experimentally [209] in BEC. Faraday type modulation in trapped short-range interacting condensates can be achieved by modulating either the interatomic interaction or the external trap. In the experiment [209], a modulation of the trap was employed for a cigar-shaped BEC. The wavelength of the pattern is typically determined by the wavenumber associated with the Bogoliubov excitation in resonance with half of the forcing frequency. In this sense, the experiments on Faraday patterns in BEC are certainly interesting, since they allow for the study of collective excitations in a relatively simple way [209, 208].

The study of collective excitations is very essential for the understanding of the macroscopic behavior of atomic BECs. Low-lying excitations in trapped short-range interacting BECs have been studied [210, 211, 212], in which trap modulation and Bragg spectroscopy was employed. The experimental results show an excellent agreement with the results of mean-field calculations [213, 192]. The excitations in strongly interacting Bose gases [214, 215] were also studied using Bragg spectroscopy [216, 217]. As mentioned in Chapter 1 contrary to the phonon-single particle spectrum of short range BECs, dipolar gases may present a roton-maxon excitation spectrum due to the momentum dependence of the anisotropic long-range DDI [144].

In this chapter, we show that pattern formation is crucially modified in dipolar BECs with a roton-maxon spectrum. Remarkably, contrary to many pattern forming systems, including non-dipolar BECs, the first unstable mode does not necessarily determine the emerging pattern, which may be dominated by harmonics of the driving frequency with energies close to the roton minimum. As a result of that and of the multi-valued character of the roton-maxon spectrum the pattern size presents a highly non trivial dependence with the driving frequency characterized even for shallow roton minima by abrupt transitions in the pattern size. These transitions, which are especially pronounced when the DDI is modulated, may be employed to reveal easily the appearance of a roton-minimum in experiments on dipolar BECs.

## 6.1. Faraday Instability in Short-range Interacting Condensates

First, we briefly discuss the formation of Faraday patterns in short-range interacting condensates as studied in [206]. We consider a 2D homogeneous repulsive BEC realized by a strong confinement in the $z$ axis. We assume a periodically modulated $s$-wave scattering length in time: $a(t) = \bar{a}[a + 2\alpha\cos(2\omega t)]$ around its mean value $\bar{a}$ with a modulation frequency $\omega$. The system is decribed by a reduced 2D-GP equation:

$$i\hbar\frac{\partial}{\partial t}\Psi(\vec{\rho},t) = \left(-\frac{\hbar^2}{2m}\nabla^2_{x,y} + g(t)|\Psi|^2\right)\Psi(\vec{\rho},t), \tag{6.1}$$

where $g(t) = \bar{g}[a + 2\alpha\cos(2\omega t)] = 4\pi\hbar^2 a(t)/m$. The spatially homogeneous, temporally periodic solution of Eq. (6.1) is $\Psi_{hom}(t) = \exp[-i\mu(t + \alpha/\omega\sin(2\omega t))/\hbar]$. The periodic modulation in short-range interaction induce spontaneous spatial-symmetry breaking of the homogeneous state, and results in the formation of Faraday patterns. In order to study the symmetry breaking, we perform a linear stability analysis with a suitable ansatz:

$$\Psi(\vec{\rho},t) = \Psi_{hom}(t)[1 + w(t)\cos(\vec{k}\cdot\vec{\rho})], \tag{6.2}$$

where $w$ is the complex-valued amplitude of the perturbation and $\vec{k}$ is the momentum vector in the $xy$ plane. Using Eq. (6.2) in Eq. (6.1) we obtain the following Mathieu equation in $u = Re(w)$:

$$\frac{d^2u}{dt^2} + \frac{1}{\hbar^2}\left[\epsilon(k)^2 + 4\alpha g_{2d}n_{2d}E_k\cos(2\omega t)\right]u = 0, \tag{6.3}$$

where $\epsilon(k) = \sqrt{E_k^2 + 2g_{2d}n_{2d}E_k}$ is the Bogoliubov excitations with $E_k = \hbar^2k^2/2m$, $g_{2d} = \bar{g}/\sqrt{2\pi}l_z$ and $n_{2d}$ is the 2D homogeneous density. Following Floquet Theorem, the solutions of Eq. (6.3) are of the form $u(t) = c(t)\exp\sigma t$, where $c(t) = c(t + 2\pi/\omega)$ and $\sigma(k,\omega,\alpha)$ is the so-called Floquet exponent. If $\mathrm{Re}(\sigma) > 0$ the homogeneous BEC is dynamically unstable against the formation of Faraday patterns, whose typical wavelength is dominated by the most unstable mode i.e. the one with the largest $\mathrm{Re}(\sigma) > 0$. For vanishing modulation the system becomes unstable at the parametric resonances $\epsilon(k) = n\hbar\omega$ $(n = 1, 2, ...)$. Similar wavenumber selection is also found in parametrically forced spatially extended systems, such as in the Faraday instability of vertically vibrated fluids [218, 219].

The neutral stability diagram obtained by analyzing the Floquet exponent is shown in the Fig. (6.1(a)). We have numerically studied the dynamical instability induced by the modulation and the corresponding Faraday patterns (see Fig. (6.1(b))) by simulating Eq. (6.1) with periodic boundary conditions and an overimposed random noise provided by a tiny random local phase ($< 10^{-3}\pi$) on the homogeneous solution. The numerical calculations show excellent agreement with the Foquet analysis. Since BECs with repulsive short-range interactions exhibit a spectrum $\epsilon(k)^2 = E_k[E_k + 2g_{2d}n_{2d}]$, characterized by phonon-like excitations at low $k$ and single-particle excitations at large $k$. For any given driving frequency the most unstable mode is always provided by the

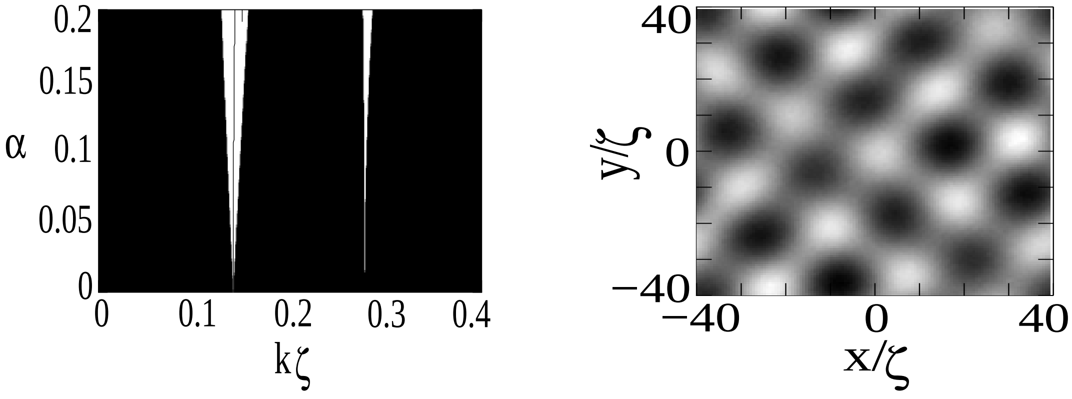

(a)

(b)

**Figure 6.1.:** Resonant tongues and corresponding Faraday pattern for the parametric instability in short-range interacting condensates. The white domains indicate the instability regions where the homogeneous state is unstable as following from the Floquet analysis of Eq. (6.3). The plot is for $\omega = 0.2$, and $\zeta = \sqrt{\hbar^2/2m\mu}$ with $\mu$ is the chemical potential.

first resonance $\epsilon(k) = \hbar\omega$, and hence the wavenumber $k = \epsilon^{-1}(\hbar\omega)$ determines the typical inverse size of the Faraday pattern [220]. As a consequence a larger driving frequency leads to a pattern of smaller size, as shown in recent experiments [209]. In the following, we will show that the physics of Faraday patterns is remarkably much richer, and the wavenumber selection has no more trivial monotonous character when the Bogoliubov spectrum has a roton-maxon character.

## 6.2. Faraday Instability in Dipolar Condensates

In the following we discuss the formation of Faraday patterns in dipolar BECs, in particular the case of dipolar BECs exhibiting roton-maxon Bogoliubov spectrum. We show that the rich physics offered by the roton-maxon spectrum in Faraday patterns can be used to probe such excitations in dipolar BEC, where the rotonic excitations are fundamentally important.

### 6.2.1. Model of the Problem

We consider a BEC of $N$ particles with mass $m$ and electric dipole $d$ (the results are equally valid for magnetic dipoles) oriented in the $z$-direction by a sufficiently large external field. The dipoles interact via a dipole-dipole potential: $V_d(\vec{r}) = d^2(1-3\cos^2(\theta))/r^3$, where $\theta$ is the angle formed by the vector joining the interacting particles and the dipole orientation. We assume a strong harmonic confinement $V(z) = m\omega_z^2 z^2/2$ along the $z$-direction, whereas for simplicity of our discussion we consider no $xy$ trapping. At sufficiently low temperatures, the physics is described by a reduced-2D GP equation (see Chapter 2):

$$i\hbar\frac{\partial}{\partial t}\psi(\vec{\rho}) = \left[-\frac{\hbar^2}{2m}\nabla^2 + g_{2d}|\psi(\vec{\rho})|^2 \right. \\ \left. +\frac{4\pi}{3}\beta g_{2d}\int\frac{d^2k}{(2\pi)^2}e^{i\vec{k}\cdot\vec{\rho}}\tilde{n}(\vec{k})h_{2d}\left(\frac{kl_z}{\sqrt{2}}\right)\right]\psi(\vec{\rho}), \tag{6.4}$$

where $\vec{k}$ is the $xy$-momentum, $l_z \equiv \sqrt{\hbar/m\omega_z}$ is the oscillator length, $g_{2d} \equiv g/\sqrt{2\pi}l_z$ is the 2D short-range coupling constant, $\tilde{n}(\vec{k})$ is the Fourier transform of $|\psi(\vec{\rho})|^2$, and $h_{2d}(\vec{k}) = 2 - 3\sqrt{\pi}ke^{k^2}\text{erfc}(k)$, with erfc$(k)$ the complementary error function. The parameter $\beta = d^2/g$ characterizes the DDI strength compared to the short-range interaction. In the following we assume $g < 0$.

### 6.2.2. Bogoliubov Excitations

The homogeneous solution of (6.4) is $\psi(\vec{\rho}, t) = \sqrt{n_{2d}}\exp\left[-i\mu_{2d}t/\hbar\right]$, with $n_{2d}$ the 2D density, and $\mu_{2d} = g_{2d}n_{2d}(1+8\pi\beta/3)$ the chemical potential. The elementary excitations of the homogeneous 2D BEC are plane waves with 2D wave number $\vec{k}$ and dispersion (see Chapter 5)

$$\epsilon(k)^2 = E_k\left[E_k + 2g_{2d}n_{2d}\left[1+\frac{4\pi\beta}{3}h_{2d}\left(\frac{kl_z}{\sqrt{2}}\right)\right]\right] \tag{6.5}$$

If $\beta = 0$ and since $a < 0$ then $\epsilon(k \to 0)^2 < 0$ and phonon instability occurs, followed by the well-known collapse for attractive short-range interacting BECs (see Chapter 5). This instability is prevented for sufficiently large DDI such that $g + 8\pi d^2/3 > 0$. At moderate $d$ values, and due to the $k$-dependence of the DDI through $h_{2d}$ function, $\epsilon(k)$ may develop a roton-like minimum for intermediate $k$ values (see Fig. (6.2)). The roton-maxon spectrum constitutes one of the most relevant novel features in dipolar gases. We show below that this roton minimum may be easily probed even for shallow roton minima by modulating the system nonlinearity.

### 6.2.3. Modulation of Short-range Interaction

#### Mathieu Equation and Floquet Analysis

We consider a modulation $a(t) = \bar{a}[1+2\alpha\cos(2\omega t)]$ about its mean $\bar{a}$. The homogeneous 2D solution is $\psi_H(\vec{\rho}, t) = \sqrt{n_{2d}}\exp\left[-i(t+\frac{\gamma}{\omega}\sin(2\omega t))\mu_{2d}/\hbar\right]$, with $\gamma = \alpha/(1+8\pi\beta/3)$. The driving may induce a dynamical instability breaking the translational symmetry. This destabilization is best studied with an ansatz $\psi(\vec{\rho}, t) = \psi_H(t)[1 + w(t)\cos(\vec{k}\cdot\vec{r})]$, where $w(t)$ is the complex perturbation amplitude. Inserting this ansatz into (6.4) we obtain a Mathieu equation for $u$ =Re$(w)$:

$$\frac{d^2u}{dt^2} + \frac{1}{\hbar^2}\left[\epsilon(k)^2 + 2b(\omega, k, \alpha)(\hbar\omega)^2\cos(2\omega t)\right]u = 0, \tag{6.6}$$

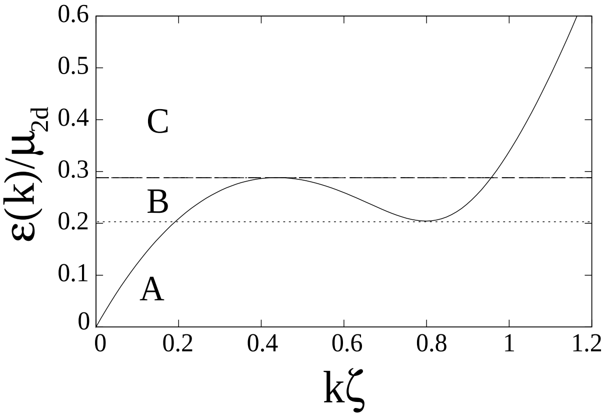

**Figure 6.2.:** Dispersion of a 2D homogeneous BEC of $^{52}$Cr with $a = -0.54$nm ($\beta = -0.375$), a 3D density $\bar{n}_{2d}/\sqrt{2\pi}l_z = 10^{14}cm^{-3}$, $\hbar\omega_z = \mu_{2d}/2$, and $\zeta = \hbar/\sqrt{2m\mu_{2d}} = 0.59\mu$m.

where $b(\omega, k, \alpha) \equiv 2\alpha g_{2d} n_{2d} T(k)/(\hbar\omega)^2$. As we discussed above, following Floquet Theorem, the solutions of (6.6) are of the form $u(t) = c(t) \exp \sigma t$ and if $\mathrm{Re}(\sigma) > 0$ the homogeneous BEC is dynamically unstable against the formation of Faraday patterns, whose typical wavelength is dominated by the most unstable mode (that with the largest $\mathrm{Re}(\sigma) > 0$). For vanishing modulation the system becomes unstable at the parametric resonances $\epsilon(k) = n\hbar\omega$ $(n = 1, 2, ...)$.

As mentioned above, for intermediate $d$ values $\epsilon(k)$ shows a roton minimum (with energy $\hbar\omega_r$) and a maxon maximum ($\hbar\omega_m$). Hence, as a function of the modulation frequency $2\omega$ we may distinguish three driving regimes: (A) $\omega < \omega_r$, (B) $\omega_r \leq \omega \leq \omega_m$ and (C) $\omega > \omega_m$ (see Fig. 6.2). The latter regime is relatively uninteresting, since, as for non-dipolar BECs, the spectrum is uni-valued and the most unstable mode is provided by $\epsilon(k) = \hbar\omega$. The regime B on the contrary is multi-valued, and the condition $\epsilon(k) = \hbar\omega$ is satisfied by a triplet $k_1 < k_2 < k_3$. These three resonant momenta lead to three instability tongues for growing modulation amplitude $\alpha$ (Fig. (6.3(a))). Among the three resonant momenta, $\mathrm{Re}(\sigma)$ is found to be large for $k_3$ and is represented by a line in the Fig. (6.3(a)). This numerical results agrees very well with the following analytical results obtained via Hill's solution method [220, 221]. Upto the fourth order in $b(\omega, k, \alpha)$ the Hill's solution method provides an expression for $\sigma$:

$$\sigma = \frac{i}{\pi} \arccos \left[ \left( 1 - \frac{b^4 \pi^2}{32 q^2 (1-q^2)^2} \right) \cos q\pi + \left( -\frac{b^2 \pi}{4q(1-q^2)} + \frac{15q^4 - 35q^2 + 8}{64 q^3 (1-q^2)^3 (4-q^2)} b^4 \pi \right) \sin q\pi \right], \tag{6.7}$$

with $q = \epsilon(k)^2/(\hbar\omega)^2$. For the lowest resonance $\epsilon(k) = \hbar\omega$ (q=1), one obtain the Floquet exponent for small $b$, by using the Eq. (6.7) as

$$\sigma_1 = b(\omega, k, \alpha)/2 \propto k^2/(\hbar\omega)^2. \tag{6.8}$$

Hence the most unstable mode in regime B is always given by the largest momentum

$k_3$, which dominates the Faraday pattern formation.

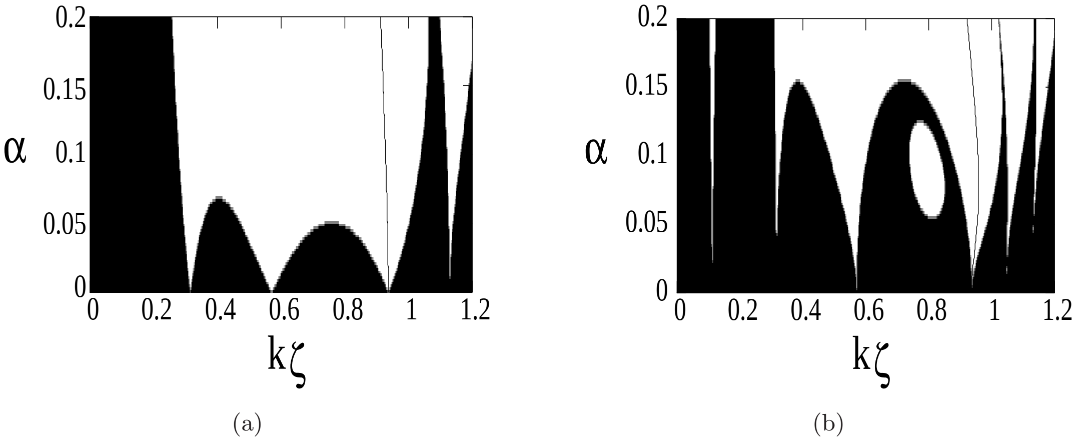

(a)

(b)

**Figure 6.3.:** Stability diagram (dark regions are stable) for the parameters of Fig. (6.2) as a function of $\alpha$ and $k$. (6.3(a)) $\hbar\omega/\mu = 0.268$ (regime B). (6.3(b)) $\hbar\omega/\mu = 0.134$ (regime A). The most unstable modes are indicated by a solid line.

For regimes B and C the Faraday pattern is, as for non-dipolar BECs, provided by $\epsilon(k) = \hbar\omega$. The situation is remarkably different for regime A. The latter is better understood by considering the ratio $\sigma_2/\sigma_1$ between the Floquet exponents for the second ($\epsilon(k) = 2\hbar\omega$) and the first ($\epsilon(k) = \hbar\omega$) resonance condition. Again using the Eq. (6.7) we obtain,

$$\sigma_2 = \frac{\sqrt{5}}{48} b^2. \tag{6.9}$$

Hence the ratio between $\sigma_1$ and $\sigma_2$ can be written as,

$$\frac{\sigma_2}{\sigma_1} = \frac{\sqrt{5}\alpha}{12(8\pi|\beta|/3 - 1)} \left(\frac{\mu_{2d}}{\hbar\omega}\right)^2 \zeta^2 \frac{[\epsilon^{-1}(2\hbar\omega)]^4}{[\epsilon^{-1}(\hbar\omega)]^2}. \tag{6.10}$$

Not surprisingly, the first resonance dominates for $\alpha \to 0$. However, contrary to the short-range interacting case, for $\alpha$ surpassing a very small $\omega$-dependent critical $\alpha$ the situation changes completely. Fig. 6.4(a) depicts the ratio $\sigma_2/\sigma_1$ as a function of $\omega$ for a small $\alpha = 0.04$. Note that for $\omega > \omega_r$ $\sigma_2 < \sigma_1$, and as expected, for regimes B and C the instability is dominated by the resonance $\epsilon(k) = \hbar\omega$. On the contrary for $\omega < \omega_r$, $\sigma_2 > \sigma_1$ even for such a small value of $\alpha$, and hence the lowest resonance is not any more the most unstable one. This surprising result is a direct consequence of the non-monotonous character of the roton-maxon dispersion law.

Our numerical Floquet analysis shows indeed (see Fig. (6.4(b))) that for $\alpha > \alpha_{cr}$ (for the parameters of Figs. (6.2) $\alpha_{cr} \simeq 0.027$) the most unstable mode for all driving frequencies within the regime A is given by the largest momenta $k$ compatible with the first harmonic

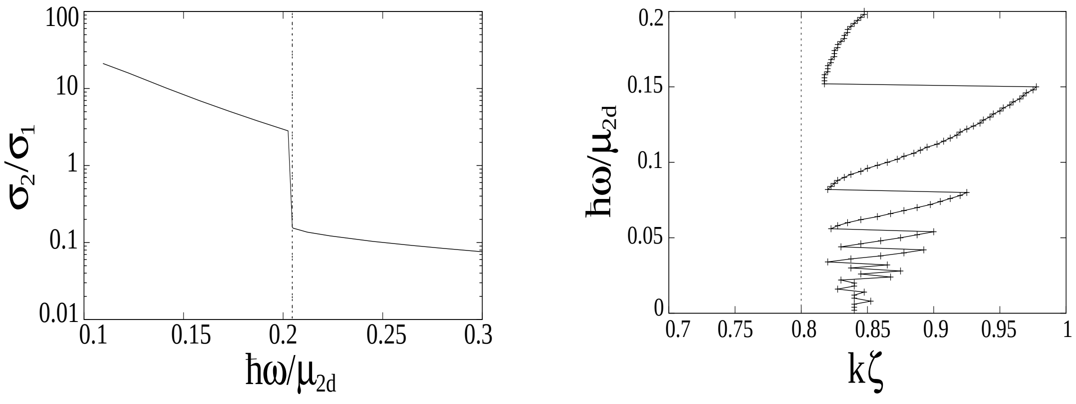

(a)

(b)

**Figure 6.4.:** 6.4(a): Ratio between the Floquet exponent $\sigma_1$ for $\epsilon = \hbar\omega$ and $\sigma_2$ for $\epsilon = 2\hbar\omega$. 6.4(b):Most unstable $k$ as a function of $\omega$ in the regime A. We use the same parameters as for Fig. 6.2. The dashed line indicates the roton frequency or momentum.

$\epsilon(k) = n\hbar\omega$ lying in the regime B (or, if none, the first lying in regime C). This has important consequences for the wavenumber selection as a function of the driving $\omega$, which, as shown in Fig. (6.4(b)), is remarkably different than that for the non-dipolar case. The pattern size does not decrease monotonously with growing $\omega$, but on the contrary oscillates in the vicinity of the roton momentum, presenting abrupt changes of the pattern size at specific driving frequencies. These oscillations are the result of the subsequent destabilization of higher harmonics in regime B.

This distorted wave number selection is directly mirrored into the spatial form of the corresponding Faraday patterns. We have studied the dynamical instability induced by the modulation and the corresponding Faraday patterns by simulating Eq. (6.4) numerically with periodic boundary conditions and an overimposed random noise provided by a tiny random local phase ($< 10^{-3}\pi$) on the homogeneous solution. Our direct numerical calculations is in excellent agreement with our Floquet analysis. Fig. (6.5(a)) depicts the case of a frequency $\omega_r < \omega_0 < \omega_m$, where as expected the Faraday pattern is indeed given by the largest resonant momentum. In Fig. (6.5(b)) we consider $\omega = \omega_0/2$ which is within the regime A. Strikingly, due to the discussed selection of higher harmonics, the Faraday pattern is basically the same as for a double driving frequency $\omega_0$. This quasi-insensitivity becomes quantitatively evident after Fourier transforming the pattern (see Fig. (6.5)).

## 6.3. Modulation of Dipolar Interaction

In the previous discussion we considered the modulation of the $s$-wave scattering length $a(t)$. A dipolar BEC offers, however, an additional novel way of modifying the system

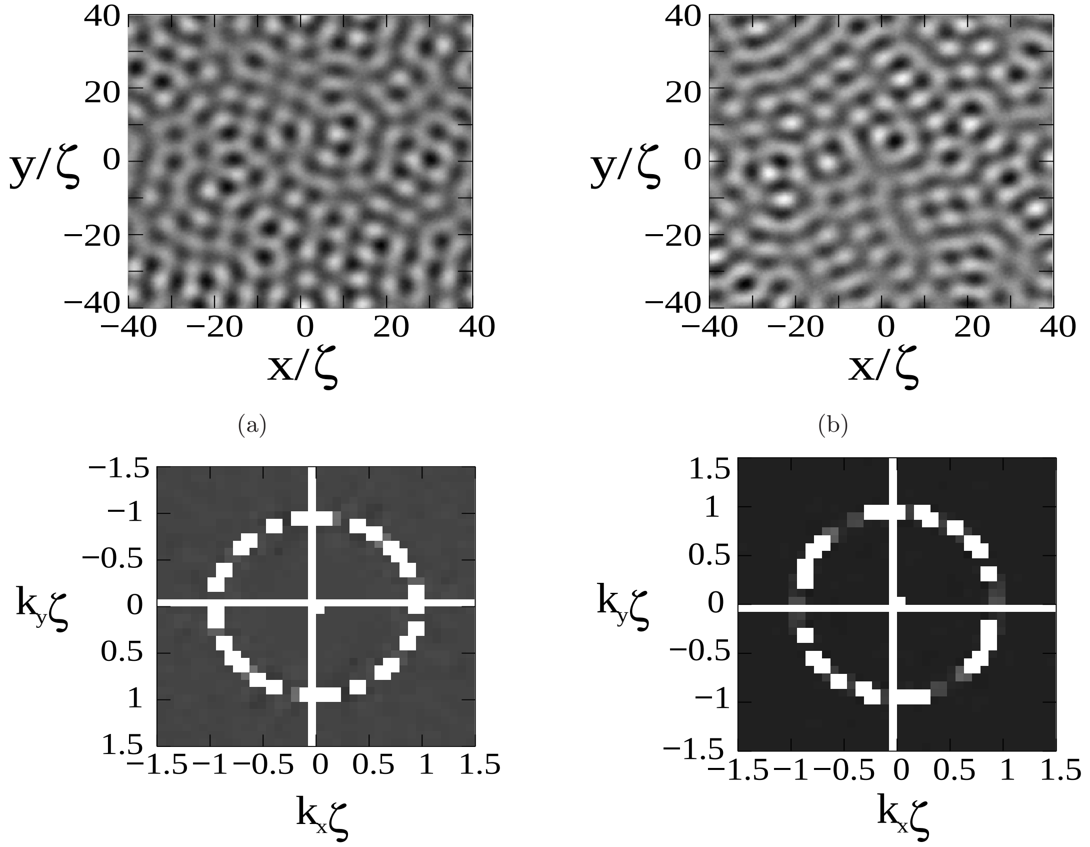

(a)

(b)

(c)

(d)

**Figure 6.5.:** Faraday patterns for $\hbar\omega/\mu = 0.268$ at $t = 40.6$ ms (Fig. (6.5(a))) and $\hbar\omega/\mu = 0.134$ at $t = 93.2$ ms (Fig. (6.5(b))), and the same parameters as in Fig. (6.2). Figs. (6.5(c)) and (6.5(d)) shows the corresponding Fourier spectrum of Faraday patterns Figs. (6.5(a)) and (6.5(a)) respectively.

nonlinearity by a time-dependent DDI. This may be achieved by modulating slightly the intensity of the polarizing field (e.g. the electric field orienting a polar molecule) or by introducing a slight precession of the direction of the external field (e.g. by additional transversal magnetic fields in the case of atomic dipoles). In the following we show that the Faraday patterns obtained by means of a modulated DDI differ very significantly from those obtained by modulating $a(t)$.

We consider a temporal modulation of the DDI $d^2 = g\beta(t)$, with $\beta(t) = \bar{\beta}[1+2\alpha\cos(2\omega t)]$ about its mean value $\bar{\beta}$. Following a similar procedure as that discussed above for the case of modulated $a(t)$, we obtain the Mathieu equation for the real part of the perturbation amplitude. This equation is of the same form as Eq. (6.6) but with

$$b(\omega, k, \alpha) = \frac{8\pi\alpha|\bar{\beta}g_{2d}|n_{2d}}{3(\hbar\omega)^2} T(k) h_{2d}\left(\frac{kl_z}{\sqrt{2}}\right). \tag{6.11}$$

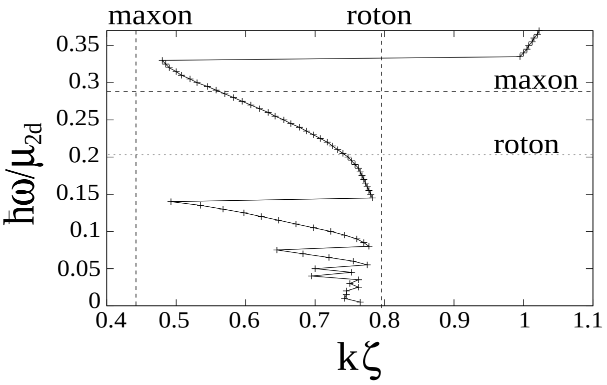

**Figure 6.6.:** Most unstable $k$ as a function of $\omega$ for modulated $\beta(t)$, $\alpha = 0.12$, and the same parameters as for Fig. 1.6. We indicate the roton and maxon frequencies and momenta.

The modified $k$-dependence of $b(\omega, k, \alpha)$ has crucial consequences for the formation of Faraday patterns. Similarly as above we may obtain from Hill's solution method the Floquet exponent for the first resonance $\epsilon(k) = \hbar\omega$,

$$\sigma_1 \propto k^2 h_{2d}(kl_z/\sqrt{2}). \tag{6.12}$$

This leads to a remarkably different selection rule for $\omega$ values within the regime B. Contrary to the case of modulated $a(t)$, it is the intermediate momentum $k_2$ and not the largest one $k_3$ the most unstable within regime B. This leads to a remarkably abrupt change in the Faraday pattern size in the vicinity of $\omega_m$ [1]. In addition, and similar to the case of modulated $a(t)$, driving with $\omega < \omega_r$ may be dominated by higher harmonics. Fig. (6.6) shows the most unstable $k$ as a function of $\omega$ for a typical case of modulated $\beta(t)$. Note not only the above mentioned abrupt jump in the vicinity of $\omega_m$ but also at other $\omega$ values within the regime A. As for the case of modulated $a(t)$ these jumps represent abrupt transitions in the Faraday pattern size, which are certainly much more marked than for the modulated $a$ case. Figs. (6.7) show the abrupt change in the patterns for two driving frequencies right below and above the transition close to $\omega_m$.

## 6.4. Experimental Feasibility

In our calculations we have assumed for simplicity no trapping on the $xy$ plane. An harmonic $xy$-confinement (with frequency $\omega_\perp$) leads to a finite momentum cut-off $k_c = \sqrt{m\omega_\perp/\hbar}$. In a good approximation all features in the excitation spectrum with momenta $k \gg k_c$ are not affected by the inhomogeneous trapping. For typical roton momenta $k\zeta \simeq 0.5$ and $\zeta \simeq 0.6\mu m$ in our figures, $k \gg k_c$ demands for $^{52}$Cr a transversal frequency $\omega_\perp < 130$Hz, which can be considered a typical experimental condition. Finally, we stress that Faraday patterns are a transient phenomenon, and that for the

---

[1] For finite $\alpha$ the transitions slightly shift from their values at $\alpha \cong 0$

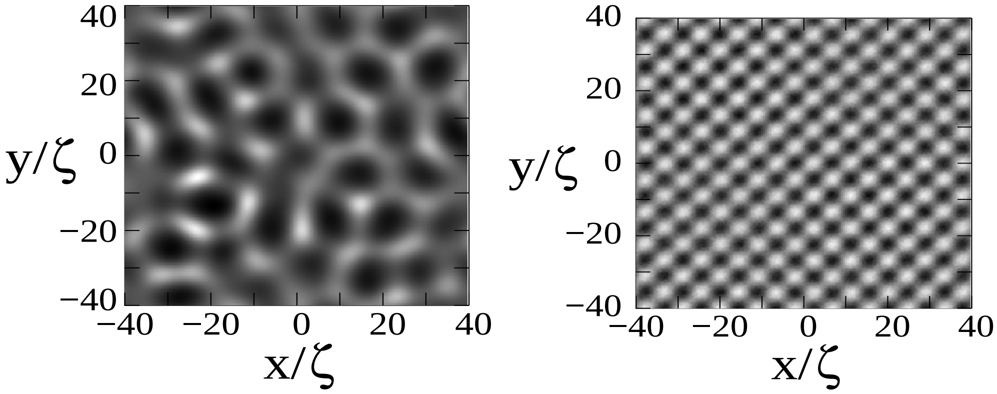

**Figure 6.7.:** Faraday patterns for $\hbar\omega/\mu = 0.32$ at $t = 116.7$ ms (left) and $\hbar\omega/\mu = 0.34$ at $t = 405.1$ ms (right), and the same parameters as in Fig. 5.5.

case discussed here ($a < 0$) pattern formation is followed by collapse (and consequent violation of the two-dimensional condition).

## 6.5. Summary

In summary, the physics of Faraday patterns is largely modified in dipolar BECs in the presence of even shallow roton minima. Whereas in non-dipolar BECs the Faraday pattern size decreases monotonously with the driving frequency $2\omega$, in dipolar BECs the patterns show a $\omega$-dependence characterized by abrupt changes in the pattern size, which are especially remarkable when the dipole itself is modulated. Faraday patterns constitute hence an excellent tool to probe the onset of rotonization in on-going experiments with dipolar condensates.

# 7. Summary

In this thesis, we have studied novel nonlinear properties introduced by the DDI in the physics of dipolar BECs.

The nonlocal nonlinearity resulting from the DDI leads to fascinating links between BEC physics and the physics of other nonlocal nonlinear media, as plasmas and nematic liquid crystals. In this thesis we have studied these nonlocal nonlinear effects in dipolar BECs, with particular emphasis on BEC stability (and the corresponding post-instability dynamics), soliton physics and pattern formation.

In Chapter 2, we have studied 2D dipolar bright solitons, which as shown in Refs. [152, 153] may be stabilized in dipolar BECs. We extended the study on the properties of 2D anisotropic solitons [153], and shown that anisotropic solitons exhibit a 2D collapse if the number of particles in the soliton exceeds a critical number. The latter may be crucial in future experiments.

In Chapter 3, we have discussed the scattering dynamics of 2D bright solitons in dipolar BECs placed at unconnected layers of a 1D optical lattice. Interlayer effects between the unconnected layers, which are a fundamentally new feature introduced by the DDI, induce an inelastic soliton-soliton scattering, that for low relative velocities, leads to the inelastic fusion into a soliton molecule. Interestingly, the inelastic losses do not increase monotonically for decreasing relative velocities, but on the contrary show strong resonances at intermediate velocities, at which, after interacting, the soliton widths are strongly modified, eventually leading to soliton destruction. This effect appears, because, due to the relatively low excitation frequencies of the solitons, a resonant coupling between incoming kinetic energy and internal soliton modes is possible for low relative velocities well within the inelastic regime. We have shown that a similar effects should be observable in 1D geometries, where the experimental requirements may be easily fulfilled in on-going Chromium experiments. Finally, we have considered the 2D scattering of dipolar solitons, a unique possibility offered by the dipolar interactions in cold gases. We have shown that due to the combination of inelastic trapping and initial angular momentum a spiraling motion is possible, offering fascinating links to similar physics in photorrefractive materials.

In the future, we would like to investigate the physics of a stack of 2D dipolar solitons, in particular to study the ground state, and the excitations in the system. There may be a possibility to observe structured ground states for the solitons in optical lattices, e.g. a zigzag structure, due to the long range character of the DDI.

In Chapter 4, we have analyzed the stability of a stationary dark soliton in a 3D dipolar BEC by means of Bogoliubov theory and variational calculations. Both approaches have shown an excellent agreement with each other. Contrary to short-range interacting BECs, where snake instability is just prevented by a sufficiently strong transverse confinement, dipolar BECs allow for stable dark solitons of arbitrarily large transversal sizes, opening a qualitatively novel scenario in nonlinear atom optics. We have obtained the stability conditions, which demand a sufficiently large dipole and a sufficiently deep optical lattice in the nodal plane. We stress that the stabilization of nodal planes against snake instability is purely linked to the long-range nature of the DDI.

In Chapter 5 we have studied the post-phonon-instability (post-PI) dynamics of 2D dipolar BECs with and without an external confinement. We have shown that the post-PI dynamics of a 2D dipolar BEC differs qualitatively from 2D and 3D short-range interacting gases, and 3D dipolar BECs. Contrary to these cases, the PI is not necessarily followed by the collapse of the gas, but on the contrary leads to a transient regime characterized by the formation of a gas of attractive inelastic 2D bright solitons, which eventually undergo fusion, leading to the creation of a single excited stable bright soliton. If the dipoles are normal to the trap plane these solitons are stable as long as the gas remains 2D, whereas if the dipoles are parallel to the trap plane the (anisotropic) solitons may become unstable even in 2D for a critical number of particles per soliton. We have shown that the phonon-like instability in the presence of an harmonic confinement is followed by the creation of transient ring-like and anisotropic patterns, which eventually lead to the creation of a single excited 2D soliton. Finally, we have analyzed the post-PI dynamics in 1D dipolar BECs characterized by the formation of attractive solitons which merge into a single one, differing from the usual repulsive soliton train in non-dipolar BECs.

In Chapter 6, we have studied the formation of Faraday patterns in 2D dipolar BECs exhibiting a roton-maxon Bogoliubov spectrum. We have shown that the physics of Faraday patterns is largely modified in dipolar BECs in the presence of even a shallow roton minima. Whereas in non-dipolar BECs the Faraday pattern size decreases monotonously with the driving frequency $2\omega$, in dipolar BECs the patterns show a $\omega$-dependence characterized by abrupt changes in the pattern size, which are especially remarkable when the dipole itself is modulated. Faraday patterns constitute hence an excellent tool to probe the onset of rotonization in on-going experiments with dipolar condensates.

An interesting future research topic concerns the study of Faraday patterns in a stack of 2D dipolar BECs realized by means of an optical lattice. As an interesting interlayer effect, the creation of Faraday patterns in a BEC in a single layer would lead to the formation of Faraday patterns in all layers due to the dipolar coupling between the layers.

# Bibliography

[1] T. Lahaye, J. Metz, B. Fröhlich, T. Koch, M. Meister, A. Griesmaier, T. Pfau, H. Saito, Y. Kawaguchi and M. Ueda, *d-Wave Collapse and Explosion of a Dipolar Bose-Einstein Condensate*, Phys. Rev. Lett. **101**, 080401 (2008).

[2] S. Chu, L. Hollberg, J. E. Bjorkholm, A. Cable and A. Ashkin, *Three-dimensional Viscous Confinement and Cooling of Atoms by Resonance Radiation Pressure*, Phys. Rev. Lett. **55**, 48 (1985).

[3] E. L. Raab, M. Prentiss, A. Cable, S. Chu and D. E. Pritchard, *Trapping of Neutral Sodium Atoms with Radiation Pressure*, Phys. Rev. Lett. **59**, 2631 (1987).

[4] P. R. Berman, *Atom Interferometry*, Academic Press (1997).

[5] D. S. Weiss, B. C. Young and S. Chu, *Precision Measurement of the Photon Recoil of an Atom Using Atomic Interferometry*, Phys. Rev. Lett. **70**, 2706 (1993).

[6] A. Peters, K. Y. Chung and S. Chu, *Measurement of Gravitational Acceleration by Dropping Atoms*, Nature **400**, 849 (1999).

[7] G. Lamporesi, A. Bertoldi, L. Cacciapuoti, M. Prevedelli and G. M. Tino, *Determination of the Newtonian Gravitational Constant Using Atom Interferometry*, Phys. Rev. Lett. **100**, 050801 (2008).

[8] T. L. Gustavson, A. Landragin and M. A. Kasevich, *Rotation Sensing with a Dual Atom-interferometer Sagnac Gyroscope*, Class. Quantum Grav. **17**, 2385 (2000).

[9] H. Müller, S. wey Chiow, S. Herrmann, S. Chu and K.-Y. Chung, *Atom-Interferometry Tests of the Isotropy of Post-Newtonian Gravity*, Phys. Rev. Lett. **100**, 031101 (2008).

[10] A. Einstein, *Quantentheorie des einatomigen idealen Gases*, Sitzber. Kgl. Preuss. Akad. Wiss. **1**, 3 (1925).

[11] S. N. Bose, *Plancks Gesetz und Lichtquantenhypothese*, Z. Phys **26**, 178 (1924).

[12] K. Huang, *Statistical Mechanics*, Wiley. New York p. 2nd edition (1987).

[13] K. B. Davis, M.-O. Mewes, M. R. Andrews, N. J. van Druten, D. S. Durfee, D. M. Kurn and W. Ketterle, *Bose-Einstein Condensation in a Gas of Sodium Atoms*, Phys. Rev. Lett **75**, 3969 (1995).

[14] M. H. Anderson, J. R. Ensher, M. R. Matthews, C. E. Wieman and E. A. Cornell,

*Observation of Bose-Einstein Condensation in a Dilute Atomic Vapor*, Science **269**, 198 (1995).

[15] A. Griesmaier, J. Werner, S. Hensler, J. Stuhler and T. Pfau, *Bose-Einstein Condensation of Chromium*, Phys. Rev. Lett **94**, 160401 (2005).

[16] Q. Beaufils, R. Chicireanu, T. Zanon, B. Laburthe-Tolra, E. Maréchal, L. Vernac, J.-C. Keller and O. Gorceix, *All optical production of chromium Bose-Einstein Condensates*, Phys. Rev. A **77**, 061601 (R) (2008).

[17] L. V. Butov, C. W. Lai, A. L. Ivanov, A. C. Gossard and D. S. Chemla, *Towards Bose-Einstein Condensation of Excitons in Potential Traps*, Nature **417**, 47 (2002).

[18] H. Deng, G. Welhs, C. Santori, J. Bloch and Y. Yamamoto, *Condensation of Semiconductor Microcavity Exciton Polaritons*, Science **298**, 199 (2002).

[19] J. Kasprzak, M. Richard, S. Kundermann, A. Baas, P. Jeambrun, J. M. J. Keeling, F. M. Marchetti, M. H. Szymańska, R. André, J. L. Staehli, V. Savona, P. B. Littlewood, B. Deveaud and L. S. Dang, *Bose-Einstein Condensation of Exciton Polaritons*, Nature **443**, 409 (2006).

[20] S. O. Demokritov, V. E. Demidov, O. Dzyapko, G. A. Melkov, A. A. Serga, B. Hillebrands and A. N. Slavin, *Bose-Einstein Condensation of Quasi-equilibrium Magnons at Room Temperature Under Pumping*, Nature **443**, 430 (2006).

[21] D. G. Fried, T. C. Killian, L. Willmann, D. Landhuis, S. C. Moss, D. Kleppner and T. J. Greytak, *Bose-Einstein Condensation of Atomic Hydrogen*, Phys. Rev. Lett. **81**, 3811 (1998).

[22] P. W. Anderson, *Considerations on the Flow of Superfluid Helium*, Rev. Mod. Phys. **38**, 298 (1966).

[23] F. Dalfovo, L. P. Pitaevskii, S. Stringari and S. Giorgini, *Theory of Bose-Einstein Condensation in Trapped Gases*, Rev. Mod. Phys **71**, 463 (1999).

[24] J. L. Roberts, N. R. Claussen, S. L. Cornish and C. E. Wieman, *Magnetic Field Dependence of Ultracold Inelastic Collisions Near a Feshbach Resonance*, Phys. Rev. Lett. **85**, 728 (2000).

[25] A. J. Moerdijk, B. J. Verhaar and A. Axelsson, *Resonances in Ultracold Collisions of* $^6$*Li,* $^7$*Li and* $^{23}$*Na*, Phys. Rev. A **51**, 4852 (1995).

[26] E. A. Donley, N. R. Claussen, S. L. Cornish, J. L. Roberts, E. A. Cornell and C. E. Wieman, *Dynamics of Collapsing and Exploding Bose-Einstein Condensates*, Nature **412**, 295 (2001).

[27] J. M. Gerton, D. Strekalov, I. Prodan and R. G. Hulet, *Direct Observation of Growth and Collapse of a Bose-Einstein Condensate with Attractive Interactions*, Nature **408**, 692 (2000).

[28] C. C. Bradley, C. A. Sackett and R. G. Hulet, *Bose-Einstein Condensation of Lithium: Observation of Limited Condensate Number*, Phys. Rev. Lett **78**, 985 (1997).

[29] L. Khaykovich, F. Schreck, G. Ferrari, T. Bourdel, J. Cubizolles, L. D. Carr and Y. Castin, *Formation of Matter-Wave Bright Soliton*, Science **296**, 1290 (2002).

[30] K. E. Strecker, G. B. Patridge, A. G. Truscott and R. G. Hulet, *Formation and propagation of Matter-Wave Soliton Trains*, Nature **417**, 150 (2002).

[31] S. L. Cornish, S. T. Thompson and C. E. Wieman, *Formation of Bright Matter-wave Solitons during the collapse of Attractive Bose-Einstein Condensates*, Phys. Rev. Lett. **96**, 170401 (2006).

[32] N. N. Bogoliubov, *Theory of Superfluidity*, j. Phys (Moscow) **11**, 23 (1947).

[33] A. J. Leggett, *Bose-Einstein condensation in the alkali gases: Some fundamental concepts*, Rev. Mod. Phys. **73**, 307 (2001).

[34] C. J. Pethick and H. Smith, *Bose-Einstein Condensation in Dilute Gases*, Cambridge University Press (2002).

[35] L. P. Pitaevskii and S. Stringari, *Bose-Einstein Condensation*, Oxford University Press (2003).

[36] E. P. Gross, *Structure of a Quantized Vortex in Boson Systems*, Nuovo Cimento **20**, 454 (1961).

[37] E. P. Gross, *Hydrodynamics of a Superfluid Condensate*, J. Math. Phys **4**, 195 (1963).

[38] L. P. Pitaevskii, *Vortex Lines in an Imperfect Bose Gas*, Sov. Phys. JETP **13**, 451 (1961).

[39] E. H. Lieb, R. Seiringer and J. Yngvason, *Bosons in a Trap: A Rigorous Derivation of the Gross-Pitaevskii Energy Functional*, Phys. Rev. A **61**, 043602 (2000).

[40] E. H. Lieb, R. Seiringer, J. P. Solovej and J. Yngvason, *The Mathematics of Bose Gas and its Condensation*, arXiv:0610117 .

[41] C. Sulem and P. L. Sulem, *The Nonlinear Schrödinger Equation*, Springer-Verlag, New York (1999).

[42] Y. S. Kivshar and G. P. Agrawal, *Optical Solitons: From Fibers to Photonic Crystals*, Academic Press (2003).

[43] I. S. Aranson and L. Kramer, *The World of the Complex Ginzburg-Landau Equation*, Rev. Mod. Phys. **74**, 99 (2002).

[44] M. C. Cross and P. C. Hohenberg, *Pattern Formation Outside of Equilibrium*, Rev. Mod. Phys. **65**, 851 (1993).

[45] E. A. Cornell and C. E. Wieman, *Nobel Lecture: Bose-Einstein condensation in a dilute gas, the first 70 years and some recent experiments*, Rev. Mod. Phys. **74**, 875 (2002).

[46] W. Ketterle, *Nobel lecture: When atoms behave as waves: Bose-Einstein condensation and the atom laser*, Rev. Mod. Phys. **74**, 1131 (2002).

[47] A. L. Migdall, J. V. Prodan, W. D. Phillips, T. H. Bergeman and H. J. Metcalf, *First Observation of Magnetically Trapped Neutral Atoms*, Phys. Rev. Lett. **54**, 2596 (1985).

[48] T. Bergeman, G. Erez and H. J. Metcalf, *Magnetostatic Trapping Fields for Neutral Atoms*, Phys. Rev. A **35**, 1535 (1987).

[49] R. Grimm, M. Weidemüller and Y. B. Ovchinnikov, *Optical Dipole Traps for Neutral Atoms*, Adv. At., Mol., Opt. Phys. **42**, 95 (2000).

[50] D. M. Stamper-Kurn, M. R. Andrews, A. P. Chikkatur, S. Inouye, H.-J. Miesner, J. Stenger and W. Ketterle, *Optical Confinement of a Bose-Einstein Condensate*, Phys. Rev. Lett. **80**, 2027 (1998).

[51] M. D. Barrett, J. A. Sauer and M. S. Chapman, *All-Optical Formation of an Atomic Bose-Einstein Condensate*, Phys. Rev. Lett. **87** 1, 010404 (2001).

[52] J. Weiner, V. S. Bagnato, S. Zilio and P. S. Julienne, *Experiments and theory in cold and ultracold collisions*, Rev. Mod. Phys. **71**, 1 (1999).

[53] I. Bloch, *Ultracold Quantum Gases in Optical Lattices*, Nature Phys. **1**, 23 (2005).

[54] I. Bloch, *Exploring Quantum Matter with Ultracold Atoms in Optical Lattices*, J. Phys. B: At. Mol. Opt. Phys. **38**, S629 (2005).

[55] O. Morsch and M. Oberthaler, *Dynamics of Bose-Einstein condensates in optical lattices*, Rev. of Mod. Phys. **78**, 179 (2006).

[56] M. R. Andrews, C. G. Townsend, H.-J. Miesner, D. S. Durfee, D. M. Kurn and W. Ketterle, *Observation of Interference Between Two Bose Condensates*, Science **275**, 637 (1997).

[57] M. R. Andrews, M.-O. Mewes, N. J. van Druten, D. S. Durfee, D. M. Kurn and W. Ketterle, *Direct, Nondestructive Observation of a Bose Condensate*, Science **273**, 84 (1996).

[58] D. S. Petrov, G. V. Shlyapnikov and J. T. M. Walraven, *Regimes of Quantum Degeneracy in Trapped 1D Gases*, Phys. Rev. Lett. **85**, 3745 (2000).

[59] J. O. Anderson, U. A. Khawaja and H. T. C. Stoof, *Phase Fluctuations in Atomic Bose Gases*, Phys. Rev. Lett. **88**, 070407 (2002).

[60] U. A. Khawaja, J. O. Anderson, N. P. Proukakis and H. T. C. Stoof, *Low Dimensional Bose Gases*, Phys. Rev. A **66**, 013615 (2002).

[61] D. L. Luxat and A. Griffin, *Dynamic Correlation Functions in One-dimensional quasicondensates*, Phys. Rev. A **67**, 043603 (2003).

[62] C. Mora and Y. Castin, *Extension of Bogoliubov Theory to Quasicondensates*, Phys. Rev. A **67**, 053615 (2003).

[63] A. Görlitz, J. M. Vogels, A. E. Leanhardt, C. Raman, T. L. Gustavson, J. R. Abo-shaeer, A. P. Chikkatur, S. Gupta, S. Inouye, T. Rosenband and W. Ketterle, *Realization of Bose-Einstein Condensates in Lower Dimensions*, Phys. Rev. Lett. **87**, 130402 (2001).

[64] M. Greiner, I. Bloch, O. Mandel, T. W. Hänsch and T. Esslinger, *Exploring Phase Coherence in a 2D Lattice of Bose-Einstein Condensates*, Phys. Rev. Lett. **87**, 160405 (2001).

[65] S. Burger, F. S. Cataliotti, C. Fort, P. Madadaloni, F. Minardi and M. Inguscio, *Quasi-2D Bose-Eisntein Condensation in an Optical Lattice*, Europhys. Lett. **57**, 1 (2002).

[66] F. S. Cataliotti, S. Burger, C. Fort, P. Madadaloni, F. Minardi, A. Trombettoni, A. Smerzi and M. Inguscio, *Josephson Junction Arrays with Bose-Einstein Condensates*, Science **293**, 843 (2001).

[67] W. Hänsel, P. Hommelhoff, T. W. Hänsch and J. Reichel, *Bose-Einstein Condensation on a Microelectronic Chip*, Nature **413**, 498 (2001).

[68] H. Ott, J. Fortagh, G. Schlotterbeck, A. Grossmann and C. Zimmermann, *Bose-Einstein Condensation in a Surface Microtrap*, Phys. Rev. Lett. **87**, 230401 (2001).

[69] V. V. Konotop and M. Salerno, *Modulational Instability in Bose-Einstein Condensates in Optical Lattices*, Phys. Rev. A **65**, 021602 (2002).

[70] F. K. Abdullaev, A. M. Kamchatnov, V. V. Konotop and V. A. Brazhnyi, *Adiabatic Dynamics of Periodic Waves in Bose-Einstein Condensates with Time Dependent Atomic Scattering Length*, Phys. Rev. Lett. **90**, 230402 (2003).

[71] Y. S. Kivshar and B. A. Malomed, *Dynamics of Solitons in Nearly Integrable Systems*, Rev. Mod. Phys. **61**, 763 (1989).

[72] V. E. Zakharov and A. B. Shabat, *Exact Theory of Two-dimensional Selffocusing and One- dimensional Selfmodulation of Waves in Nonlinear Media*, Sov. Phys. JETP **34**, 62 (1972).

[73] D. J. Kaup, *Exact Quantization of the Nonlinear Schr[o-umlaut]dinger Equation*, J. Math. Phys. **16**, 2036 (1975).

[74] I. M. Uzunov and V. S. Gerdjikov, *Self-frequency Shift of Dark Solitons in Optical Fibers*, Phys. Rev. A **47**, 1582 (1993).

[75] Y. S. Kivshar and X. Yang, *Perturbation-induced dynamics of dark solitons*, Phys. Rev. E **49**, 1657 (1994).

[76] E. M. Lifshitz and L. P. Pitaevskii, *Statistical Physics Part 2: Landau and Lifshitz Course of Theoretical Physics*, Pergamon Press **9** (1989).

[77] S. Ospelkaus, A. Peer, K.-K. Ni, J. J. Zirbel, B.Neyenhuis, S. Kotochigova, P. S. Julienne, J. Ye and D. S. Jin, *Efficient State Transfer in an Ultracold Dense Gas of Heteronuclear Molecules*, Natur. Phys. **4**, 622 (2008).

[78] J. Deiglmayr, A. Grochola, M. Repp, K. Mörtlbauer, C. Glück, J. Lange, O. Dulieu, R. Wester and M. Weidemüller, *Formation of Ultracold Polar Molecules in the Rovibrational Ground State*, Phys. Rev. Lett. **101**, 133004 (2008).

[79] T. Lahaye, T. Koch, B. Fröhlich, M. Fattori, J. Metz, A. Griesmaier, S. Giovanazzi and T. Pfau, *Strong Dipolar Effects in a Quantum Ferrofluid*, Nature **448**, 672 (2007).

[80] S. Yi and L. You, *Trapped condensates of atoms with dipole interactions*, Phys. Rev. A **63**, 053607 (2001).

[81] K. Góral, K. Rzażewski and T. Pfau, *Bose-Einstein Condensation with Magnetic Dipole-dipole Forces*, Phys. Rev. A **61**, 051601 (2000).

[82] J.-P. Martikainen, M. Mackie and K.-A. Suominen, *Comment on "Bose-Einstein Condensation with Magnetic Dipole-dipole Forces"*, Phys. Rev. A **64**, 037601 (2001).

[83] L. Santos, G. V. Shlyapnikov, P. Zoller and M. Lewenstein, *Bose-Einstein Condensation in Trapped Dipolar Gases*, Phys. Rev. Lett **85**, 1791 (2000).

[84] L. Santos, G. V. Shlyapnikov, P. Zoller and M. Lewenstein, *Erratum: Bose-Einstein Condensation in Trapped Dipolar Gases [Phys. Rev. Lett. 85, 1791 (2000)]*, Phys. Rev. Lett. **88**, 139904 (2002).

[85] S. Giovanazzi, D. O'Dell and G. Kurizki, *Density Modulations of Bose-Einstein Condensates via Laser-Induced Interactions*, Phys. Rev. Lett. **88**, 130402 (2002).

[86] K. Góral, L. Santos and M. Lewenstein, *Quantum Phases of Dipolar Bosons in Optical Lattices*, Phys. Rev. Lett. **88**, 170406 (2002).

[87] H. Pu, W. Zhang and P. Meystre, *Ferromagnetism in a Lattice of Bose-Einstein Condensates*, Phys. Rev. Lett. **87**, 140405 (2001).

[88] W. Zhang, H. Pu, C. Search and P. Meystre, *Spin Waves in a Bose-Einstein–Condensed Atomic Spin Chain*, Phys. Rev. Lett. **88**, 060401 (2002).

[89] M. Klawunn, R. Nath, P. Pedri and L. Santos, *Transverse Instability of Straight Vortex Lines in Dipolar Bose-Einstein Condensates*, Phys. Rev. Lett. **100**, 240403 (2008).

[90] D. DeMille, *Quantum Computation with Trapped Polar Molecules*, Phys. Rev. Lett. **88**, 067901 (2002).

[91] M. Vengalattore, S. R. Leslie, J. Guzman and D. M. Stamper-Kurn, *Spontaneously Modulated Spin Textures in a Dipolar Spinor Bose-Einstein Condensate*, Phys. Rev. Lett **100**, 170403 (2008).

[92] M. Fattori, G. Roati, B. Deissler, C. D'Errico, M. Zaccanti, M. Jona-Lasinio, L. Santos, M. Inguscio and G. Modugno, *Magnetic Dipolar Interaction in a Bose-Einstein Condensate Atomic Interferometer*, Phys. Rev. Lett **101**, 190405 (2008).

[93] M. Marinescu and L. You, *Controlling Atom-Atom Interaction at Ultralow Temperatures by dc Electric Fields*, Phys. Rev. Lett. **81**, 4596 (1998).

[94] B. Deb and L. You, *Low-energy atomic collision with dipole interactions*, Phys. Rev. A **64**, 022717 (2001).

[95] C. Ticknor and J. L. Bohn, *Long-range scattering resonances in strong-field-seeking states of polar molecules*, Phys. Rev. A **72**, 032717 (2005).

[96] S. Yi and L. You, *Trapped atomic condensates with anisotropic interactions*, Phys. Rev. A **61**, 041604 (2000).

[97] D. C. E. Bortolotti, S. Ronen, J. L. Bohn and D. Blume, *Scattering Length Instability in Dipolar Bose-Einstein Condensates*, Phys. Rev. Lett. **97**, 160402 (2006).

[98] S. Ronen, D. C. E. Bortolotti, D. Blume and J. L. Bohn, *Dipolar Bose-Einstein Condensates with Dipole-dependent Scattering Length*, Phys. Rev. A **74**, 033611 (2006).

[99] A. Derevianko, *Anisotropic pseudopotential for polarized dilute quantum gases*, Phys. Rev. A **67**, 033607 (2003).

[100] S. Giovanazzi, A. Görlitz and T. Pfau, *Tuning the Dipolar Interaction in Quantum Gases*, Phys. Rev. Lett. **89**, 130401 (2002).

[101] A. G. Litvak, *Self-focusing of Powerful Light Beams by Thermal Effects*, JETP Lett. **4**, 230 (1966).

[102] A. G. Litvak, V. A. Mironov, G. M. Fraiman and A. D. Yunakovskii, *Thermal Self-effect of Wave Beams in a Plasma with a Nonlocal Nonlinearity*, Soviet Journal of Plasma Physics **1**, 31 (1975).

[103] C. Rotschild, O. Cohen, O. Manela, M. Segev and T. Carmon, *Solitons in Nonlinear Media with an Infinite Range of Nonlocality: First Observation of Coherent Elliptic Solitons and of Vortex-Ring Solitons*, Phys. Rev. Lett. **95**, 213904 (2005).

[104] M. Segev, B. Crosignani, A. Yariv and B. Fischer, *Spatial Solitons in Photorefractive Media*, Phys. Rev. Lett. **68**, 923 (1992).

[105] E. M. Wright, W. J. Firth and I. Galbraith, *Beam propagation in a medium with a diffusive Kerr-type nonlinearity*, J. Opt. Soc. Am. B: Opt. Phys. **2**, 383 (1985).

[106] E. A. Ultanir, G. Stegeman, C. H. Lange and F. Lederer, *Coherent interactions of dissipative spatial solitons*, Opt. Lett. **29**, 283 (2004).

[107] E. A. Ultanir, D. Michaelis, F. Lederer and G. I. Stegeman, *Stable spatial solitons in semiconductor optical amplifiers*, Optics Letters **28**, 251 (2003).

[108] A. C. Tam and W. Happer, *Long-Range Interactions between cw Self-Focused Laser Beams in an Atomic Vapor*, Phys. Rev. Lett. **38**, 278 (1977).

[109] D. Suter and T. Blasberg, *Stabilization of Transverse Solitary Waves by a Nonlocal Response of the Nonlinear Medium*, Phys. Rev. A **48**, 4583 (1993).

[110] D. W. McLaughlin, D. J. Muraki, M. J. Shelley and X. Wang, *A Paraxial Model for Optical Self-focussing in a Nematic Liquid Crystal*, Physica D: Nonlinear Phenomena **88**, 55 (1995).

[111] G. Assanto and M. Peccianti, *Spatial Solitons in Nematic Liquid Crystals*, Quantum Electronics, IEEE Journal of **39**, 13 (2003).

[112] C. Conti, M. Peccianti and G. Assanto, *Observation of Optical Spatial Solitons in a Highly Nonlocal Medium*, Phys. Rev. Lett. **92**, 113902 (2004).

[113] M. Peccianti, C. Conti and G. Assanto, *Interplay between Nonlocality and Nonlinearity in Nematic Liquid Crystals*, Opt. Lett. **30**, 415 (2005).

[114] C. Conti, M. Peccianti and G. Assanto, *Route to Nonlocality and Observation of Accessible Solitons*, Phys. Rev. Lett. **91**, 073901 (2003).

[115] M. Peccianti, C. Conti, G. Assanto, A. D. Luca and C. Umeton, *Routing of Anisotropic Spatial Solitons and Modulational Instability in Liquid Crystals*, Nature **432**, 733 (2004).

[116] H. L. Pecseli and J. J. Rasmussen, *Nonlinear Electron Waves in Strongly Magnetized Plasmas*, Plasma Physics **22**, 421 (1980).

[117] A. G. Litvak, V. A. Mironov, G. M. Fraiman and A. D. Yunakovskii, *Thermal Self-effect of Wave Beams in a Plasma with a Nonlocal Nonlinearity*, Soviet Journal of Plasma Physics **1**, 31 (1975).

[118] G. C. Duree, J. L. Shultz, G. J. Salamo, M. Segev, A. Yariv, B. Crosignani, P. Di Porto, E. J. Sharp and R. R. Neurgaonkar, *Observation of Self-trapping of an Optical Beam due to the Photorefractive Effect*, Phys. Rev. Lett. **71**, 533 (1993).

[119] A. V. Mamaev, A. A. Zozulya, V. K. Mezentsev, D. Z. Anderson and M. Saffman, *Bound Dipole Solitary Solutions in Anisotropic Nonlocal Self-focusing Media*, Phys. Rev. A **56**, R1110 (1997).

[120] E. DelRe, A. Ciattoni and A. J. Agranat, *Anisotropic Charge Displacement Supporting Isolated Photorefractive Optical Needles*, Opt. Lett. **26**, 908 (2001).

[121] A. Dreischuh, G. G. Paulus, F. Zacher, F. Grasbon and H. Walther, *Generation of Multiple-charged Optical Vortex Solitons in a Saturable Nonlinear Medium*, Phys. Rev. E **60**, 6111 (1999).

[122] F. W. Dabby and J. R. Whinnery, *Thermal Self-focusing of Laser Beams in Lead Glasses*, App. Phys. Lett. **13**, 284 (1968).

[123] J. F. Henninot, M. Debailleul and M. Warenghem, *Tunable Non-locality of Thermal Non-linearity in Dye Doped Nematic Liquid Crystal*, Mol. Cryst. Liq. Cryst. **375**, 631 (2002).

[124] M. D. I. Castillo, J. J. Sanchez-Mondragon and S. Stepanov, *Formation of Steady-state Cylindrical Thermal Lenses in Dark Stripes*, Optics Letters **21**, 1622 (1996).

[125] W. Krolikowski, O. Bang, J. J. Rasmussen and J. Wyller, *Modulational Instability in Nonloacal Nonlinear Kerr Media*, Phys. Rev. E **64**, 016612 (2001).

[126] W. Krolikowski, O. Bang, J. Wyller and J. Rasmussen, *Optical Beams in Nonlocal Nonlinear media*, Acta Phys. Pol. A **103**, 133 (2003).

[127] J. Wyller, W. Krolikowski, O. Bang and J. J. Rasmussen, *Generic Features of Modulational Instability in Nonlocal Kerr Media*, Phys. Rev. E **66**, 066615 (2002).

[128] W. Krolikowski, O. Bang, N. I. Nikolov, D. Neshev, J. Wyller, J. J. Rasmussen and D. Edmundson, *Modulational Instability, Solitons and Beam Propagation in Spatially Nonlocal Nonlinear Media*, Journal of Optics B: Quantum and Semiclassical Optics **6**, S288 (2004).

[129] S. K. Turitsyn, *Spatial Dispersion of Nonlinearity and Stability of Multidimensional Solitons*, Theor. Math. Phys **64**, 226 (1985).

[130] O. Bang, W. Krolikowski, J. Wyller and J. J. Rasmussen, *Collapse Arrest and Soliton Stabilization in Nonlocal Nonlinear Media*, Phys. Rev. E **66**, 046619 (2002).

[131] N. I. Nikolov, D. Neshev, O. Bang and W. Z. Królikowski, *Quadratic Solitons as Nonlocal Solitons*, Phys. Rev. E **68**, 036614 (R) (2003).

[132] P. V. Larsen, M. P. S. rensen, O. Bang, W. Z. Królikowski and S. Trillo, *Nonlocal Description of X waves in Quadratic Nonlinear Materials*, Phys. Rev. E **73**, 036614 (2006).

[133] A. Fratalocchi, M. Peccianti, C. Conti and G. Assanto, *Spiraling and Cyclic Dynamics of Nematicons*, Mol. Cryst. Liq. Cryst. **421**, 197 (2004).

[134] N. I. Nikolov, D. Neshev, W. Krolikowski, O. Bang, J. J. Rasmussen and P. L. Christiansen, *Attraction of Nonloacal Dark Optical Solitons*, Opt. Lett. **29**, 286 (2004).

[135] A. Dreischuh, D. N. Neshev, D. E. Petersen, O. Bang and W. Krolikowski, *Observation of Attraction between Dark Solitons*, Physical Review Letters **96**, 043901 (2006).

[136] P. D. Rasmussen, O. Bang and W. Królikowski, *Theory of Nonlocal Soliton Interaction in Nematic Liquid Crystals*, Phys. Rev. E **72**, 066611 (2005).

[137] V. A. Mironov, A. M. Sergeev and E. M. Sher, *Multidimensional bound solitons in nonlinear field equations*, Sov. Phys. Dokl. **26**, 861 (1981).

[138] S. Lopez-Aguayo, A. S. Desyatnikov and Y. S. Kivshar, *Azimuthos in Nonlocal Nonlinear Media*, Opt. Express **14**, 7903 (2006).

[139] D. Briedis, D. Petersen, D. Edmundson, W. Krolikowski and O. Bang, *Ring Vortex Solitons in Nonlocal Nonlinear Media*, Opt. Express **13**, 435 (2005).

[140] A. I. Yakimenko, Y. A. Zaliznyak and Y. Kivshar, *Stable Vortex Solitons in Nonlocal Self-focusing Nonlinear Media*, Phys. Rev. E **71**, 065603 (2005).

[141] K. Góral and L. Santos, *Ground state and elementary excitations of single and binary Bose-Einstein condensates of trapped dipolar gases*, Phys. Rev. A **66**, 023613 (2002).

[142] S. Ronen, D. C. E. Bortolotti and J. L. Bohn, *Radial and Angular Rotons in Trapped Dipolar Gases*, Phys. Rev. Lett. **98**, 030406 (2007).

[143] O. Dutta and P. Meystre, *Ground-state structure and stability of dipolar condensates in anisotropic traps*, Phys. Rev. A **75**, 053604 (2007).

[144] L. Santos, G. V. Shlyapnikov and M. Lewenstein, *Roton-Maxon Spectrum and Stability of Trapped Dipolar Bose-Einstein Condensates*, Phys. Rev. Lett. **90**, 250403 (2003).

[145] L. Landau, *Theory of Superfluidity of Helium II*, J. Phys. U.S.S.R **11**, 91 (1947).

[146] R. P. Feynman, *Atomic Theory of the Two-Fluid Model of Liquid Helium*, Phys. Rev. **94**, 262 (1954).

[147] S. Stringari, *Dynamics of Bose-Einstein condensed gases in highly deformed traps*, Phys. Rev. A **58**, 2385 (1998).

[148] U. R. Fischer, *Stability of quasi-two-dimensional Bose-Einstein condensates with dominant dipole-dipole interactions*, Phys. Rev. A **73**, 031602 (2006).

[149] D. H. J. O'Dell, S. Giovanazzi and G. Kurizki, *Rotons in Gaseous Bose-Einstein Condensates Irradiated by a Laser*, Phys. Rev. Lett. **90** 11, 110402 (2003).

[150] S. Giovanazzi and D. H. J. O'Dell, *Instabilities and the Roton Spectrum of a Quasi-1D Bose-Einstein Condensed Gas with Dipole-dipole Interactions*, Eur. Phys. J. D **31**, 439 (2004).

[151] S. Komineas and N. R. Cooper, *Vortex lattices in Bose-Einstein condensates with dipolar interactions beyond the weak-interaction limit*, Physical Review A (Atomic, Molecular, and Optical Physics) **75**, 023623 (2007).

[152] P. Pedri and L. Santos, *Two-Dimensional Bright Solitons in Dipolar Bose-Einstein Condensates*, Phys. Rev. Lett. **95**, 200404 (2005).

[153] I. Tikhonenkov, B. A. Malomed and A. Vardi, *Anisotropic Solitons in Dipolar Bose-Einstein Condensates*, Phys. Rev. Lett. **100**, 090406 (2008).

[154] M. Peccianti, K. A. Brzdkiewicz and G. Assanto, *Nonlocal Spatial Soliton Interactions in Nematic Liquid Crystals*, Opt. Lett. **27**, 1460 (2002).

[155] M. feng Shih, M. Segev and G. Salamo, *Three-dimensional Spiraling of Interacting Spatial Solitons*, Phys. Rev. Lett. **78**, 2551 (1997).

[156] X. Liu, K. Beckwitt and F. Wise, *Transverse Instability of Optical Spatiotemporal Solitons in Quadratic Media*, Phys. Rev. Lett. **85**, 1871 (2000).

[157] X. Liu, K. Beckwitt and F. Wise, *Two-dimensional Optical Spatiotemporal Solitons in Quadratic Media*, Phys. Rev. E **62**, 1328 (2000).

[158] B. Eiermann, T. Anker, M. Albiez, M. Taglieber, P. Treutlein, K.-P. Marzlin and M. K. Oberthaler, *Bright Bose-Einstein Gap Solitons of Atoms with Repulsive Interaction*, Phys. Rev. Lett. **92**, 230401 (2004).

[159] E. A. Ostrovskaya and Y. S. Kivshar, *Matter-Wave Gap Solitons in Atomic Band-Gap Structures*, Phys. Rev. Lett. **90**, 160407 (2003).

[160] H. Saito and M. Ueda, *Dynamically Stabilized Bright Solitons in a Two-Dimensional Bose-Einstein Condensate*, Phys. Rev. Lett. **90** 4, 040403 (2003).

[161] G. B. Arfken and H. J. Weber, *Mathematical Methods for Physicists*, Academic Press .

[162] I. S. Gradshteyn and I. M. Ryzbik, *Table of Integrals, Series, and Products*, Academic Press p. Sixth Edition (2000).

[163] V. M. Pérez-García, H. Michinel, J. I. Cirac, M. Lewenstein and P. Zoller, *Low Energy Excitations of a Bose-Einstein Condensate: A Time-Dependent Variational Analysis*, Phys. Rev. Lett. **77**, 5320 (1996).

[164] V. M. Pérez-García, H. Michinel, J. I. Cirac, M. Lewenstein and P. Zoller, *Dynamics of Bose-Einstein condensates: Variational solutions of the Gross-Pitaevskii equations*, Phys. Rev. A **56**, 1424 (1997).

[165] D. S. Jin, M. R. Matthews, J. R. Ensher, C. E. Wieman and E. A. Cornell, *Temperature-Dependent Damping and Frequency Shifts in Collective Excitations of a Dilute Bose-Einstein Condensate*, Phys. Rev. Lett. **78**, 764 (1997).

[166] U. Al Khawaja and H. T. C. Stoof, *Kinetic theory of collective excitations and damping in Bose-Einstein condensed gases*, Phys. Rev. A **62**, 053602 (2000).

[167] S. Yi and L. You, *Probing dipolar effects with condensate shape oscillation*, Phys. Rev. A **66**, 013607 (2002).

[168] R. Nath, P. Pedri and L. Santos, *Phonon Instability with Respect to Soliton Formation in Two-Dimensional Dipolar Bose-Einstein Condensates*, Phys. Rev. Lett. **102**, 050401 (2009).

[169] J. P. Gordon, *Interaction Forces among Solitons in Optical Fibers*, Opt. Lett. **8**, 596 (1983).

[170] A. D. Martin, C. S. Adams and S. A. Gardiner, *Bright Matter-Wave Soliton Collisions in a Harmonic Trap: Regular and Chaotic Dynamics*, Phys. Rev. Lett. **98**, 020402 (2007).

[171] L. D. Carr and J. Brand, *Pulsed atomic soliton laser*, Phys. Rev. A **70**, 033607 (2004).

[172] L. Khaykovich and B. A. Malomed, *Deviation from one dimensionality in stationary properties and collisional dynamics of matter-wave solitons*, Phys. Rev. A **74**, 023607 (2006).

[173] R. Nath, P. Pedri and L. Santos, *Soliton-soliton scattering in dipolar Bose-Einstein condensates*, Physical Review A (Atomic, Molecular, and Optical Physics) **76**, 013606 (2007).

[174] L. Poladian, A. Snyder and D. Mitchell, *Spiralling Spatial Solitons*, Optics Communications **85**, 59 (1991).

[175] J. Werner, A. Griesmaier, S. Hensler, J. Stuhler, T. Pfau, A. Simoni and E. Tiesinga, *Observation of Feshbach Resonances in an Ultracold Gas of* $Cr52$, Phys. Rev. Lett. **94**, 183201 (2005).

[176] D.-W. Wang, M. D. Lukin and E. Demler, *Quantum Fluids of Self-Assembled Chains of Polar Molecules*, Phys. Rev. Lett. **97**, 180413 (2006).

[177] Y. S. Kivshar and B. Luther-Davies, *Dark optical solitons: physics and applications*, Phys. Rep. **298**, 81 (1998).

[178] P. O. Fedichev, A. E. Muryshev and G. V. Shlyapnikov, *Dissipative dynamics of a kink state in a Bose-condensed gas*, Phys. Rev. A **60**, 3220 (1999).

[179] J. Dziarmaga, Z. P. Karkuszewski and K. Sacha, *Images of the dark soliton in a depleted condensate*, Journal of Physics B: Atomic, Molecular and Optical Physics **36**, 1217 (2003).

[180] D. L. Feder, M. S. Pindzola, L. A. Collins, B. I. Schneider and C. W. Clark, *Dark-soliton states of Bose-Einstein condensates in anisotropic traps*, Phys. Rev. A **62**, 053606 (2000).

[181] J. Brand and W. P. Reinhardt, *Solitonic vortices and the fundamental modes of the "snake instability": Possibility of observation in the gaseous Bose-Einstein condensate*, Phys. Rev. A **65**, 043612 (2002).

[182] A. Muryshev, G. V. Shlyapnikov, W. Ertmer, K. Sengstock and M. Lewenstein, *Dynamics of Dark Solitons in Elongated Bose-Einstein Condensates*, Phys. Rev. Lett. **89**, 110401 (2002).

[183] B. P. Anderson, P. C. Haljan, C. A. Regal, D. L. Feder, L. A. Collins, C. W. Clark and E. A. Cornell, *Watching Dark Solitons Decay into Vortex Rings in a Bose-Einstein Condensate*, Phys. Rev. Lett. **86**, 2926 (2001).

[184] A. V. Mamaev, M. Saffman and A. A. Zozulya, *Propagation of Dark Stripe Beams in Nonlinear Media: Snake Instability and Creation of Optical Vortices*, Phys. Rev. Lett. **76**, 2262 (1996).

[185] A. E. Muryshev, H. B. van Linden van den Heuvell and G. V. Shlyapnikov, *Stability of Standing Matter Waves in a Trap*, Phys. Rev. A **60**, R2665 (1999).

[186] T. Busch and J. R. Anglin, *Motion of Dark Solitons in Trapped Bose-Einstein Condensates*, Phys. Rev. Lett. **84**, 2298 (2000).

[187] G. Huang, J. Szeftel and S. Zhu, *Dynamics of dark solitons in quasi-one-dimensional Bose-Einstein condensates*, Phys. Rev. A **65**, 053605 (2002).

[188] L. D. Carr and C. W. Clark, *Vortices and Ring Solitons in Bose-Einstein condensates*, Phys. Rev. A **74** 4, 043613 (2006).

[189] G. Theocharis, D. J. Frantzeskakis, P. G. Kevrekidis, B. A. Malomed and Y. S. Kivshar, *Ring Dark Solitons and Vortex Necklaces in Bose-Einstein Condensates*, Phys. Rev. Lett. **90**, 120403 (2003).

[190] R. Nath, P. Pedri and L. Santos, *Stability of Dark Solitons in Three Dimensional Dipolar Bose-Einstein Condensates*, Phys. Rev. Lett. **101**, 210402 (2008).

[191] A. Trombettoni and A. Smerzi, *Discrete Solitons and Breathers with Dilute Bose-Einstein Condensates*, Phys. Rev. Lett. **86**, 2353 (2001).

[192] M. Krämer, L. Pitaevskii and S. Stringari, *Macroscopic Dynamics of a Trapped Bose-Einstein Condensate in the Presence of 1D and 2D Optical Lattices*, Phys. Rev. Lett. **88**, 180404 (2002).

[193] V. Tikhonenko, J. Christou, B. Luther-Davies and Y. S. Kivshar, *Observation of vortex solitons created by the instability of dark soliton stripes*, Opt. Lett. **21** 15, 1129 (1996).

[194] J. Dziarmaga, Z. P. Karkuszewski and K. Sacha, *Quantum depletion of an excited condensate*, Phys. Rev. A **66**, 043615 (2002).

[195] C. C. Bradley, C. A. Sackett, J. J. Tollett and R. G. Hulet, *Evidence of Bose-Einstein Condensation in an Atomic Gas with Attractive Interactions*, Phys. Rev. Lett. **75**, 1687 (1995).

[196] C. C. Bradley, C. A. Sackett, J. J. Tollett and R. G. Hulet, *Evidence of Bose-Einstein Condensation in an Atomic Gas with Attractive Interactions [Phys. Rev. Lett. 75, 1687 (1995)]*, Phys. Rev. Lett. **79**, 1170 (1997).

[197] J. L. Roberts, N. R. Claussen, S. L. Cornish, E. A. Donley, E. A. Cornell and C. E. Wieman, *Controlled Collapse of a Bose-Einstein Condensate*, Phys. Rev. Lett. **86**, 4211 (2001).

[198] M. Ueda and A. J. Leggett, *Macroscopic Quantum Tunneling of a Bose-Einstein Condensate with Attractive Interaction*, Phys. Rev. Lett. **80**, 1576 (1998).

[199] S. L. Cornish, N. R. Claussen, J. L. Roberts, E. A. Cornell and C. E. Wieman, *Stable 85Rb Bose-Einstein Condensates with Widely Tunable Interactions*, Phys. Rev. Lett. **85**, 1795 (2000).

[200] Y. Kagan, A. E. Muryshev and G. V. Shlyapnikov, *Collapse and Bose-Einstein Condensation in a Trapped Bose Gas with Negative Scattering Length*, Phys. Rev. Lett. **81**, 933 (1998).

[201] H. Saito and M. Ueda, *Intermittent Implosion and Pattern Formation of Trapped Bose-Einstein Condensates with an Attractive Interaction*, Phys. Rev. Lett. **86**, 1406 (2001).

[202] H. Saito and M. Ueda, *Mean-field analysis of collapsing and exploding Bose-Einstein condensates*, Phys. Rev. A **65**, 033624 (2002).

[203] A. I. Yakimenko, V. M. Lashkin and O. O. Prikhodko, *Dynamics of two-dimensional coherent structures in nonlocal nonlinear media*, Phys. Rev. E **73**, 066605 (2006).

[204] V. M. Lashkin, *Two-dimensional nonlocal vortices, multipole solitons, and rotating multisolitons in dipolar Bose-Einstein condensates*, Physical Review A (Atomic, Molecular, and Optical Physics) **75**, 043607 (2007).

[205] C. Bowman and A. C. Newell, *Natural patterns and wavelets*, Rev. Mod. Phys. **70**, 289 (1998).

[206] K. Staliunas, S. Longhi and G. J. de Valcárcel, *Faraday Patterns in Bose-Einstein Condensates*, Phys. Rev. Lett. **89**, 210406 (2002).

[207] K. Staliunas, S. Longhi and G. J. de Valcárcel, *Faraday patterns in low-dimensional Bose-Einstein condensates*, Phys. Rev. A **70**, 011601 (2004).

[208] M. Modugno, C. Tozzo and F. Dalfovo, *Detecting phonons and persistent currents in toroidal Bose-Einstein condensates by means of pattern formation*, Phys. Rev. A **74**, 061601 (2006).

[209] P. Engels, C. Atherton and M. A. Hoefer, *Observation of Faraday Waves in a Bose-Einstein Condensate*, Phys. Rev. Lett. **98**, 095301 (2007).

[210] C. Fort, F. S. Cataliotti, L. Fallani, F. Ferlaino, P. Maddaloni and M. Inguscio, *Collective Excitations of a Trapped Bose-Einstein Condensate in the Presence of a 1D Optical Lattice*, Phys. Rev. Lett. **90**, 140405 (2003).

[211] D. S. Jin, J. R. Ensher, M. R. Matthews, C. E. Wieman and E. A. Cornell, *Collective Excitations of a Bose-Einstein Condensate in a Dilute Gas*, Phys. Rev. Lett. **77**, 420 (1996).

[212] M.-O. Mewes, M. R. Andrews, N. J. van Druten, D. M. Kurn, D. S. Durfee, C. G. Townsend and W. Ketterle, *Collective Excitations of a Bose-Einstein Condensate in a Magnetic Trap*, Phys. Rev. Lett. **77**, 988 (1996).

[213] S. Stringari, *Collective Excitations of a Trapped Bose-Condensed Gas*, Phys. Rev. Lett. **77**, 2360 (1996).

[214] S. B. Papp, J. M. Pino, R. J. Wild, S. Ronen, C. E. Wieman, D. S. Jin and E. A. Cornell, *Bragg Spectroscopy of a Strongly Interacting Rb Bose-Einstein Condensate*, Phys. Rev. Lett. **101**, 135301 (2008).

[215] D. Clément, N. Fabbri, L. Fallani, C. Fort and M. Inguscio, *Exploring Correlated 1D Bose Gases from the Superfluid to the Mott-Insulator State by Inelastic Light Scattering*, Phys. Rev. Lett. **102**, 155301 (2009).

[216] J. Stenger, S. Inouye, A. P. Chikkatur, D. M. Stamper-Kurn, D. E. Pritchard and W. Ketterle, *Bragg Spectroscopy of a Bose-Einstein Condensate*, Phys. Rev. Lett. **82**, 4569 (1999).

[217] D. M. Stamper-Kurn, A. P. Chikkatur, A. Görlitz, S. Inouye, S. Gupta, D. E. Pritchard and W. Ketterle, *Excitation of Phonons in a Bose-Einstein Condensate by Light Scattering*, Phys. Rev. Lett. **83**, 2876 (1999).

[218] P. Coullet, T. Frisch and G. Sonnino, *Dispersion-induced patterns*, Phys. Rev. E **49**, 2087 (1994).

[219] W. Zhang and J. Viñals, *Square patterns and quasipatterns in weakly damped Faraday waves*, Phys. Rev. E **53**, R4283 (1996).

[220] A. I. Nicolin, R. Carretero-González and P. G. Kevrekidis, *Faraday Waves in Bose-Einstein condensates*, Phys. Rev. A **76**, 063609 (2007).

[221] A. I. Nicolin, *PhD Thesis, Copenhagen* (2008).

# Selbstständigkeitserklärung

Hiermit versichere ich, die vorliegende Doktorarbeit selbstständig und unter ausschließlicher Verwendung der angegebenen Hilfsmittel angefertigt zu haben.

Hannover, den 30. April 2009

Rejish Nath

# Acknowledgments

My research and this thesis would have not materialized if I did not have the invaluable support, and encouragement from a number of individuals. First, I take this oppurtunity to express my deepest gratitude and indebtedness to Prof. Dr. Luis Santos, for his unstilted help, valuable advices and constant encouragement throughout the course of this work. Second, I thank Dr. Paolo Pedri for his valuable guidance and enlightening discussions which have helped me to constitute foundations in the field of ultra cold atoms.

In the last three and a half years, Arturo Arguelles has been my office colleague who has become a close friend. I have benefited from him ideas concerning numerical simulations, which have helped me in the course of my PhD thesis. My special thanks also goes to Karen Rodriguez for giving a good company and, especially for the lively parties we have organized at her place on X’mas nights. At this moment I also thanks to Prof. Luis Santos wife, Rocio for making a homely atmosphere at her home at different occasions.

Special thanks goes to Carsten v. Zobeltitz and Alex Cojuhovschi for their kind help on a number of computer-related problems.

I have also benefited from fruitful discussions with numerous people. I can’t express my gratitude to Michael Klawunn for the discussions we had on dipolar gases, Garu Gebreyesus for intial discussions on dark solitons and later on the subject of spinor condensates. From Andreas Jacob I gained an invaluable basics about non-abelian atom optics. Special thanks also goes to Kazimierz Łakomy for the valuable discussions on the topics of dipolar gases and also for his valuable suggestions, and corrections he suggested for this thesis.

Here, I cannot also forget the names of previous member’s of Prof. Santos group, especially Dr. Subhasis Sinha for his kind guidance in the intial stages of my research at university of Stuttgart, and Dr. Philipp Hyllus and Dr. Giovanni Mazarella for their invaluable support during their stay at Hannover. I am also thankful to Jimmy Sebastian for supporting me, and giving me a good company during my stay at Stuttgart.

My friends and colleagues made Hannover not only a great place to work, but also a wonderful place to live. I warmly thank all the members of the Institute of Theoretical Physics and Institute of Quantum Optics at University of Hannover. I particularly enjoyed the company of Ajith Parameswaran, Sajan D. George, Catherine Aresipathi, Jinu John and her aunt’s family. I also acknowledge my friends back at home, and at the various parts of the world.

The administrative and supportive staff of Institute of Theoretical Physics and University of Hannover have been very helpful throughout these years. I thank Ms. Gitta Richter, Ms. Schwebs Emma, Ms. Elke Hünitzsch, Ms. Guhild Faber, Ms. Ute Reuter and Ms. Ildiko Poljak (Stuttgart).

I am also grateful to Dr. B Premlet, Dr. M V Satyanarayana, and Prof. Purusattam Ray for their kind support in starting my career in physics.

I am greatly thankful to the financial support provided by SFB-TR21 (Stuttgart) and SFB 407 (Hannover). Without that this thesis would not have been finished.

Finally, but immensely, I thank my family back home for their love, understanding and support.

Rejish Nath

# Curriculum Vitae

Rejish Nath Gopinathan Rejani
Gerhardtstr. 5, 30167 Hannover, Germany
E-mail: rejish@itp.uni-hannover.de
Homepage: http://www.itp.uni-hannover.de/tqowww/rejish/index.xht

### Personal profile

| | | |
|---|---|---|
| Date of Birth | : | 12 February 1982 |
| Place of Birth | : | Kollam, Kerala, India |
| Sex | : | Male |
| Marital Status | : | Single |
| Nationality | : | Indian |

### Education

*Ph. D. Physics:* Institute of Theoretical Physics3, University of Stuttgart, Stuttgart, Germany. (2005-2006)
Institute of Theoretical Physics, Leibniz University of Hannover, Hannover, Germany. (2006 – 2009)

*M. Sc. Physics:* Indian Institute of Technology Madras, Chennai, India. (2002 – 2004).

*B. Sc. Physics:* University of Kerala, Thiruvananthapuram, India. (1999 – 2002).

*Pre Degree (Physics, Mathematics, Chemistry):* University of Kerala, Thiruvananthapuram, India. (1995 – 1997).

*Primary and Secondary School:* Mount Carmel English Medium High School, Mathilakom, Kerala, India. (1987 – 1997).

### Research experience

- ⇝ Graduate student at University of Stuttgart (August 2005-April 2006) and at Leibniz University of Hannover, Germany (May 2006-June 2009).
  Thesis Title: Non-linear Phenomena in Dipolar Bose-Einstein Condensates.
  Advisor: Prof. Luis Santos.

- ⇝ Visiting student at 1st Physikalisches Institute, University of Stuttgart, Stuttgart, Germany (February 2005-July 2005).
  Field: Molecular Magnets.
  Advisor: Dr. Joris van Slageren.
- ⇝ Visiting student at Centre for Non-destructive Evaluation, Indian Institute of Technology Madras, Chennai, India (September 2004-December 2004).
  Field: Wave Propagation in Complex Media.
  Advisor: Prof. Krishnan Balasubramaniam.
- ⇝ Summer student at Institute of Mathematical Sciences, Chennai, India (summer 2003 and summer 2004).
  Field: Spin Glasses.
  Advisor: Prof. Purusattam Ray.
- ⇝ Master Thesis at Indian Institute of Technology Madras, Chennai, India (August 2003-April 2004).
  Thesis Title: Electrostatics and Zeros of Orthogonal Polynomials.
  Advisor: Dr. M. V. Satyanarayana.

# List of Publications

1. R. Nath and L. Santos, *Faraday Patterns in Dipolar Bose-Einstein Condensates*, submitted to Phys. Rev. Lett. (2009), arXiv:0902:3969
2. R. Nath, P. Pedri and L. Santos, *Phonon Instability with Respect to Soliton Formation in Two-Dimensional Dipolar Bose-Einstein Condensates*, Phys. Rev. Lett. **102** 050401 (2009).
3. R. Nath, P. Pedri and L. Santos, *Stability of Dark Solitons in Three-Dimensional Dipolar Bose-Einstein Condensates*, Phys. Rev. Lett. **101** 210402 (2008).
4. M. Klawunn, R. Nath, P. Pedri and L. Santos, *Transverse Instability of Straight Vortex Lines in Dipolar Bose-Einstein Condensates*, Phys. Rev. Lett. **100** 240403 (2008).
5. R. Nath, P. Pedri and L. Santos, *Soliton-soliton Scattering in Dipolar Bose-Einstein Condensates*, Phys. Rev. A **76** 013606 (2007).